

DIGITAL ACCESS TO SCHOLARSHIP AT HARVARD

Microbe-electrode interactions: The chemico-physical environment and electron transfer

The Harvard community has made this article openly available. Please share how this access benefits you. Your story matters.

Citation	Gardel, Emily Jeanette. 2013. Microbe-electrode interactions: The chemico-physical environment and electron transfer. Doctoral dissertation, Harvard University.
Accessed	April 17, 2018 4:24:46 PM EDT
Citable Link	http://nrs.harvard.edu/urn-3:HUL.InstRepos:11169781
Terms of Use	This article was downloaded from Harvard University's DASH repository, and is made available under the terms and conditions applicable to Other Posted Material, as set forth at http://nrs.harvard.edu/urn-3:HUL.InstRepos:dash.current.terms-of-use#LAA

(Article begins on next page)

Microbe-electrode interactions: The chemico-physical environment and electron transfer

A dissertation presented

by

Emily Jeanette Gardel

to

The School of Engineering and Applied Sciences

in partial fulfillment of the requirements

for the degree of

Doctor of Philosophy

in the subject of

Applied Physics

Harvard University

Cambridge, Massachusetts

September 2013

©2013 – Emily Jeanette Gardel

All rights reserved.

Thesis advisor

Peter R. Girguis

Author

Emily Jeanette Gardel

Microbe-electrode interactions: The chemico-physical environment and electron transfer

Abstract

This thesis presents studies that examine microbial extracellular electron transfer that an emphasis characterizing how environmental conditions influence electron flux between microbes and a solid-phase electron donor or acceptor. I used bioelectrochemical systems (BESs), fluorescence and electron microscopy, chemical measurements, 16S rRNA analysis, and qRT-PCR to study these relationships among chemical, physical and biological parameters and processes.

Chapter 1 introduces the concepts of microorganisms, microbial metabolism, extracellular electron transfer, and the value of BESs to provide essential background and motivation for the projects in this thesis.

Chapter 2 presents how variations in the time an anode is connected influences cumulative charge, current and microbial community composition in an environmental BES. When disconnection times are sufficiently short, the current decreases due to an increase in the overall electrode reaction resistance. These results indicate that replenishment of depleted electron

donors within the biofilm and surrounding diffusion layer is necessary for maximum electron transfer. Such experiments are valuable in determining performance factors of BESs and in optimizing field-deployed systems.

Chapter 3 aims at demonstrating if an iron-oxidizing photoautotroph can take up electrons from a poised electrode. The subject of this study is *Rhodopseudomonas palustris* TIE-1, which can oxidize Fe^{2+} to Fe^{3+} with light for energy generation. The results indicate TIE-1 can accept electrons from a poised electrode, with carbon dioxide as the sole carbon source/electron donor. Genes encoding for membrane proteins implicated in iron oxidation (the *pioABC* operon) play a role in electron uptake. This reveals a previously unknown metabolic versatility of photoferrotrophs to use extracellular electron transfer for electron uptake in the presence of light.

Chapter 4 aims at determining if microbial methane production can be stimulated using BESs. This study examines two methanogens, *Methanosarcina barkeri* Fusaro and *Methanosarcina acetivorans* C2A, at different electrode potentials. While *M. barkeri* has hydrogenases with metalloprotein subunits, *M. acetivorans* does not. A poised electrode stimulates methanogenesis for *M. barkeri* but not for *M. acetivorans*, implicating the role of these hydrogenases in microbial extracellular electron transfer. These data demonstrate of the viability of microbial electrosynthesis and indicate how media composition influences net current in BESs.

Contents

Citations to Work

Chapter 2 is from the manuscript:

"Duty-Cycling Influences Current Generation in Multi-Anode Environmental Microbial Fuel Cells", E.J. Gardel, M.E. Nielsen, P.T.Grisdela, P.E. Girguis *Environ. Sci. Technol.* **46**, 5222-5229 (2012).

The content from Chapter 3 is from the paper:

"Mechanisms and implications of electron uptake by iron oxidizing phototrophic bacteria:, A. Bose, E.J. Gardel, C. Vidoudez, E.A. Parra, P.R. Girguis, in review at *Nat. Commun.*

Acknowledgements

Without a doubt there are many people to recognize who have helped me along the way and I am greatly appreciative for their cumulative efforts. Whether it is helping me figure out an experiment, talking about life, or providing support after a tough day, all of these actions contributed to this accomplishment.

First, I'd like to thank Peter Girguis for taking a chance on me and allowing a physicist into his lab. I truly appreciate his ability to think outside the box and bridge across different scientific areas. To his credit, I'm not quite sure what to call myself anymore, and I consider that a good thing.

I will always feel indebted to members of the Girguis lab for their never-tiring guidance, companionship, mentorship, and support. This is especially true of Arpita Bose and Charles Vidoudez—I feel so blessed to have worked on projects with both of them. Not only did I learn so much about designing experiments and interpreting results from them, but their continued support and friendship helped me through this thesis. I would also like to thank Mark Nielsen for introducing me to the world of microbial fuel cells and support with my first project. Thanks goes out to former microbial EET group members –Erika Parra, Allon Hochbaum, Sage Radachowsky, Israel Figureoa, and Tom Weller.

Jennifer Delany and Stephanie Hillsgrove—words can't express my gratitude for all your help. I would also like to thank Melissa Adams, Jon Sanders, Vicky Bertics, Ulli Jaekel, Dan Rogers, Kiana Frank, Heather Olins, John Skutnik, and Roxie Beinart for being fantastic co-workers and colleagues.

I would like to thank the Department of Energy and their Office of Science Graduate Research Fellowship program, especially Ping Ge, Cayla Stephenson, and all the other DOE SCGF fellows. It was truly an honor to be a part of the inaugural fellowship program and learn about role of the DOE in our country's science and technology efforts. Additionally, I thank the National Science Foundation and there Graduate Fellowship program for funding me during the early graduate school years.

Many others at Harvard have helped me in a variety of ways. Being a part of Harvard Graduate Women in Science has been immensely rewarding and allowed me to form friendships with other graduate students outside my lab—Karen Ruff, Eliza Morris, Erin Boyd, Sarah Ballard, Shan Lou, Risa Kawai, Dilani Kahawala, and all the others who worked towards building community for women graduate students. It was pleasure to get to know Margot Gill, Garth McCavana, John McNally, and Liz Nunez during many HGWISE efforts. I thank Laura Malisheski and Amy Sanford at the Office of Career Services for providing wonderful advice and support. Members of my mentoring group—Rachelle Gaudet, Elise Novitski, Laura Brittain, Elizabeth Templeton-

Barrett—for being there to talk about science, life, career aspirations, and emotional support. Kathryn Hollar for involving me in such great science outreach activities. Dina Aronzon and Eleanor Millman—you two are among the most courageous people I know.

Finally, my friends, family, and animal companions provide me both exceptional support and joy. I feel so fortunate to have a network of friends who are there when I need them. I thank Elizabeth Youngblood for taking me on adventures and always encouraging me through these past years. I would like to thank my parents Linda Gardner and Jim O'Dell for their love, support, and encouragement and for raising me to be the curious person that I am today. To my sister, Margaret Gardel, you have always been a bedrock of support for me throughout my life. At times, when I've expressed doubt you were there to shove it vigorously out of the way. My wife, Nicole Mushero—you mean the world to me and I love you so much sometimes I can't believe it. It is true what you always told me—if I wasn't here, I wouldn't have met you. Pooka—thank you for your company and soft, furry, chatty self. Jeeves, thank you for teaching me to sit down and enjoy life's simple pleasures—may you always have a lap to sit on.

Overview

The energy for all forms of life comes from the flow of electrons in energetically favorable pairings of oxidation and reduction reactions. While animals and plants typically use complex carbon molecules (e.g. sugar) as electron donors and oxygen as the electron acceptor during respiration, bacteria and other microorganisms have diverse metabolisms. Most microorganisms respire with soluble compounds (e.g. oxygen, nitrate, and sulfate); however, some microorganisms are able to use a conductive mineral (e.g. rust, goethite, magnetite) as either an electron donor or acceptor in a process called extracellular electron transfer (*1*, *2*). Metabolizing insoluble compounds require microorganisms to electrically interact with a stationary material outside the cell. This process differs significantly than using a soluble compound that can enter the cell.

Microorganisms that electrically interact with solids are diverse and inhabit a variety of ecosystems with examples from biogeochemical cycles (e.g. iron, manganese), medicine (e.g. medical implants, tooth decay), and corrosion. Some

microorganisms are known to create conductive contacts with a solid either through electron-carrying cell membrane proteins or cellular appendages (*3*), and elucidating how these biomaterials initiate, maintain, and respond to varying redox potentials would reveal insights into microbial physiology. This would lead to further development of biotechnological applications such as current generation, bioelectronics, chemical production, detoxification of harmful compounds, and biofuels (*4–6*).

This ability of microbes to electrically interact with conductive solids is harnessed in a bioelectrochemical system. While focus on these bioelectrochemical systems has largely been for energy generation, they are a unique experimental design for studying the ability of microorganisms to metabolically use different redox potentials as well as discovering microorganisms capable of electron transfer with a solid. Bioelectrochemical systems are used both to study a single microbial species and microbial communities in environmental samples. Using bioelectrochemical systems to study microbial growth and physiology of microorganisms undergoing extracellular electron transfer processes elucidates microbial interactions with solid-phase electron donors or acceptors and determine how redox potential influences microbial growth. These questions require the versatility of bioelectrochemical systems to enable systematic experiments with the ability to control specific redox potentials and reduce abiotic reactions by using an inert,

conductive electrode. Such studies will help to establish an understanding of how microorganisms electrically interact with solid-phase materials, including how electron transfer initiates and occurs, and will tie in with molecular and cellular microbiology. Moreover, these results will enable the development of biotechnologies which harness microbial metabolisms for electricity, industrial processes, or bioremediation.

Chapter 1

Introduction

1.1 Microbes and microbial metabolism

Microorganisms are single cellular organisms that are distinct from the cells of animals and plants—macroorganisms. Cells of plants and animals are unable to live alone in nature and exist only as parts of multicellular structures, such as the organ systems of animals or the structural components of plants. By contrast, most microorganisms can carry out their life processes of growth, energy generation, and reproduction independently of other cells.

In general, microbial cells are very small, particularly prokaryotic cells that consist of the *Bacteria* and *Archaea*. For example, a rod-shaped prokaryote is typically about 1-5 micrometers (μm) long and about 1 μm wide and thus is invisible to the naked eye. To grasp their size, consider that 500 bacteria each 1

μm long could be placed end-to-end across the period at the end of this sentence (*7*).

Microbes are small, but mighty; they play an important role in the web of life on Earth and are central to the very functioning of the biosphere. Digging up one gram of soil uncovers at least a million microbial cells (*8*). Plants and animals are intimately tied to microbial activities for the recycling of key nutrients and for degrading organic matter. Since microorganisms existed on Earth for billions of years before plants and animals appeared, they have a broad evolutionary diversity as a result. This huge diversity accounts for some of the spectacular properties of microorganisms, such as their diverse physiological capacities that allow them to live in environments unsuitable for animals or plants. In essence, microbes can be viewed as vessels that ferry metabolic machines through environmental perturbations into a wide variety of geological landscapes, harnessing biological energy from oxidation-reduction reactions. Combined, they can be considered Earth's greatest chemists.

The chemistry of life is based on redox reactions, and electron flows are inherent to microbial metabolisms. Microorganisms transfer electrons from an electron donor (lower potential) to an electron acceptor (higher potential). These electron-transfer metabolisms allow microbes to capture, store, and release energy. Substrates that are oxidized (give up electrons) are termed electron donors (i.e. reductants) while substrates that are reduced (gain

electrons) are termed electron acceptors (i.e. oxidants). The electron acceptor can be external, in which case the metabolism is called respiration. If the electron acceptor is internal, the metabolism is called fermentation. Not all electron donors can be fermented, mainly due to thermodynamic constraints.

A convenient way of viewing electron transfer reactions in biological systems and their importance to bioenergetics is to imagine a vertical tower (Table 1.1). The tower represents the range of reduction potentials possible for redox couples in nature, from those with the most negative reduction potentials (E_0') on the top to those with the most positive E_0's at the bottom. The reduced substance in the redox pair at the top of the tower has the greatest tendency to donate electrons, whereas the oxidized substance in the couple at the bottom of the tower has the greatest tendency to accept electrons. It is important to note that not all predicted pathways of possible redox reactions have been found. Microorganisms will, within their capacity, attempt to maximize their energy gain by selecting the electron acceptor with the highest potential available. One of the most exciting traits of bacteria and archaea is their ability to extract energy from sources that are inaccessible to other life forms. For example, animals can only use oxygen as a terminal electron acceptor while different species of microbes can use a variety of electron acceptors besides oxygen, including iron, sulfate, and nitrate.

Table 1.1 The electron tower. Redox couples (oxidized/reduced forms) are arranged from the strongest reductants (negative reduction potential) at the top to the strongest oxidants (positive reduction potentials) at the bottom. As electrons are donated from the top of the tower, then can be "caught" by acceptors at various levels. The farther the electrons fall before they are caught, the greater the difference in reduction potential between electron donor and electron acceptor and the more energy released. (*7, 9*)

Redox Couple (Oxidized/Reduced Form)	**E_0' (mV)**
CO_2/glucose	-430
$2H^+/H_2$	-410
Fd (ox/red), *Clostridium*	-410
CO_2/methanol	-380
NAD^+/NADH	-320
FeS (ox/red), mitochondria	-305
CO_2/acetate	-280
S^0/H_2S	-270
$FAD/FADH_2$	-220
SO_4^{2-}/H_2S	-220
$FMN/FMNH_2$	-190
Pyruvate/lactate	-185
Menaquinone (ox/red)	-74
Cytochrome b_{558} (ox/red)	-75 to -43
$S_4O_6^{2-}/S_2O_3^2$	+20
Fumarate/succinate	+33
Cytochrome b_{556} (ox/red)	+46 to +129
Ubiquinone (ox/red)	+100
Cytochrome b_{562} (ox/red)	+125 to +260
Fe^{3+}/Fe^{2+}(pH 7)	+200
Cytochrome d (ox/red)	+260 to +280
FeS (ox/red), mitochondria	+280
Cytochrome a (ox/red)	+290
Cytochrome c_{555} (ox/red)	+355
Cytochrome a_3 (ox/red)	+385
NO^{3-}/NO^{2-}	+421
$NO^{3-}/\frac{1}{2}N_2$	+740
Fe^{3+}/Fe^{2+} (pH 2)	+771
$\frac{1}{2}O_2/H_2O$	+815

The theoretical energy gain ΔG (kJ/mol) for microorganisms relates directly to the potential difference between the donor and the acceptor, $\Delta E_0'$, with n electrons exchanged in the reaction (F is Faraday's number, 96485 C/mol) (Eq. 1.1). In general, the larger the potential difference between electron donor and acceptor, the more energy gained by the microorganism. Inherent inefficiencies during the metabolic process will decrease this energy gain, but in general this is a useful way of understanding microbial metabolism.

$$\Delta G = -nF\Delta \mathrm{E}_0' \tag{1.1}$$

Not everything can be explained from a thermodynamic perspective. This is because metabolic reactions must not only be thermodynamically favorable, but kinetically favorable as well. Abiotic reactions must proceed slowly enough that microorganisms can take advantage of the reaction while the substrates used must be in a form that is accessible to the microorganisms. Finally, even if a substrate is thermodynamically and kinetically favorable, an organism must possess the machinery required to recognize it.

A minimal constraint for any catabolic (i.e. energy-yielding) pathway is the generation of a proton motive force (Δp) across the cytoplasmic membrane that can be harnessed to energize membrane transporters, drive flagellar rotation, and synthesize adenosine triphosphate (ATP), the energy currency molecule for

biological life. Microbes have diverse ways of doing this, ranging from using coupling sites in the electron transport chain to running the ATP synthase in reverse (*9*).

During metabolism, protons are pumped across the cellular membrane generating an electrochemical gradient of protons across the membrane that can then be used to do useful work when the protons return across the membrane to the lower potential. Bacterial membranes are energized by proton currents. The return of the protons across the membrane is through transmembrane proteins; proton conductors that couple the translocation of protons to do useful cellular work.

The cell membrane is similar to a battery in that it maintains a potential difference between the inside and outside, except that the current that flows is one of protons rather than electrons (Fig. 1.1). The potential difference is maintained by reactions that translocate protons to the outside. These reactions include redox reactions that occur during electron transport and when ATP synthase uses ATP to pump protons outside the cell. The higher proton concentration outside the cell compared to inside the cell creates a concentration gradient. The cell membrane does work when protons enter the cell for activities such as extrusion of sodium ions, solute transport, flagellar rotation, and the synthesis of ATP via the ATP synthase. Note that ATP synthase has these two roles; the primary function of synthesizing ATP and the

reverse reaction of transmembrane proton pumping powered by ATP hydrolysis.

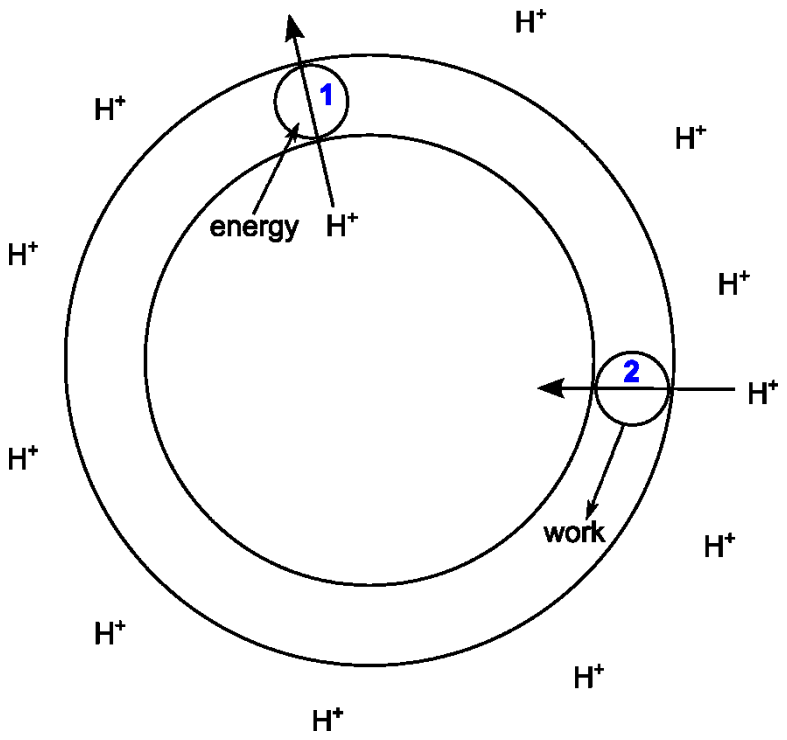

Figure 1.1 The proton current. There is a proton circuit transversing the bacterial cell membrane. Protons translocated to the cell surface, driven there by either chemical or light energy through a proton pump (1) and returned through special proton transporters (2) that do work, including the formation of ATP via ATP synthase. The accumulation of protons on the outside surface of the membrane establishes an electrochemical membrane potential gradient, outside positive or acidic and the interior is alkaline and negative. (*9*, *140*)

The translocation of protons out of the cells is an energy-requiring process (Eq. 1.2). The amount of energy required to translocate y moles of protons out of the cell is $yF\Delta p$ joules. This is the same energy, but opposite sign, when the

protons enter the cell. Therefore, the ΔG of the driving reaction must be equal to or greater than the $yF\Delta p$ joules. The most common classes of driving reactions are oxidation-reduction reactions that occur during respiration and photosynthetic electron transport, and ATP hydrolysis. Energy released from oxidation-reduction reactions can generate a Δp because the redox reactions are coupled to proton translocation.

$$\Delta G = yF\Delta \mathrm{p} \tag{1.2}$$

These two reactions (Eqs. 1.1 and 1.2) are coupled, close to equilibrium, and can proceed in either direction. Therefore, the total force available from the redox reaction is equal to the total force of the proton potential (Eq. 1.3). This relationship between ΔE_0' of an oxidation-reduction reaction during respiration and the Δp that can be generated at a coupling site, and subsequently used to generate ATP, is the central concept in microbial metabolism.

$$\Delta G/F = -n\Delta \mathrm{E_0}' = y\Delta \mathrm{p} \tag{1.3}$$

1.2 Electron transport carriers

Electrons from microbial redox reactions flow spontaneously down an energy gradient through a series of electron carriers. Some of these carry hydrogen as well as electrons, and some carry only electrons. Each of the electron carriers has a different electrode potential, and the electrons are transferred

sequentially to a carrier of a higher potential to the final acceptor, which has the highest potential (Table 1.1). Electron carriers can be divided into two classes: those that are freely diffusible (coenzymes) and those that are firmly attached to enzymes in the cytoplasmic membrane (prosthetic groups).

Common diffusible carriers include the coenzymes nicotinamide-adenine dinucleotide (NAD^+) and NAD-phosphate ($NADP^+$). NAD^+ and $NADP^+$ are electron and hydrogen carriers. Both have a reduction potential at -0.32 V, placing them fairly high on the electron tower, making NADH (or NADPH) a good electron donor. Although they have the same reduction potentials, they generally have different capabilities in the cell. NAD^+/NADH is directly involved in energy-generating (catabolic) reactions, whereas $NADP^+$/NADPH is involved in primarily biosynthetic (anabolic) reactions.

Common membrane-associated electron carriers are:

1. NADH dehydrogenases (hydrogen and electron carriers)
2. Flavoproteins (hydrogen and electron carriers)
3. Quinones (hydrogen and electron carriers)
4. Iron-sulfur proteins (electron carriers)
5. Cytochromes (electron carriers)

The quinones are lipids, whereas the other electron carriers are proteins, which exist in multiprotein enzyme complexes called oxidoreductases. The electrons

are not carried in the protein, but in a nonprotein molecule bound to the protein called a prosthetic group.

1.2.1 NADH dehydrogenases

NADH dehydrogenases are proteins bound to the inside of the surface of the cytoplasmic membrane. They have an active site that binds NADH and accepts $2e^-$ and $2H^+$ when NADH is converted to NAD^+. The electrons and hydrogen ions are passed onto flavoproteins.

1.2.2 Flavoproteins

The prosthetic group in flavoproteins (Fp) is a flavin, which can be either flavin adenine dinucleotide (FAD) or flavin mononucleotide (FMN). The flavins FAD and FMN are synthesized by cells from the vitamin riboflavin (vitamin B_2). When flavins are reduced they carry two electrons and two protons. There are many different flavoproteins, and they catalyze diverse oxidation-reduction reactions in the cytoplasm, not merely those of the electron transport chain in the membranes. Although all the flavoproteins have FAD or FMN as their prosthetic group, they catalyze different oxidations and have different redox potentials. These differences are due to the protein component of the enzyme, not the flavin itself.

1.2.3 Quinones

The quinones are lipids which can carry both hydrogen and electrons. Some are believed to be highly mobile in the lipid phase of the membrane, carrying hydrogen and electrons to and from the complexes of protein electron carriers that are not mobile, such as from ATP synthase to cytochromes. Bacteria make two types of quinone that function during respiration: ubiquinone (UQ), a quinone also found in mitochondira, and menaquinone (MQ). Menaquinones have a much lower electrode potential than ubiquinones and are predominantly used during anaerobic respiration, where the electron acceptor has a low potential. A third type of quinone, plastoquinone, occurs in chloroplasts and cyanobacteria, and functions in photosynthetic electron transport.

1.2.4 Iron-Sulfur proteins

The prosthetic group in iron-sulfur proteins (FeS) is a cluster of iron and sulfur atoms commonly in arrangements of Fe_2S_2 and Fe_4S_4. Enzyme complexes can contain multiple FeS clusters, for example, in mitochondria the complex that oxidizes NADH has at least four. The FeS clusters have different E_0' values, and the electron travels from one FeS cluster to the next toward the higher E_0'. The electron may not be localized on any particular iron atom, and the entire FeS cluster should be thought of as carrying one electron, regardless

of the number of Fe atoms. The iron-sulfur proteins cover a very wide range of potentials, from approximately -400 mV to +350 mV. They therefore can carry out oxidation-reduction reactions at both the low-potential end and the high-potential end of the electron transport chain, and indeed are found in several locations. Ferredoxin (Fd) is a common iron-sulfur protein in biological systems and has a Fe_2S_2 configuration.

1.2.5 Cytochromes

The prosthetic group in cytochromes is a heme. Hemes are placed in different classes (a, b, c, and d) and in the center of each heme there is an iron atom. The iron is the electron carrier and is oxidized to ferric or reduced to ferrous ion during electron transport. Cytochromes are therefore one electron carriers. Cytochromes can act as capacitors to store electrons in the periplasm and outer membrane when external electron acceptors are not immediately available (*10*). The E_0' values of the different cytochromes vary depending on the protein and the molecular interactions with surrounding molecules. Occasionally, cytochromes form tight complexes with other cytochromes or with iron-sulfur proteins.

1.3 Extracellular electron transfer

Often soluble electron acceptors are depleted in the microbial environment. Microorganisms can then turn to fermentation or use non-soluble electron acceptors. In the latter case, microorganisms have to transport the electrons outside the cell to a solid oxidant to achieve reduction. This process is called extracellular electron transfer (EET). Similarly to electron acceptors, soluble electron donors may become depleted, in which case microorganisms can oxidize insoluble electron donors via EET. Thus, EET relates to electron transport both in and out of the cell when a redox active or conductive solid is used either for an electron donor or acceptor during microbial metabolism. Microbial EET is ubiquitous in nature, and previous research has been mainly on minerals containing iron and manganese oxides being reduced. Conductive solids, such as electrodes used in bioelectrochemical systems discussed throughout the rest of this thesis, can also function as electron acceptors or donors for microbial EET.

Iron and manganese may represent the primary electron acceptors for organic matter oxidation in sedimentary environments where they are enriched. In marine sediments, iron and manganese reduction would likely be important in the zone between the region of oxygen removal and the region of sulfate reduction. In freshwater sediments, metal reduction would occur

between the regions of oxygen depletion and carbon dioxide reduction (methanogenesis) (*11*). Upon isolating Fe(III)- and Mn(IV)-reducing microorganisms, additional studies have shown that these microbes can completely oxidize organic compounds with Fe(III) or Mn(IV) as the sole electron acceptor and that oxidation of organic matter coupled to dissimilatory Fe(III) or Mn(IV) reduction can yield energy for microbial growth (*11*, *12*). *Shewanella oneidensis* MR-1 and *Geobacter sulferreducens* are two well-studied metal-reducing bacteria (*11*, *12*).

Several mechanisms have been described for EET in the past years. They can be placed in two categories: direct and indirect EET. Many studies indicate that based on their innate capabilities microorganisms use multiple strategies simultaneously, maximizing the use of available resources.

1.3.1 Direct EET

In general, direct EET is defined as a process not requiring diffusion of a mobile component to and from the cell for electron transport. This includes mechanisms that require physical connections between bacteria and the redox active surface. Direct transfer typically involves at least a series of periplasmic and outermembrane complexes. These are usually produced by the bacteria and include membrane bound or associated enzyme complexes and exocellular

appendages, such as conductive pili or pilus-like structures (Fig. 1.2). Two microorganisms that have been widely studied are *Shewanella oneidensis* MR-1 and *Geobacter sulferreducens*, both metal-reducing bacteria (*11*, *13*).

For *S. oneidensis*, the apparent terminal cell-bound complex is MtrC, a decaheme cytochrome located on the outside of the membrane and capable of donating electrons in a broad potential range. Electrons are transported from the periplasm to MtrC through a transmembrane electron transfer module consisting of MtrA, the transporting protein, incorporated inside MtrB, a sheath protein (*14*). Electron transfer through the *S. oneidensis* outer membrane occurs through the MtrAB complex. Similar complexes seem to be ubiquitous in other species.

For *G. sulfurreducens*, a similar dependency on membrane-bound cytochromes has been well documented (*15*). In recent years, the involvement of pili or pilus-like appendages (called nanowires in this context) was established (*16*). These seem to be essential for high levels of current production in *G. sulfurreducens*, in conjunction with OmcZ, a matrix-located cytochrome (*17*). It is possible that nanowires also establish electron transport between different microorganisms in a community.

1.3.2 Indirect EET

Indirect EET involves the production and/or use of electron shuttles, which transport the electrons between the microbe and the insoluble electron donor/acceptor (Fig. 1.2). These soluble shuttles can be either organic or inorganic. The soluble compound is reduced or oxidized at the cell and subsequently diffuses towards the insoluble electron acceptor/donor. These shuttle molecules are soluble, yet are reduced or oxidized outside the cell because they are too large to enter the cell, as is probably the case for humic substances (*10*).

Examples of electron shuttles produced as secondary metabolites by organisms include phenazines and flavins. *S. oneidensis* MR1 was found to excrete flavins, a quinone-like molecule, that serves as an electron shuttle (*18*). A phenazine derivative has been shown to function as a key membrane bound electron shuttle during methanogenesis (*19*). While humic substances are electron shuttles not produced by the cell, they are present in many sediment environments. Previous studies show that inorganic shuttles, such as neutral red, can be used as a true driver for microbial conversions and the generation of a proton motive force (*20*).

Indirect extracellular electron transfer is most likely to take place in an environment where a terminal oxidant is not easily accessible, due to poor

solubility and/or diffusion limitations, and where excreted shuttles can be recycled. A biofilm community on an iron mineral surface is a good example of such an environment because there is a high cell density that would allow the build-up of the shuttle (*2*).

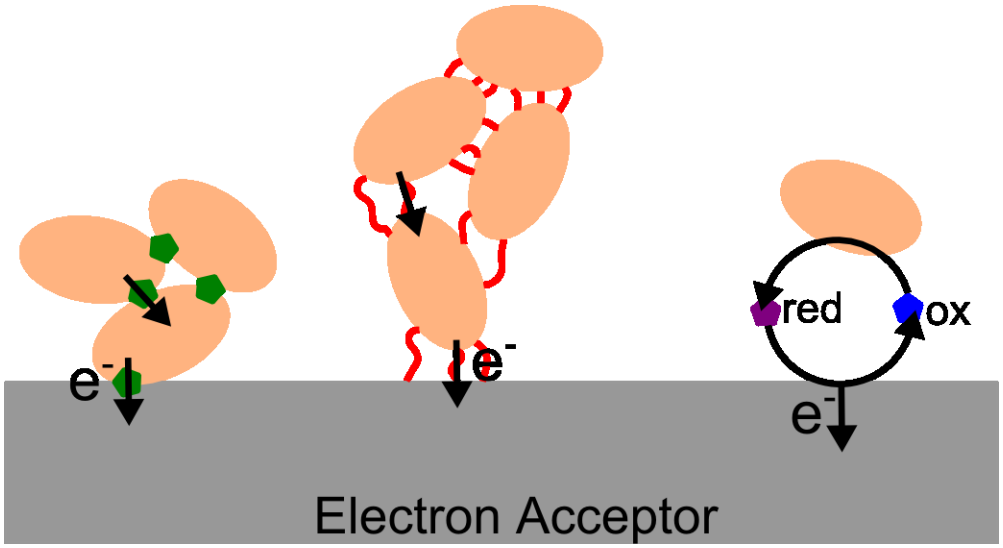

Figure 1.2. Modes of extracellular electron transfer. Direct EET occurs through conductive **membrane proteins** (i.e. cytochromes) or **cellular appendages** (i.e. pili). Indirect EET occurs via soluble **redox active molecules** either biologically produced or already present in the environment. The direction of electron transfer presented in this figure is where the solid-phase material (either metal or electrode) is an electron acceptor. Depending on the microorganism, the reverse pathway can also occur and then the solid would be an electron donor.

1.4 Bioelectrochemical systems

In 1910, M. C. Potter wrote that "The disintegration of organic compounds by microorganisms is accompanied by the liberation of electrical energy"(*21*). This

finding, made using *Saccharomyces cerevisiae*, was perhaps the first observation of microbial EET using a bioelectrochemical system (*21*).

Bioelectrochemical systems (BESs) harness the ability of microbes to transfer electrons to and from insoluble materials by allowing the microbe to interact with a conductive electrode instead of a redox active mineral. The electrode acts as either an electron donor or acceptor depending on the experimental conditions, which include electrode potential and species or community of microbes present. BESs differ in design, but the underlining principle is an electron transfer between microbial activity and electrical current.

The general design of a BES is a three-electrode setup consisting of a working, counter, and reference electrodes (Fig. 1.3). The working and counter electrodes are electrically connected through a potentiostat or resistor to allow current to flow. When using a potentiostat, the potential of the working electrode is held at a specific potential versus the reference electrode. The working electrode is generally where the microorganisms are present and it behaves as either an anode or cathode depending on the potential difference across the two electrodes. When the microbes are donating electrons to the electrode and producing electricity, the BES is called a microbial fuel cell (MFC). If the microbes are instead accepting electrons from the electrode and consuming electrical current, the BES is typically called a microbial electrolysis

cell (MEC). These systems can be setup both in the lab and in environment to study isolated microbial species or microbial communities.

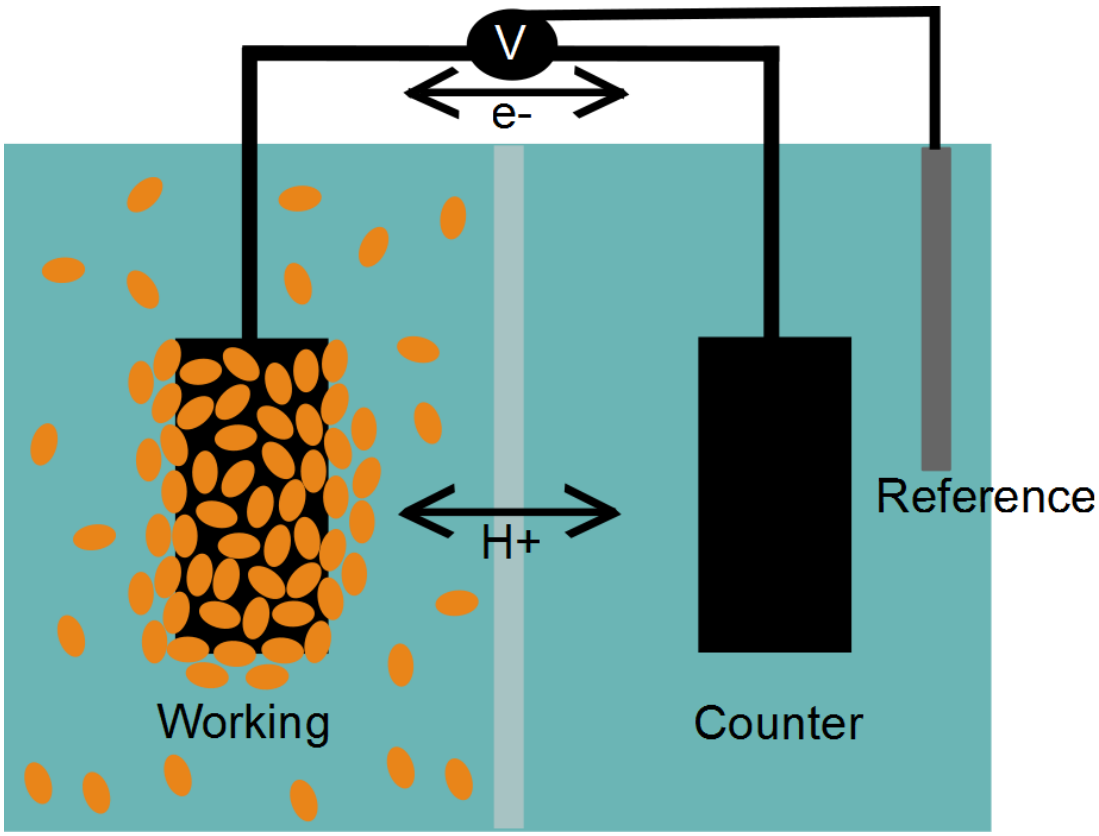

Figure 1.3 General bioelectrochemical system (BES) design. A BES consists of at least working and counter electrodes and, in most cases, a reference electrode. The working electrode can act as either an anode or cathode depending on the direction of electron flow towards or away from the counter electrode. This allows microorganisms to either use the working electrode as an electron donor or acceptor as part of their metabolism.

BESs are powerful tools for studying microorganisms that use solid minerals during respiration because one of the half reactions in the overall metabolic redox reaction can be controlled by varying the working electrode potential,

instead of relying on the inherent redox potentials of metabolic compounds. The majority of microbial physiology research depends on demonstrating a microorganism's ability to use specific electron donors and acceptors for growth, which can prove to be a difficult endeavor because experimental design may change based on the compounds tested. Additionally, it can be difficult to uncouple biotic and abiotic changes because the products of microbial metabolism are identical or similar to those of a chemical reaction of the mineral. These problems are resolvable with bioelectrochemical systems, which use an inert electrode, typically graphite based, to mimic conductive minerals (6). While focus on these systems has largely been for energy generation, they are a unique experimental design for studying the ability of microorganisms to metabolically use different redox potentials, as well as discovering microorganisms capable of extracellular electron transfer. The inert electrode removes abiotic reactions from the mineral, allowing only microbial processes to be studied. The potentiostat allows a range of redox potentials to be explored with a single experimental setup, simplifying and broadening the different types of experimental questions that can be addressed. At the same time, current is either generated or consumed by microorganisms and can be measured as a proxy for microbial activity.

1.4.1 Biotechnology applications

Microbial EET has the potential to be used in many biotechnological applications such as current generation, bioelectronics, chemical production, and detoxification of harmful compounds (4–6). Combining the enzymatic versatility of microorganisms with the robustness of electrochemical cells, BESs have the potential to become a key technology in the bioenergy industry. As a result, there is significant interest in learning more about overall microbial EET processes in order to both understand the role of these microorganisms in nature and to benefit microbial based technologies.

The practical use of electricity from environmental BESs is useful in remote locations with long-term usage. Low power sensor and monitoring systems are widely used in both science and industry to increase data collection or monitor materials and infrastructure. Examples of parameters that are of interest to both science and industry include temperature, salinity, water level, irradiance, pressure, pH, fluid flow including tidal patterns, migration patterns of fish and other animals, pollution monitoring, and seismic activity. Long-term monitoring requires instrumentation that is powered to collect, store, and transmit data. Solar systems are of limited long-term use above certain latitudes, and batteries, while improving in energy density and duration, are typically unable to provide power for any deployment longer than two or three

years (depending on the sensor system). With respect to oceanographic applications, batteries can typically power a sensor for about one year. For logistical and financial reasons, this limits the ability of the end user to deploy extensive sensor systems in nature. The practical use of electricity from environmental BESs requires power management systems that have the following three requirements: 1) current is produced at a low voltage and must be converted to higher voltages to satisfy sensor requirements, 2) modest and steady power production requires storage to satisfy variable load cycles, and 3) cell voltage should be regulated to operate at the most efficient and maximum sustainable level. In general, the low voltages generated by most environmental BESs limits the use of commercial electronics for power management and there is interest in increasing the voltages produced by these systems.

Microbial electrosynthesis is defined as supplying electrons to microorganisms at a cathode to permit them to catalyze useful processes (*5*). This offers the possibility of converting renewable but intermittent forms of energy, such as solar and wind, into liquid transportation fuels or desirable chemicals much more efficiently and with less potential environmental degradation than biomass-based strategies (*5*). Especially if using an alternative energy source as the electron source, it could be a way for storing energy as a biofuel. Microorganisms have been shown to decrease the

overpotentials at both anodes and cathodes, resulting in improved performance of a desired electrosynthetic reaction (*5*). Microbial electrosynthesis also does not require arable land, the large quantities of water required for growing biomass and then processing biomass to fuel, and can avoid the environmental degradation associated with large-scale biomass production (*22*). It would be conceivable to use microbial electrosynthesis as a carbon sequestration process, producing organic compounds that are resistant to degradation for long-term carbon removal (*22*).

Chapter 2

Duty Cycling an Environmental Microbial Fuel Cell

2.1 Introduction

Microbial fuel cells (MFCs) harness the catabolic activity of microorganisms to convert chemical energy into electrical energy (*23*, *24*). Electroactive microorganisms facilitate the exchange of electrons to and from solid-phase electron acceptors or donors through diverse physiological mechanisms that are broadly referred to as extracellular electron transfer (EET) (*2*, *17*, *18*, *24–28*). MFCs operated in nature, or in comparable, industrial conditions such as sewage treatment plants, are referred to herein as environmental microbial fuel cells (eMFCs), and typically host a diversity of microbes on the anode that may be directly or indirectly involved in EET (*6*, *24*, *29*).

MFCs have been the subject of much research in the last decade (*4*, *30*, *31*), largely driven by the possibility to produce substantial amounts of carbon-neutral energy from organic matter, including wastewater, as well as the promise of catalyzing the efficiency of industrial processes that rely on microbial catabolism (*32–36*). There have been a number of suitable implementations of eMFCs for small-scale power generation, such as unattended power supplies for distributed sensors (*20*, *21*), though power from eMFCs is often below the amount required for most conventional external devices. For example, numerous eMFC studies report power densities ranging from 20-1500 $mW \cdot m^{-2}$ normalized to anode area (*39–44*), with systems using pure chemicals producing more power in general (*29*). Moreover, additional losses are often incurred when scaling up MFCs, which result from design and technological constraints (*45–47*). Several researchers have aimed at developing scalable designs (*45*, *48*), but so far no study has demonstrated that the respective designs can indeed be operated satisfactorily beyond the liter-scale. Additionally, many of the problems that can occur in laboratory-scale systems occur in these scale-up designs, including leakages, clogging of electrodes, membrane damage and short circuits, all of which call for flexible designs. Technological constraints that might not be important on the lab scale can gain importance at large scale, such as the effects of increased current, the membrane choice, and hydrodynamics (*49*). Scaling up without paying

attention to these factors will inevitably lead to further reductions in efficiency and additional energy losses. The design of an implemented bioelectrochemical system should consider and accommodate these different physical and chemical factors.

To increase the efficacy of MFCs, in particular eMFCs, in power production, recent studies have endeavored to increase power through the use of particular microbial phylotypes (*50–53*), varying electron donors (*54–56*), electrode materials (*57*, *58*), the addition of electrochemically active compounds (*26*, *27*, *59*, *60*) to facilitate electron transfer between the microbes and the electrode, and optimizing system function and architecture, through various buffers (*44*, *61*) and use of selective membranes (*62*).

While the influence of design factors on MFC performance has been extensively studied, the extent to which duty cycling affects MFC performance has only been of recent interest and is further addressed in this study. Recent duty cycling experiments performed by connecting and disconnecting to an external resistor in an MFC concluded that shorter cycles lead to optimal power production which resolved the mismatch between the internal resistance of the MFC and external resistance of what the MFC was powering (*63*). Previously, a capacitor has been used in the external circuit to accumulate charge and release bursts of current discharged either through an external resistor (*64*) or channeled back to the anode as in a microbial electrolysis cell (*65*). In these

studies, the circuit design resulted in a variable anode potential that can influence microbial colonization and activity (*66*, *67*).

Importantly, there is interest in on how to best capture charge at the highest practical potential since this is where voltage converters are most efficient. A recent study developed a power management system that enabled sufficient power to be harnessed from a eMFC with a voltage comparator and DC-DC converter to boost the voltage to 3.3 V, which is sufficient to power most solid-state devices (*68*). This and equivalent systems exhibit efficiencies up to 80% when the voltage potential is greater than approximately 0.6V, and exhibit much lower efficiencies – approximately 10% – when voltage potentials are less than 0.4V.

Fundamental to all MFCs are the limitations imposed by the diffusion of substrates and products into and out of microbial cells and, in some cases, into and out of the microbial biofilm. Recent laboratory studies using pure or defined cultures reveal that substrate diffusion in the biofilm (*69*) and proton diffusion away from the anode (*61*) limit current generation. These studies highlight important factors that influence the electrode reaction kinetics associated with MFC performance: donor-substrate availability and utilization, electron transfer to the anode, and proton diffusion away from the anode.

It is equally important to consider how these and other factor(s) might govern power production in eMFCs. For example, the extent to which the surrounding

geochemical environment or microbial community composition influences bulk transport, alleviates diffusion limitation and, ultimately, affects power production is unknown. To this end, I conducted a series of experiments in which I operated a multiple anode eMFC (specifically a chambered MFC placed atop marine sediments) to interrogate how three key factors –substrate and endproduct diffusion into and out of the biofilm, microbial community composition, and geochemical conditions –, influence power production. Through cycling continuity between anode and cathode at varying frequencies, geochemical analyses and molecular microbial phylogenetic analyses, I characterized the relationship between current production and cycling frequency, seawater geochemical composition and pH, biofilm thickness, and microbial community composition. The potential was held constant with a programmable load during these experiments, to eliminate variable potential as a confounding factor. These data suggest that replenishment of depleted chemical species within the biofilm and surrounding diffusion layer, on the time scale of ~5-10 seconds, is what likely governs maximum charge transfer in these eMFCs. It is also worth noting that duty cycling had no discernible effect on microbial community composition, suggesting that gross community composition is unaltered by duty cycling in these experiments. In brief, these data collectively underscore the importance of considering a variety of

operational, geochemical and microbial factors when characterizing or optimizing MFC performance.

2.2 Experimental design and methods

2.2.1 System and operating conditions

A multi-anode chambered benthic MFC (Fig. 2.1) was built in an aquarium (40 cm depth x 60 cm length x 30 cm height), filled with salt marsh sediment recovered from Winthrop Harbor, MA to a height of approximately 24 cm. The remainder of the tank was filled with natural aerated seawater. The multi-anode MFC consisted of 15 graphite anodes, housed in sets of three, in five independent semi-enclosed acrylic chambers. Anodes were fabricated from cylindrical graphite rods (1.25 cm diameter x 1.25 cm height). Each chamber was 7 cm in diameter and 15 cm in height, and were pushed approximately 10 cm into the sediment. The top of each chamber was fitted with a gastight septum to enable fluid sampling. All the anodes were connected to a programmable relay board (model 34903A; Agilent Inc.) that enabled the independent connection of each anode to a custom-built programmable load (North-West Metasystems, Inc.) (*43*). The circuit effectively adjusts the external resistance to maintain a user defined whole-cell potential (in our case 0.5 V), so long as actual whole-cell potential is not below the user-defined

setpoint. To eliminate variations in cathode performance, a single 1 m long graphite brush was used as the cathode for all experiments. The cathode was placed in the overlying, air-sparged seawater (S = 30 ppt, T = 10 °C) overlying the sediment in the aquarium. My measurements of constant cathode potential during all duty-cycling treatments indicate that this system was not cathode-limiting. An Ag/AgCl electrode (MI-402; Microelectrodes, Inc.) was used as a reference electrode in the overlying water. Electrode potentials and current were measured using a digital multimeter (34970A; Agilent Inc.) with 6½ digits of resolution, 0.004% direct current (DC) voltage, and isolated from the earth-referenced circuitry and computer interface. A 20-channel multiplexer and 2 current channels module (34901A; Agilent Inc.) with a 60 channel • s^{-1} scan speed and 120 channel • s^{-1} open/close speed was used to input electrode potential and current for measurement.

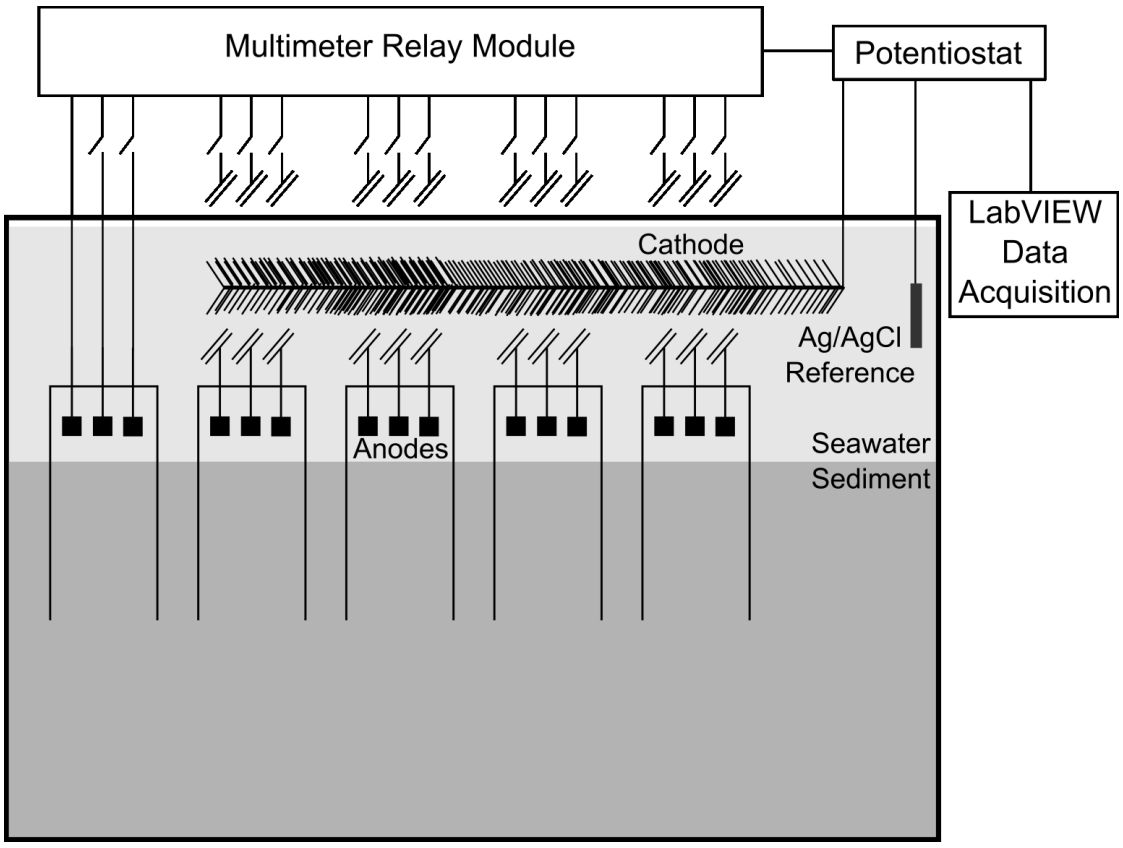

Figure 2.1. Experimental setup showing the five chambers, each containing three anodes (to minimize complexity, only one of the chambers is shown as being connected to the relay module). The relay module included the capacity to connect or disconnect each anode independently, allowing cycling of individual anodes and/or among multiple anodes. A large, graphite brush electrode was placed in the overlaying, aerated seawater and was used as the cathode for all experiments.

The multimeter and relay bank were controlled through a custom-designed LabVIEW interface with the capability to execute a number of different experiments; 1) cycling among all 15 anodes with a set switching interval (1.5 s data acquisition), 2) cycling a single anode through variable ON and OFF times (600 ms data acquisition), and 3) maintenance of the anodes at a constant state

(i.e. always ON or always OFF). Cycling among all 15 anodes sequentially allowed current to be drawn from one anode at a time, and single experiments were conducted at different anode switching intervals (3s, 7.5s, 15s, 30s, 60s). The "ON" time was the switching interval, i, and the "OFF" time was the total amount of time it took to cycle back to the same anode, $(n-1)\times i$ for the general case of n anodes and $14\times i$ for my case of 15 anodes. Later, a single electrode was used for select duty cycling experiments (where each condition was performed once), wherein each set of cycling conditions was followed by a period at open circuit until anode potential was within 1.5% of the original open circuit value (to remove any experimental carryover effects). Using a single anode in this manner enabled the ON and OFF times to be investigated independently to measure total cumulative current passed by the anode. Selection of the cycling conditions, the ON and OFF times, between consecutive experiments was varied to reduce any bias in the system. In these experiments, the total sum of ON times was normalized to one hour in order to compare how the OFF time interval influenced total cumulative charge. Maintaining constant continuity with a steady whole cell potential was used to study pH changes within the pore water inside the core tube.

2.2.2 pH measurements

pH was monitored inside one chamber for nine consecutive days, during which the three electrodes in the chamber were kept in the ON state. Fluid samples (2 mL) were collected from within the chamber through the septa in the lid at regular intervals, decanted into a 2 mL centrifuge tube immersed in a 10˚C cold bath, and measured with a needle pH electrode (MI-407; Microelectrodes, Inc.) with an Ag/AgCl electrode (MI-402; Microelectrodes, Inc.) as reference using an pH meter (AR20 Accumet; Fisher Scientific). All pH samples and measurements were conducted in duplicate.

2.2.3 Dissolved sulfide measurements

Anode chamber fluid was collected through the septa, and dissolved sulfide was measured with a spectrophotometric sulfide kit scaled down to handle sample volumes of 1 mL (LaMotte, Inc.). Absorbance was measured with spectrophotometer (DU-650; Beckman-Coulter) and was compared to a standard curve of known concentration sodium sulfide samples prepared anaerobically. Both chamber fluid and a 10x dilution with MilliQ water were measured for an accurate reading on the standardization curve.

2.2.4 Anode biofilm diversity characterization

Microbial diversity was assessed by examining the community diversity of the electrogenic biofilm growing on four representative anodes maintained at four different duty cycles: a) always ON, b) 1.8 s ON and 0.6 s OFF, c) 1.8 s ON 41.4 s OFF, and d) always OFF. After operating at these conditions for four months, electrodes were removed from the system and scraped with a sterile razor blade. Shavings were scraped into sterile cryovials. In addition, sediments underlying the electrodes were sampled using syringes with the tips removed, and biofilm from inside each chamber were sampled using sterile wipes (Kimberley Clark, Inc.). All samples were flash frozen in liquid nitrogen and then kept at -80 ˚C until further processing.

DNA was extracted using a PowerSoil® DNA Isolation Kit (Mo-Bio, Inc.) following the manufacturers' protocol, with an additional cell lysis protocol consisting of heating to 85 °C and bead beating (FastPrep-24, MP Bio, Inc.) for 60 s at 6.5 m/s after the initial extraction. DNA extractions were quantified using a fluorometric assay (Qubit; Invitrogen, Inc.), and ranged from 25-300 ng of DNA • cm^{-2} of electrode, with the anode in the always OFF state having the least concentration.

16S rRNA genes were amplified by PCR with 28F and 519R primers (Table 2.1) and amplicons were sequenced via 454 Titanium pyrosequencing (*70*).

Sequence sff files were analyzed with Qiime version 1.3.0 (*71*), OTUs were picked with the optimal flag passed in UCLUST with a 0.97 similarity threshold and a representative set was selected based on the most abundant sequence and aligned with PyNAST using the UCLUST pairwise alignment method with a 0.75 minimum percent sequence identity to closest BLAST hit to include sequence in alignment. ChimeraSlayer was used to identify chimeric sequences before the OTUs were assigned taxonomy with the RDP database at a minimum confidence level of 80%.

Sequence sff files are available through the National Center for Biotechnology Information Sequence Read Archive (NCBI SRA) database under submission identification SRA049469.

Table 2.1. Primers used for bacterial and archaeal PCR.

Primer name	Sequence	Primer target	Reference
28F	5′-GAGTTTGATYMTGGCTC	Bacteria	(*72*)
519R	5’-GTATTACCGCGGCTGGCTG	Bacteria	(*72*)
21F	5′-TTCCGGTTGATCCYGCCGGA	Archaea	(*73*)
958R	5′-YCCGGCGTTGAMTCCAATT	Archaea	(*73*)
337F	5’-AGGTCCTACGGGACGCAT-3’	ANME-1a	(*74*)
724R	5’-GGTCAGACGCCTTCGCT-3’	ANME-1a	(*74*)
468F	5’-CGCACAAGATAGCAAGGG-3’	ANME-2c	(*75*)
736R	5’-CGTCAGACCCGTTCTGGTA-3’	ANME-2c	(*75*)

PCR for Archaeal and ANME DNA

To detect the presence of archaea and anaerobic methane oxidizers (ANME) on the electrode surface, extracted DNA (described above) was amplified using

16S rRNA general archaeal primers (21F and 958R), ANME-1a (337F and 724R), and ANME-2c (468F and 736R) targeted primers. Each 25 µl reaction mixture contained 12.5 µl of FailSafe™ PCR premix D, 0.25 µl of FailSafe™ enzyme mix (Epicentre Biotechnologies, Madision, WI, U.S.A.), 1 µl of each reverse and forward primers (25 µM in 10mM TRIS) for a given target, and 2 µl of DNA template (~0.3 µg/mL). Positive controls are from clone libraries already known to contain ANME DNA. Negative controls substituted PCR quality water in replacement of DNA for the template. PCR amplifications were carried out at the following touchdown program: 58°C for 45s, 72°C for 105s, 94°C for 60s, 56°C for 45s, 72°C for 105s, 94°C for 60s, 54°C for 45s, 72°C for 105s, followed by 35 cycles of 94°C for 60s, 52°C for 45s, 72°C for 105s, followed by 72°C for 5 minutes. The amplified DNA from each PCR was stained by adding 5 µl of 10X BlueJuice™ Gel Loading Buffer (Life Technologies) to each 25 µl reaction volume and loaded in a agarose gel (1% in TAE electrophoresis buffer) containing SYBR® Safe DNA Gel Stain (1 µl/10 mL). A 1 kb ladder (New England Biolabs, Inc.) and the different PCR products were loaded in the agarose gel and DNA was separated based on size via electrophoresis (60 V for 20-30 minutes). The gel was imaged under a UV lamp with camera (Stratagene Transilluminator 2020E).

2.2.5 Microscopy

Scanning Electron Microscopy (SEM) Sample Preparation and Imaging

Anode subsamples for SEM imaging were collected at the same time as those for DNA extraction. A section of the anode was removed using a sterile cutter and immediately placed in 2 mL of sterile 5% glutaraldehyde in phosphate buffered saline (PBS), in a sterile 2 mL centrifuge tube and held at 4 °C for 24 hours. The samples were subject to ethanol dehydration by placing the sample in 10%, 25%, 50%, 75%, 100% ethanol (200 proof) PBS solutions for five minutes each. The 100% ethanol solution was changed three times and the sample was left in ethanol for critical point drying (Autosamdri 815 A; Tousimis, Inc.) with a 15 minute purge time. The samples were adhered to SEM posts with carbon tape and coated with platinum/palladium (208HR Sputter Coater) at 40 mA current for 100 seconds and then imaged with a SEM at 10kV (JEOL, Inc.).

Confocal Microscopy Sample Preparation, Imaging, and Analysis

Anode sections were sampled as above, and placed into a sterile 4% paraformaldehyde in PBS solution in a 2 mL centrifuge tube and refrigerated at 4 °C for 12 hours. Samples were placed in 100% PBS and kept at 4 °C. Prior to imaging, each sample was placed with sterile tweezers in 500 μL of PBS and

0.15 µl of SYBR® Green I (Invitrogen), wrapped in foil and kept at room temperature for at least 15 minutes. Samples were then placed in a PBS-filled glass-bottom dish (MatTek Corp.), with the side to be imaged against the coverslip, and imaged with a Zeiss 700 inverted confocal microscope using the 488 nm laser and Zeiss filter set 38. For calculating biofilm thickness measurements, confocal stacks were imaged at 20x, 40x, 63x magnifications with typical *z* distances between each slice being 1.7, 0.4, 0.3, respectively. Different magnifications were used to reduce any bias due to slice thicknesses. In total, eight confocal stacks were acquired for an Always ON, Short OFF, and Long OFF samples. Due to the inherent heterogeneity of both the graphite surface and the biofilm thickness, each image was analyzed with an ImageJ program that subdivided each stack into a 10 by 10 grid and calculated the local biofilm thickness based on signal intensity for each sub region. The average biofilm thickness is from the values for sub regions among all images for a given sample.

Fluorescence In Situ Hybridization (FISH) Microscopy

Anode sections were sampled as above, and placed into a sterile 4% paraformaldehyde in PBS solution in a 2 mL centrifuge tube and refrigerated at 4 °C for 12 hours. Samples were placed in 100% PBS and kept at 4 °C. Standard protocols were used to prepare the hybridization and washing buffers

(*76*) and are outlined in Appendix A. General archaeal (ARCH195, 5'- GTG CTC CCC CGC CAA TTC CT -3'), bacterial (EUB338, 5'- GCT GCC TCC CGT AGG AGT -3'), and control (NON338, Cy3, 5'- ACT CCT ACG GAG GCA GC -3') probes were used at a working concentration of 5 ng/µl. Hybridization buffer (Table A.1) contained 20% of formamide and washing buffer (Table A.2) had a final concentration of 0.225M NaCl. Washed anode sections were stained with a dilute 4'6'-dia- midino-2-phenylindole (DAPI) solution (5 µg/ml) for 10 minutes in the dark. Samples were kept in the dark at -20°C prior to microscopy (at least overnight). Samples were then placed in a PBS-filled glass-bottom dish (MatTek Corp.), with the side to be imaged against the coverslip, and imaged with a Zeiss 700 inverted confocal microscope with the following imaging lasers and Zeiss filters: 555 nm and 488 nm, SP490; 405 nm, SP555. This procedure and FISH probes were tested on *Escherichia coli* and *Methanosarcina acetivorans* cells fixed with 4% paraformaldehyde and prepared on microscope slides with agarose film (described in section II of Appendix A).

2.3 Results and discussion

2.3.1 Mass transfer in MFCs

In a MFC, the magnitude of the steady-state current is usually limited by one reaction, typically called the rate-determining step. The more facile reactions

are held back from their maximum rates by the slowness with which the rate-determining step disposes of their products or creates their reactants. The electron exchange reaction at the electrodes can be represented by a resistance term (R) composed of a series of resistances: mass transfer between the bulk solution and near the electrode surface, chemical reactions that occur within this region close to the electrode, and surface reactions including adsorption, or desorption, and electron transfer at the electrode (Eq. 2.1). A fast reaction step is characterized by a small resistance, while a slow step is represented by a high resistance.

$$R = R_{mass-transfer} + R_{\substack{chemical \\ reactions}} + R_{\substack{surface \\ reactions}} + R_{electron-transfer} \tag{2.1}$$

Generally, eMFC systems that are operated continuously become mass-transfer limited through depletion of soluble electron donors, such as acetate, used by the microorganisms. Previous studies have shown that the power density of an eMFC is increased four-fold by mixing the fluids in the anode chamber (*39*). Similarly, the mass-transfer resistance can be reduced by disconnecting the anode to enable substrate depletion to dissipate through diffusion. Cycling a series of anodes then is expected to lower the overall electrode reaction resistance and increase the current produced, when compared to a single anode under constant load.

2.3.2 Effect of anode switching on cumulative charge

In these experiments, seven different anode cycling intervals were tested, in which the "ON" period is defined as the length of time that a single anode was connected to a cathode. Using a metric of cumulative charge per day, we observed an optimal cycling interval of 15 seconds ON per anode (Fig. 2.2), which yielded 17 coulombs per day. This optimal cycling interval is, to a degree, a function of the number of anodes in this system, which in this case determined the extent of OFF time. Notably, the shorter time intervals of 3 and 7.5 seconds yielded less charge than the optimal 15 seconds, most likely due to a shortened OFF time, implying that there is a benefit to allowing the anodes to reside at open circuit. In addition to the OFF time interval dependence, the number of ON/OFF cycles varies with switching interval. Single anode experiments were conducted to remove the interdependence of the ON and OFF times in the 15 anode experiments. With a single anode, different combinations of ON and OFF times were selected and duty cycling continued until the total amount of ON time equaled one hour. These single-anode experiments demonstrate that select ratios of ON/OFF times yielded greater total charge normalized to one hour of total ON time (Fig. 2.3).

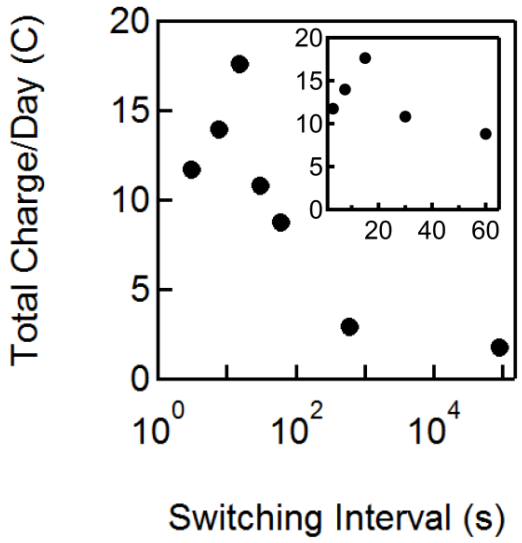

Figure 2.2. The total charge cumulated over a 24 hour period from sequentially switching among 15 anodes at a specified interval (a single anode is always connected to the cathode). The inset presents the same data plotted on a linear x-axis to resolve the shorter switching intervals.

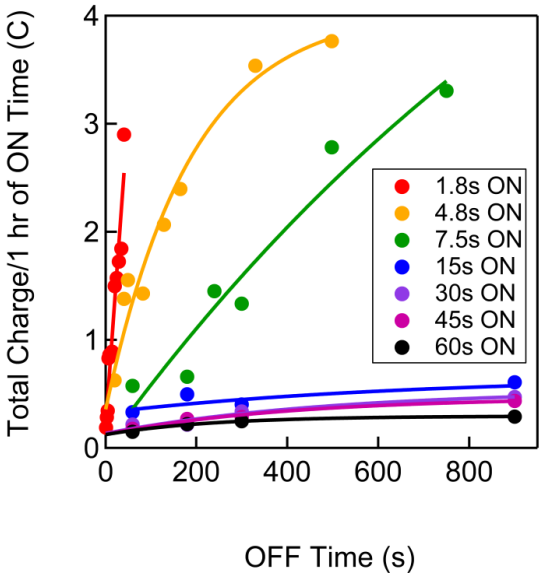

Figure 2.3. Cumulative charge per one hour of combined ON time as a function of the OFF time interval in the duty cycle experiment. Each point corresponds to a single experiment at the specified ON and OFF times. The curves are exponential fits, $y = A + Be^{-Cx}$, for illustrative purposes only.

Examining the current profile of an ON/OFF cycle in a single-anode experiment (Fig. 2.4) demonstrates how a shorter switching interval leads to more cumulated charge due to less time spent in the current profile's plateau, where current is modest. All current profiles (both single and multi-anode experiments) exhibited $\sim t^{1/2}$ decay rate that is typical when a voltage step is applied to an electrode (*77*). This most likely results from the expanding diffusion layer, $\partial_O(t)$, surrounding the electrode where the oxidizing species are depleted. The thickness of the diffusion layer depends on the time after the voltage step (t) and the diffusion coefficient of the oxidizing species (D_O), grows with $\sim t^{1/2}$ (Eq. 2.2) and reaches a maximum when the concentration gradient through the diffusion layer reaches a steady-state (*77*).

$$\partial_O(t) = 2\sqrt{D_O t} \tag{2.2}$$

Passing current during the time shortly after connection, when the diffusion layer is thin, produces maximal current because the electrode is surrounded by a high concentration of electron donors, be they reduced chemical species that are abiotically oxidized by the anode, or microbial cells replete with charge from their metabolic substrates (*43*, *69*).

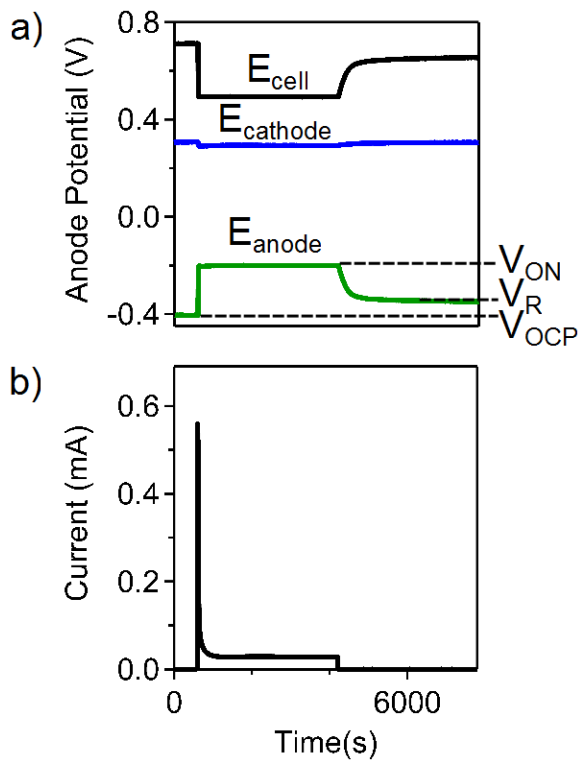

Figure 2.4. Profiles of electrode potentials (a) and current (b) collected during a cycle with 3500 seconds of ON time followed by an OFF interval. Although this ON time was not used in the experiments, these data illustrate how the system reaches a steady-state current over time. In closed circuit, the anode potential, E_{anode}, increases (V_{ON}) until the whole cell voltage, E_{cell}, set by the programmable load is reached. When the circuit is turned OFF, the anode potential recovers (V_R) over time as it returns to the anode open circuit potential (V_{OCP}). The cathode potential, $E_{cathode}$, changes minimally over the duration of the cycle. The current has an initial peak immediately after turning the switch ON that decays to a plateau region, which is the pseudo-steady state the system reaches under circuit connection.

These experiments demonstrate the value of allowing the system to spend time in open circuit if maximal current is a key characteristic being optimized. At switching intervals shorter than 15 seconds, the multi-anode experiments yielded less charge, decreasing the overall benefit of a shorter ON time. Indeed,

previous experiments using pure cultures of *S. oneidensis* MR-1 (*78*) and *Geobacter sulferreducens* (*79*) observe similar current profiles (a transient peak with ~$t^{1/2}$ decay) following circuit connection with peaks that increase in magnitude with longer time spent in open circuit. The authors attribute the increased current to the biofilm's ability to store charge that accumulated during the disconnection time. The transient current peaks observed in these experiments are consistent with the discharging of charge stored in the biofilm, but the data do not provide the resolution needed to definitively attribute the results to this phenomenon.

2.3.3 Recovery of anode potential during cycling

To further elucidate the effect of the OFF time to the overall system performance, we examined the anode potential profiles of the different switching intervals in the 15 anode experiments, and observed that anode potential prior to the next ON time –which I refer to as recovered potential– is closer to the original open circuit potential at longer time intervals (Fig. 2.5).

During these experiments, 15 seconds is the shortest switching interval where the anode potential nearly fully recovers to open circuit potential, suggesting that for any given system a specific combination of ON time and OFF time maximizes anode potential recovery while increasing total

cumulative charge. I parameterized this anode recovery by calculating the anode recovery percentage, which is defined as the ratio of the difference between the anode recovered potential, V_R, (Fig. 2.4a) and the anode closed circuit potential, V_{ON}, and the difference between original open circuit potential, V_{OCP}, and anode closed circuit potential, V_{ON} (Eq. 2.3).

$$AR\% = \frac{|V_R - V_{ON}|}{|V_{OCP} - V_{ON}|} \times 100 \tag{2.3}$$

If the anode fully recovers during the OFF time, then this anode recovery percentage is 100%. For each of the single anode experiments, the average anode recovery percentage is compared to the average height of the current peaks that occur immediately after connection of the anode to the cathode. The OFF time influences the anode potential and, when sufficient in length, allows the anode to recover to open circuit potential, which increases current when the anode is in continuity. The data reveal, not surprisingly, that the longest OFF time yields the greatest recovery (Fig. 2.6). However, at OFF times less than 10 seconds, anode recovery is never better than 20% and the average height of the current peaks drastically decreases by half. Thus, if optimizing for current, aggressive duty cycling may not be any more beneficial than leaving the electrode in continuous continuity.

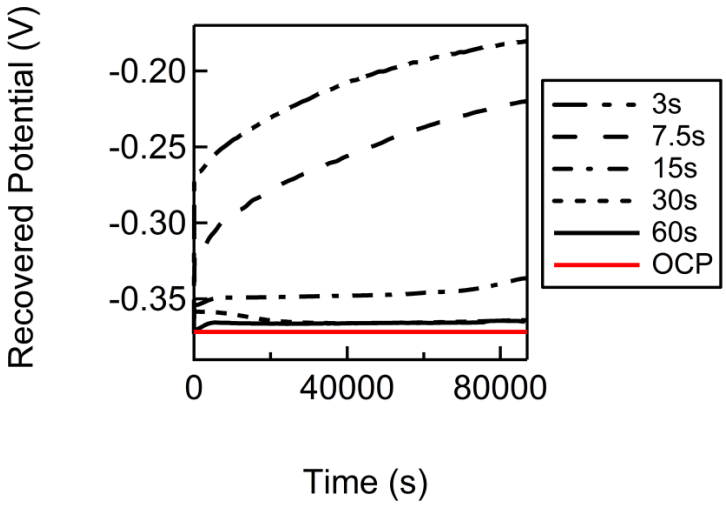

Figure 2.5. The recovered potential of a single anode measured at the end of each OFF time interval as a function of time for different switching intervals. Recovered potential is the minimum potential reached by the anode during one duty cycle. The open circuit potential (OCP) prior to the experiment is plotted in red to demonstrate the deviation of the recovered potential. OFF intervals of less than 15 seconds demonstrate an inability of the anode to recover during repeated duty cycles.

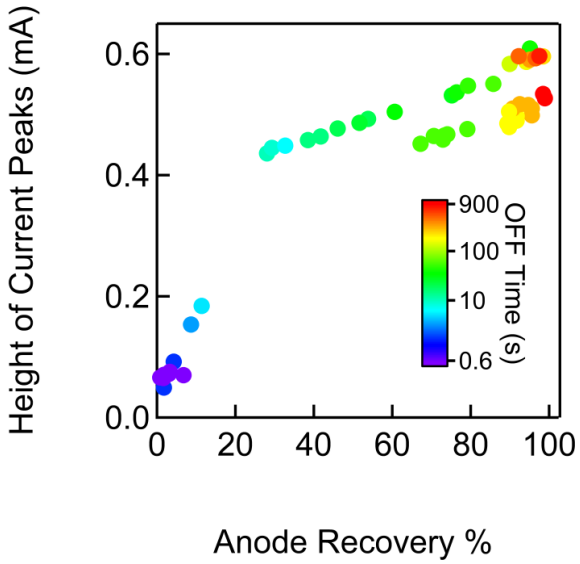

Figure 2.6. Average height of the current peaks plotted versus average anode recovery percentage. Each point represents a single experiment. The markers are color coded to the OFF time used in that experiment.

To better understand the basis of these findings, I used a resistor-capacitor series circuit, although typical equivalent circuits used to represent microbial fuel cells contain more components when more analysis is desired (*80*, *81*). An ideal voltage step experiment, where faradaic reactions occur fast and charge transfer resistance is negligible, can be represented by a bulk capacitance (C) and a resistance (R). It is the same as in an RC circuit (Eq. 2.4) where applying a potential step (V) has a current (i) and a response over time (t). At $t = 0$, the height of the current peak is equivalent to $\frac{V}{R}$. In these experiments, the anode potential is the same while connected, therefore any change in the current peak height indicates a change in the overall resistance in the electrode reactions; a lower current means the reaction rate is limited.

$$i = \frac{V}{R} e^{-t/RC} \tag{2.4}$$

When the height of successive current peaks and anode recovery percentage is followed throughout the course of the experiments, those with OFF times of less than 7 seconds show a sudden drop in current peak height around 15% anode recovery (Fig. 2.7). Recall that each experiment starts at 100% recovery because the system rested in open circuit and proceeded to lower percentage values as the experiment progressed. For the experiments with the longest

OFF time, 498 seconds, the recovery percentage never drops below 80%. These findings indicate that there is a threshold anode recovery percentage below which the current passed during ON time decreases substantially due to an increased resistance of the electrode reactions.

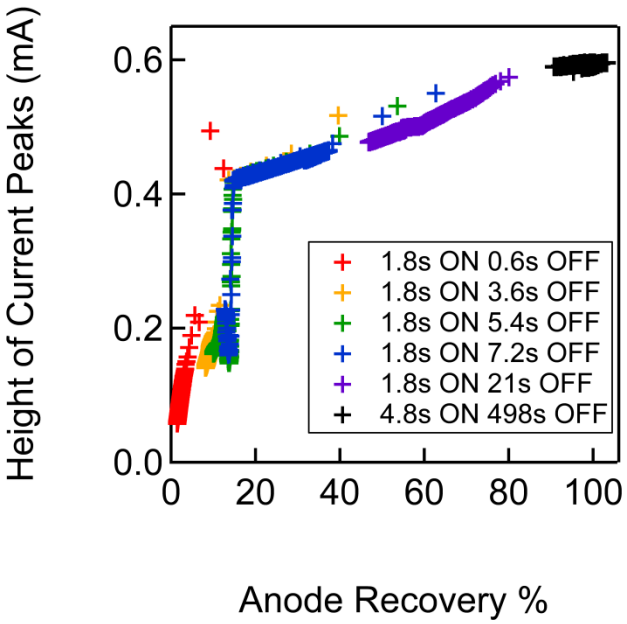

Figure 2.7. A plot of the height of each successive current peak immediately after returning to the ON state versus the corresponding anode recovery percentage. Data shown are from a selection of single anode experiments with similar ON times and varying OFF times. Each point represents the height of a discrete current peak during the course of repeated cycling. The experiments start at 100% anode recovery when the first current peak is the highest and proceeds to lower percentages, corresponding to lower current peak heights.

In order to determine whether the anode potential is important for recovery (represented by current peak height), I conducted an additional series of single anode experiments where the switching conditions were the same (1.8s ON and

0.6s OFF) but the whole cell potential were 0.25 V, 0.5 V, 0.6 V, and 0.7 V (Fig. 2.8). These data reveal that the whole cell potential modestly influences the height of the current peaks and does not alter the minimum percentage of anode potential recovery obtained during the course of the experiment, implying that OFF time is important for reaching anode recovery.

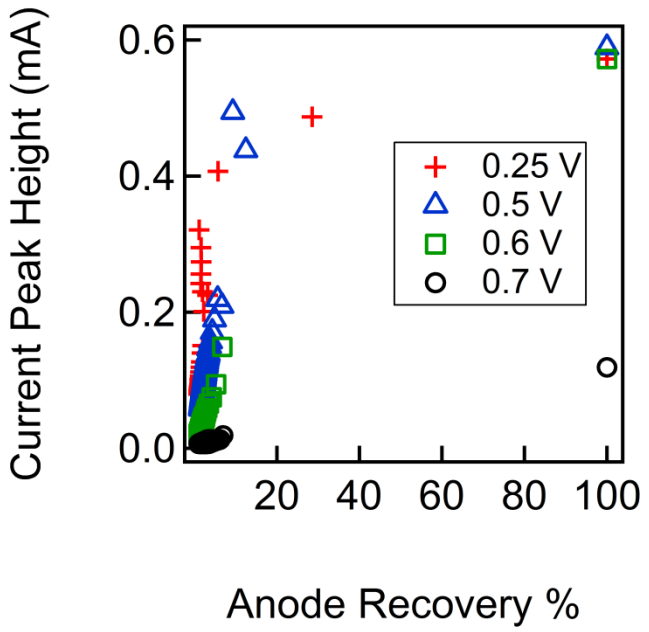

Figure 2.8. A plot of current peak height versus the corresponding anode recovery percentage. Using a single anode, the whole cell potential was poised at 0.25, 0.5, 0.6 and 0.7 volts in separate experiments where the ON and OFF times were 1.8 and 0.6 seconds, respectively. The experiments start at 100% anode recovery when the first current peak is the highest and proceed to lower percentages, corresponding to lower current peak heights.

2.3.4 Biofilm constraints on transport

Since the data suggest that time is the critical parameter, it is apparent that diffusion of metabolites, including protons, substrates, or both, within the biofilm, is the major factor that governs current production. To that end, I used the 1-D diffusion equation (Eq. 2.2) to calculate a length scale associated with this time using typical diffusion coefficients of substrates through a biofilm. With these values, I empirically estimated a length of ~100-200 μm for substrates larger than protons, which have a range of ~400-600 μm (Table 2.2). As mentioned, the relationship between time and diffusion coefficient calculates the diffusion layer boundary surrounding the anode and this layer is comprised of both biofilm and surrounding liquid. Imaging with SEM (Fig. 2.9a-b) and confocal microscopy (Fig. 2.9c) demonstrate highly comparable biomass on all active (cycled) anodes, demonstrating that interruption time does not influence overall microbial mass. Confocal microscopy shows that all active anodes have a similar thickness of 30±10 μm (Fig. 2.9c). The calculated length is larger than the thickness of the biofilm and, therefore, includes a diffusion layer beyond the biofilm surrounding the anode. If the maximum diffusion layer is on the same order of magnitude as a previous study, which calculated a maximum diffusion layer distance of ~50 μm (*69*), then 5-10 seconds corresponds to the amount of time it takes for species to sufficiently

pass through both the maximum diffusion layer and the biofilm surrounding the anode. The correspondence between time and length scales in this experiment implies that the observed increase in electrode reaction resistance may be attributable to the diffusion layer, namely when it is at its maximum.

Table 2.2. Diffusion coefficients and distances of relevant metabolites.

Diffusion coefficients, for liquid and biofilm, of metabolites relevant to this eMFC system and the corresponding length scales that correspond to the 5-10 seconds observed in experiments. The biofilm diffusion coefficient, Dbiofilm, is estimated based on the relationship Dbiofilm = 0.8*Dliquid (69) from the diffusion coefficients of that species in a liquid (77).

Metabolites	**D_{liquid}** (10^{-5} cm^2s^{-1})	**Diffusion Distance liquid (5-10 s)** (μm)	**$D_{biofilm}$** (10^{-5} cm^2s^{-1})	**Diffusion Distance biofilm (5-10 s)** (μm)
H^+	9.311	390-550	7.449	430-610
HS^-	1.731	170-240	1.385	190-260
Acetate	1.089	130-190	0.871	150-210
SO_4^{2-}	1.065	130-180	0.852	150-210
Lactate	1.033	130-180	0.826	140-200
Propionate	0.953	120-170	0.762	140-200

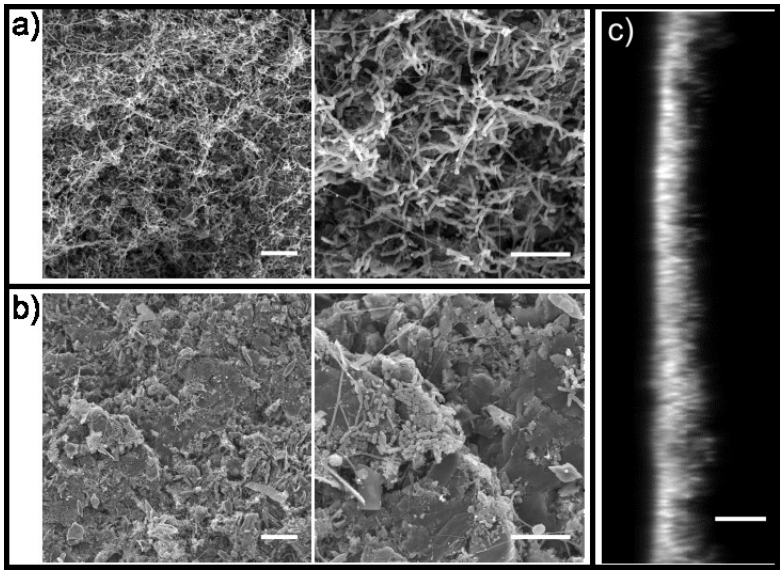

Figure 2.9. a-b) SEM images of (a) an anode that was continuously connected to a cathode, and (b) an anode that was disconnected. Each pair of images is of the same sample at two different magnifications; 600x (left) with a corresponding 20 μm scale bar and 2000x (right) with a 10 μm scale bar. c) Confocal microscopy z-profile of an always ON anode (30 μm scale bar). Confocal stacks of the two duty-cycled anodes (with short and long OFF times) have similar thicknesses.

Through this analysis I cannot infer which metabolite in particular is the limiting factor. However, it is known that protons have a very high diffusion coefficient and I posit it is unlikely that they are rate-limiting in these conditions. Previous experiments found that diffusion of protons from the anode biofilm to the cathode is the rate-limiting step in current production (*61*) and I sought to determine if this was an important factor in this system by monitoring pH in the anode chamber. Maintaining all three anodes under continuous load (which would result in the greatest excursion in pH) resulted

in a modest change in chamber seawater pH from 7.1 to 6.9 over a period of 9 days (Fig. 2.10). Seawater with 1500 μM sulfide (comparable to these conditions of 1300-1700 μM) typically has a total alkalinity of 3.1 meq • L^{-1} (*82*) and combined with alkaline sediments provides highly effective buffering capacity of the system. As previously observed, an increase in the buffering capacity of the medium in a laboratory MFC also increased current production (*61*). Conversely, a study of *Geobacter sulferreducens* biofilms on MFC anodes found a striking reduction in pH within the biofilm (*83*). Although I am unable to determine the extent to which the biofilm accumulates protons in these experiments, the modest change in seawater pH decreased seawater alkalinity by less than 20% (*84*), and the remaining buffering capacity of both the seawater and the sediments make it highly unlikely that a substantial accumulation of protons persisted within the biofilm.

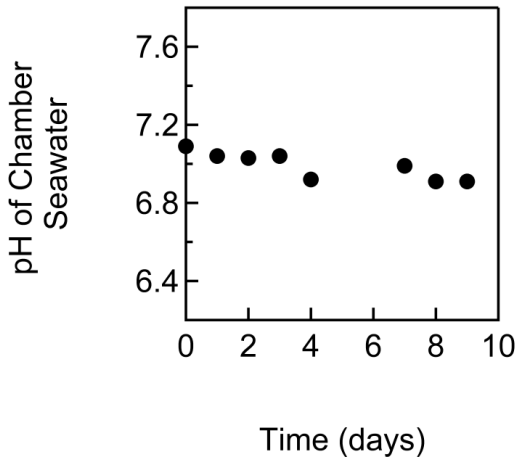

Figure 2.10. pH measurements of the seawater in the chamber when all three electrodes were in the ON state for over a week.

2.3.5 Microbial community composition

Analyses of the 16S rRNA gene sequences revealed that microbial community composition was, at a coarse level, highly similar among all active anodes (Fig. 2.11). These communities were dominated by Proteobacteria with at least 98% representation, regardless of duty cycle. In contrast, the control (open circuit) anode hosted 70% Proteobacteria. In all three active anodes, I observed a significant enrichment of δ-proteobacteria, representing ~98% of all the 16S rRNA gene sequences recovered from active anodes (Fig. 2.11). 66% of the sequences on the control electrode (always OFF) and 21% of the sequences in the sediment were assigned to the δ-proteobacteria. Sequences recovered from a non-electroactive biofilm accumulated on the inside of the chamber were enriched with 85% γ-proteobacteria and 4% α-proteobacteria. For the three active anodes, ribotypes allied to the genus *Desulfobulbus* were dominant making up 96-97% of all recovered gene sequences, but only 35%, 1%, and 0.4% of the sequences from the control anode, sediment, and inside biofilm respectively (Fig. 2.12). While these high-throughput sequence representations are not quantitative, the clear dominance of these ribotypes strongly suggest they are the dominant members of the community and -after establishment of the community- are likely the dominant contributors to power production.

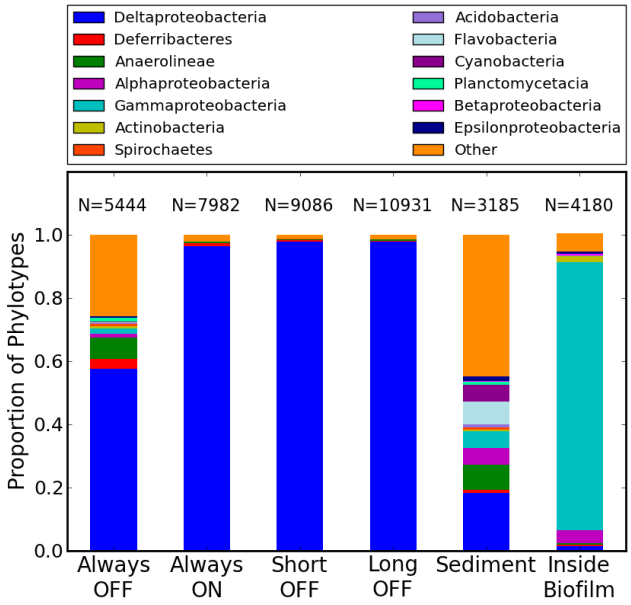

Figure 2.11. Class level representation in the one inactive anode (always OFF), the three active anodes (always ON, short OFF and long OFF), sediment, and biofilm inside the core tube. *N* = the number of sequences represented in each bar. See Experimental Methods for details.

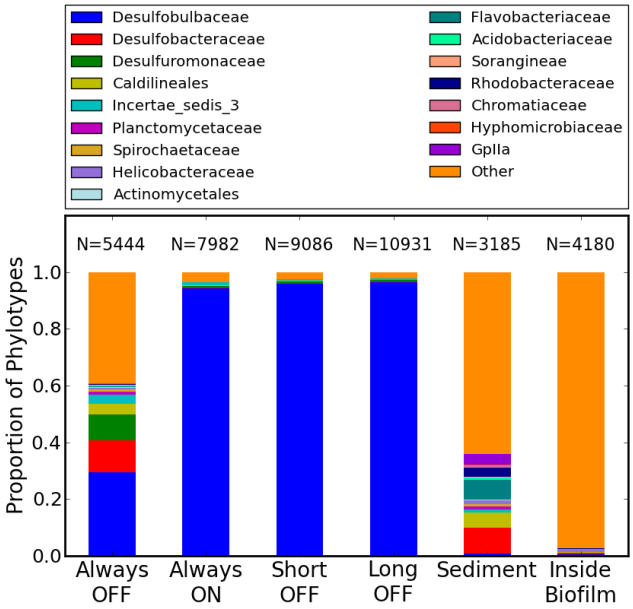

Figure 2.12. Family level representation in the one inactive anode (always OFF), the three active anodes (always ON, short OFF and long OFF), sediment, and biofilm inside the core tube. *N* = the number of sequences represented in each bar. See Experimental Methods for details.

In culture, members of the genus *Desulfobulbus* have been shown to reduce Fe(III) (*85*) as well as transfer electrons to electrodes while using propionate, lactate, and pyruvate as electron donors (*86*). In particular, *D. propionicus* can oxidize S^0 as the sole electron donor (*87*), allowing it to access the precipitated S^0 on marine sediment anodes as a result of abiotic sulfide oxidation at the anode surface (*88*). The observed 0.2 unit pH change (Fig. 2.10) was unlikely to inhibit microbial activity as members of this family (*Desulfobulbaceae*), are metabolically active over a range of pH of 6.0 to 8.2 (*89*). It has been suggested that in environments where *Desulfobulbus* species dominate the anode microbial community, reduced sulfur compounds are the primary electron donors that fuel current production (*88*). Given the low community diversity and the elevated concentrations of dissolved sulfide in this system (1300-1700 μM), sulfur cycling by δ-proteobacteria was probably a major component of power production in this system.

ANME observed on anode surface via PCR and FISH microscopy

There was a high enrichment of sulfate reducers on the anode surface with 96% Desulfobulbus species in the bacterial community detected through 454 pyrosequencing Fig. 2.12. Sulfate reducers have previously been found in consortia with anaerobic methanotropic archaea (ANME archaea) (*90*, *91*). Both ANME-3 and ANME 2c archaeal groups have been observed in close consortia

with Desulfobulbus (*90*). PCR reactions with targeted archaea and ANME primers as well as FISH microscopy with bacterial and archaeal probes were used to investigate the presence of ANMEs on the anode surface. An endpoint PCR with general archaeal, ANME-1, and ANME-2 primers were all positive for the extracted DNA (Fig. 2.13). Furthermore, FISH microscopy with general bacterial and archaeal fluorescent probes (Fig. 2.14) show a majority of bacterial cells associated with a comparable abundance of archaeal cells. Based on previous DNA sequencing (Fig. 2.12) the bacterial cells are predominately Desulfobulbus and with the results of the PCR with archaeal primers, the archaeal cells include ANMEs. It is apparent that the anode serves as an environment for enriching sulfate reducers and ANMEs may associate with these microbes. Previously, D. propionicus can oxidize S0 as the sole electron donor(*87*), allowing it to access the precipitated S^0 on marine sediment anodes as a result of abiotic sulfide oxidation at the anode surface. When S^0 was added as a potential electron donor for electron transfer to the electrode, sulfate was produced in the presence of *D. propionicus* but not in the absence of cells (*86*). Cells did not produce sulfate in the absence of the electrode. Therefore, it is possible for sulfide to electrodeposit onto the anode as elemental sulfur which serves to enrich the anode community with sulfate-reducers capable of using elemental sulfur as an electron donor and the electrode as the electron acceptor. This creates an environment suitable for anaerobic methane oxidizing

archaea (ANMEs). Further research on this topic would be required to determine this hypothesis and determine whether ANME and sulfer reducers are in fact enriched on anode surfaces.

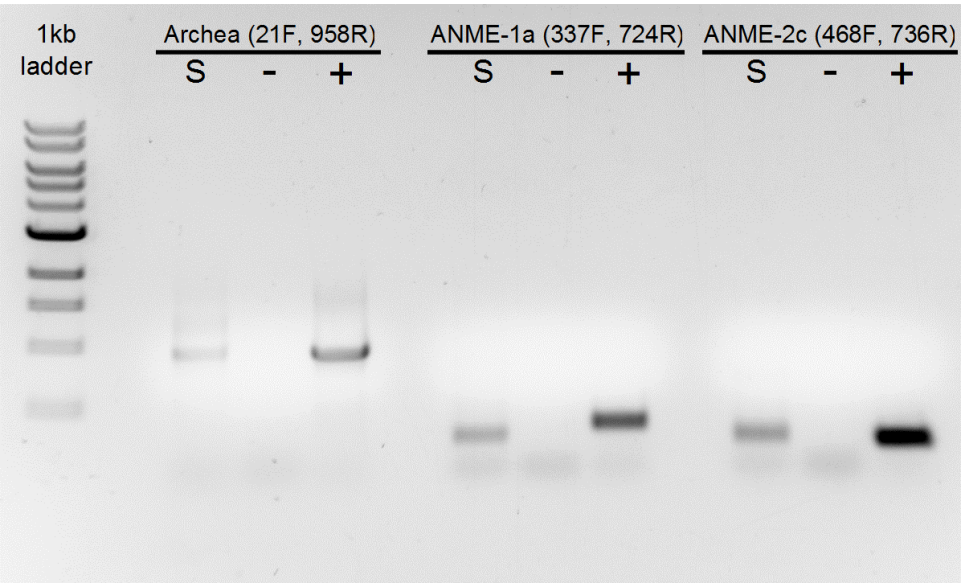

Figure 2.13. Gel of an endpoint PCR with general archaea, ANME-1a, and ANME-2c primers (Table 2.1). DNA extracted from sample and amplified with these primers (S) were all positive, indicating the presence of archaea, including ANMEs. Positive (+) and negative (-) controls are indicated.

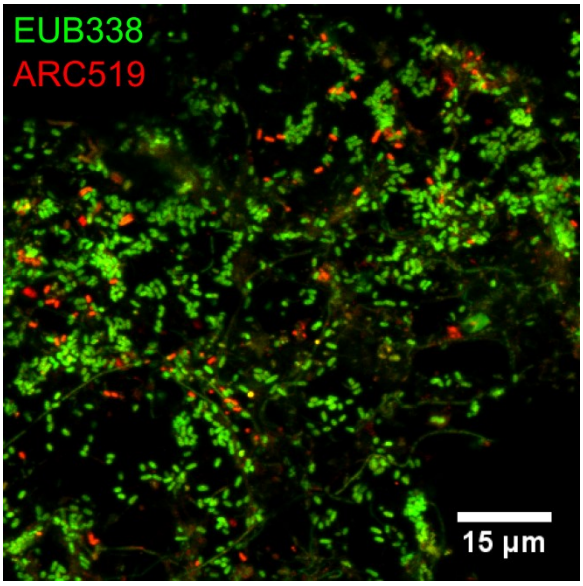

Figure 2.14. FISH microscopy of the anode surface with general bacterial (green, EUB338) and archaeal (red, ARC519) probes. While bacterial cells are in majority, there is a distribution of archaea in consortia with the bacteria.

2.4 Implications and applications

Collectively, these data provide a comprehensive empirical assessment of power production as a function of duty cycling frequency and further our understanding about which factor(s) influence and govern power density in electroactive biofilms. Previous models have suggested that proton diffusion limits power production (*61*), but in the highly buffered conditions of this experiment, which is typical of many eMFCs, and resolution of the measurements, this does not appear to be the case. Rather, replenishment of metabolic substrates via diffusion into the biofilm appears to govern power

density and varying the ON-OFF state enables these substrates to diffuse into these substantial biofilms. In general, the evaluation of power output curves in microbial fuel cells should take into account that current after disconnection events can be considerably higher than current produced under steady state conditions. I am unable to comment on the specific rate of diffusion or acquisition of metabolites into the cells, or the metabolic rate of sulfide oxidation, or electron shuttling via outer membrane cytochromes or redox active shuttles, and future experiments might aim to constrain these factors and their role in eMFC performance.

While it is apparent that the OFF time does not produce current, and as such when integrated over time that duty cycling may yield less total power, there is operational value in duty cycling. First, this is relevant to applications where voltage is boosted to harness energy or operate instrumentation, as the higher input voltage results in greater power conversion efficiency. Additionally, this may be relevant to the field of bioelectrosynthesis wherein electrodes provide electrons as reducing equivalents for the production of organic molecules, e.g. biofuels or high value pharmaceuticals. The ability of a microorganism to utilize charge from a solid-phase electron donor is influenced by the potential of that electrode, and the availability of substrates in the surrounding media, and providing electrons with higher potentials is likely a critical dimension of electrosynthesis. With the recent focus on electrosynthesis (*5*), duty-cycling to

optimize for these factors might well yield higher net product. It is equally possible that in these systems the organisms do not require a constant electrode potential to produce the desired output, and so switching anode connection could significantly reduce the operating costs of running the system. As in these experiments, there might be minimum anode potential beyond which the current significantly decreases. It is important to fully investigate the deployed system to make sure it is operating above this minimum. These results provide a comprehensive microbial, geochemical and electrochemical analysis of eMFC operations and provides insight into how to operate future eMFCs employed in the field.

Chapter 3

Electron Uptake from an Electrode by a Phototrophic Iron Oxidizer

3.1 Introduction

Iron is one of the most abundant elements in Earth's crust and is used by microbes in diverse ways. These various microbial metabolisms have a role in the iron cycle and are relevant in a variety of environments, ranging from anaerobic aquifers (*92*) and acid mines (*93*) to the deep sea (*94*). In nature, iron cycles primarily between the two oxidation states, ferrous (Fe^{2+}) and ferric (Fe^{3+}) forms. The midpoint potential of iron (Fe^{3+}/Fe^{2+}) is +0.77 V, only slightly more electronegative than O_2/H_2O at 0.82 V, and is relevant primarily under acidic conditions. At pH 7, different forms of iron have widely varying midpoint potentials ranging from -0.314 V for magnetite/Fe^{2+} to +0.385 V for Fe-citrate

(Table 3.1) that allow Fe(II) at around pH 7 to function as an electron donor for for different microbial metabolisms. Fe(II) oxidation is performed by many different types of bacteria, including autotrophs and heterotrophs, phototrophs and chemotrophs, and aerobes and anaerobes. Since Fe(II) oxidizes rapidly in the presence of oxygen at neutral pH, Fe(II)-oxidizing bacteria are limited to environments with low to no oxygen or to highly acidic environments where abiotic Fe(II) oxidation is much lower.

Table 3.1. Reduction potentials of relevant compounds.

Reduction Pair	**E_m' (V) ***
Fe^{3+}/Fe^{2+} (pH 2)	+0.77
Fe(III)-citrate/Fe(II)-citrate	+0.385
Fe(III)-NTA/Fe(II)-NTA	+0.372
$Ferrihydrite_{solid}/Fe^{2+}$	+0.1 to -0.1
$\alpha\text{-}FeOOH_{solid}/Fe^{2+}$	-0.274
$\alpha\text{-}Fe_2O_{3solid}/Fe^{2+}$	-0.287
Fe_3O_{4solid}/Fe^{2+}	-0.314

* E_m' indicates the environmentally relevant midpoint potentials: pH 7 except where noted, standard concentrations except for solid Fe minerals, for which Fe^{2+} is 100 μM. (*95*)

Since the byproduct of Fe(II) oxidation, Fe(III), precipitates rapidly as an insoluble ferric hydroxide [$Fe(OH)_3$] at neutral pH, a question in microbial metabolic iron oxidation is: where is Fe(II) oxidized? If Fe(II) oxidation occurs in the periplasm, there are several potential ways that the cell might avoid periplasmic Fe(III) precipitation, such as producing ligands to bind Fe(III) or by rapidly transporting Fe(III) out of the cell before it has a chance to precipitate intracellulary (*95*). However, no mechanisms have been found to transport

insoluble Fe(III) to outside the cell and if Fe(II) is oxidized at the cell surface no Fe(III) transport mechanism would be needed because periplasmic precipitation would be bypassed. One study of *Rhodobacter* species strain SW2 has shown that Fe precipitation takes place outside the cell on organic polymer fibers attached to the bacteria, where precipitates start as Fe(III)/Fe(II) mixed valence minerals are converted to Fe(III) minerals over time (*96*). These results are consistent either with oxidation taking place outside the cell or with Fe(III) oxidized in the periplasm being rapidly pumped out of the cell and precipitating on the surface.

Where Fe(II) oxidation occurs, which is closely tied to the Fe(III) precipitation problem, is a question that can be addressed using bioelectrochemical systems. Bioelectrochemical experimentation and cultivation offers an unique opportunity to understand the metabolism of Fe(II) oxidizing microbes by replacing the electron donor (in this case, Fe(II)) with an insoluble, biologically inert electrode and controlling its potential to act as an electron donor. If the electron transport machinery is able to oxidize metals at the outer cell surface, electrodes poised at potentials near those of natural substrates might serve as electron donors, eliminating Fe(III) end products, Fe(II) concentration issues, and abiotic reactions. Bacteria capable of oxidizing phyllosilicate-Fe(II) was found in soil samples (*97*), suggesting that some iron-oxidizers are able to use a solid-phase conductor, and potentially an electrode, as an electron donor.

Recently, a bioelectrochemical study of a neutrophilic Fe(II) oxidizing bacteria *Mariprofundus ferroxydans* PV-1 used a poised electrode as the sole energy source with a cathodic current indicating electron uptake by bacteria (*98*). These studies suggest that other Fe(II) oxidizers may also be capable of electron uptake, including the phototrophic Fe(II) oxidizing bacteria. If these microbes are capable of electron uptake from a solid-phase conductor, they might use this ability to access electrons from minerals, including conductive Fe(III) minerals precipitated on the cell surface(*99*).

Fe(II) oxidation can supply electrons to fix carbon dioxide in anoxygenic photosynthesis according to Eq. 3.1.

$$4Fe^{2+} + HCO_3^- + 10H_2O + h\nu \rightarrow [CH_2O] + 4Fe(OH)_3 + 8H^+ \qquad (3.1)$$

The unifying principle of bacterial photosynthesis is the light-driven generation of a proton-motive force, which is subsequently used by ATP synthase to form ATP, or for active transport and motility. Bacterial photosynthesis can be divided into two different types of reactions; 1) light energy is converted into ATP via a proton-motive force and a reduced redox carrier, and 2) biosynthetic carbon reduction into biomass. Understanding whether a Fe(II) oxidizing phototroph can uptake electrons from a solid-phase conductor would reveal

more about the electron transfer mechanisms involved in Fe(II) oxidizing photosynthesis.

The major aim of this study is to determine if an electrode could serve as an electron donor for *Rhodopseudomonas palustris* TIE-1, a photoautotroph capable of using a variety of electron donors, including Fe(II) for photosynthesis(*99–101*). TIE-1 is used as the model organism because it uses ferrous iron, Fe(II), as an electron donor for photosynthesis (photoferrotrophy) (*99*), and produces solid-phase oxides such as goethite and magnetite as an endproduct. These iron oxides are not only very common in nature but are conductive (*102*, *103*). These iron oxides encrust the microbial cell, indicating the possibility that these phototrophic iron oxidizers have a way of accessing electron donors via these conductive materials, making TIE-1 a possible candidate for electron uptake from an electrode in a BES.

The metabolic versatility and genetic tractability of TIE-1 allows the investigation of the conditions and mechanisms of electron uptake from a solid-phase conductor as well as its relation to photosynthesis and carbon fixation. The Pio operon (Fig. 3.1) in TIE-1 contains three genes which are required for phototrophic iron oxidation: PioA is a periplasmic decaheme c-type cytochrome, PioB is an outer membrane porin protein, and PioC is a periplasmic high-potential iron protein (HiPIP)(*100*). Both cytochromes and HiPIPs are often involved in electron transfer reactions, and it is likely that PioA and PioC

transfer electrons from Fe(II) to their destination in the cell. PioB could be involved in Fe(II) transport into or Fe(III) transport out of the cell. Since the Pio operon is essential for phototrophic iron oxidation(*100*), the Pio genes could be important in the ability of TIE-1 to accept electrons from solid-phase Fe(II) minerals and electrodes.

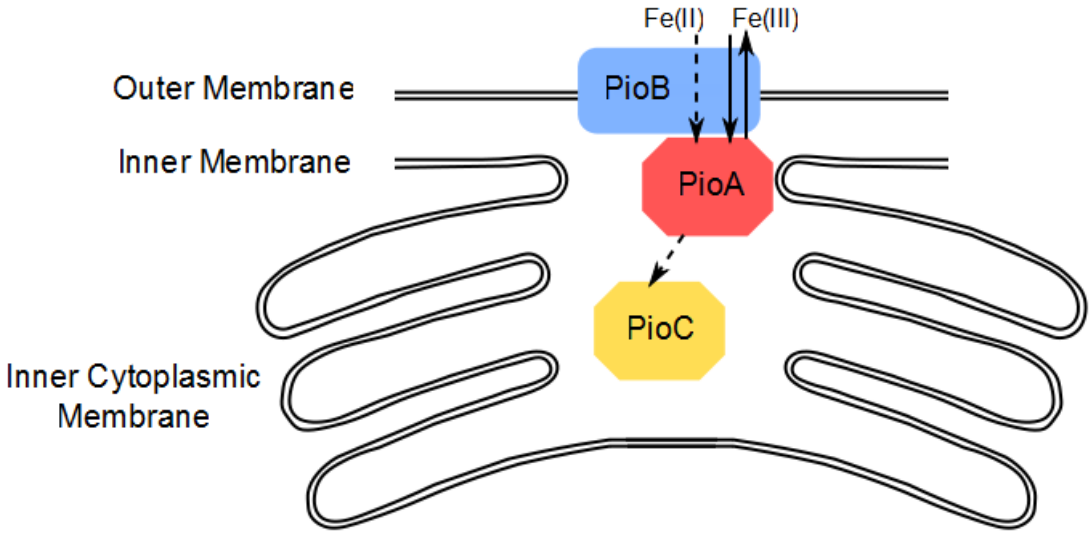

Figure 3.1. Electron transfer in the Pio system of *R. palustris* TIE-1. The outer membrane, inner membrane, and inner cytoplasmic membrane are shown. Abbreviations: PioB, outer membrane protein which might be involved in Fe transfer in and out of the cell; PioA, cytochrome; PioC, high-potential iron protein. Dotted arrows denote electron reactions. (*95*)

While microbial extracellular electron transfer as a means of accessing minerals as electron acceptors is well studied, little is understood about the role of extracellular electron transfer as an electron donating process coupled to growth. Previous studies show that mixed microbial communities facilitate cathodic reactions in bioelectrochemical systems (BESs) (*104*), suggesting

microorganisms capable of electron uptake. Studies using pure cultures capable of taking up current from an electrode are few: *Sporomusa ovata* (*105*), *Mariprofundus ferrooxydans* PV-1 (*98*), and *Shewanella oneidensis* MR-1 (*106*). Mechanistic insights were only provided for *Shewanella* (*106*) which normally uses organic carbon as an electron donor and donates electrons to insoluble metal oxides or electrodes. Characterizing how microbes accept electrons from solid-phase electron donors improves our understanding of the ecological implications of this process as well as biotechnology and bioremediation efforts that harness this ability (*5*).

3.2 Materials and methods

3.2.1 *Rhodopseudomonas palustris* strains, media, and growth conditions

General growth protocols of *Rhodopseudomonas palustris* TIE-1 followed previous methods (*101*). Cells were grown aerobically in 10 mM sodium succinate in yeast extract-peptone medium, buffered to pH 7 with 100 mM MOPS at 30°C. For experiments, cells were pre-grown autotrophically on 80% hydrogen:20% carbon dioxide (H_2:CO_2) at 200 kPa, in fresh-water medium (FW) with 20 mM bicarbonate. The Δ*pioABC* strain used herein was constructed as

previously described (*100*). Phototrophic pre-growth was at 30°C using a 60W incandescent light source providing total irradiance of ~40 W m^{-2}. Bioelectrochemical reactor studies were conducted with FW medium with 20 mM bicarbonate, buffered to pH 6.8 and with no exogenous electron-donor. All bacterial strains were routinely tested for purity by standard PCR using primers indicated in Table 3.2. Due to biological variation in the cultivation effort, which resulted in different cell densities in the inoculum and prohibits comparison across treatments, we included wild-type (WT) cells under light and electrical connectivity conditions (described below) in parallel with every individual treatment to account for these differences. All comparisons between WT and treatments are made using these paired runs.

Table 3.2. Primers used in the study in 5 to 3 direction.

Gene name (Locus tag)	Primer name	Sequence	Purpose
pioA (Rpal_0817)	pioAqRTPCRfor	AAATTTCGACGACACCATCGA	PCR, qRT-PCR(*108*)
pioA (Rpal_0817)	pioAqRTPCRrev	CTTGGCGGCGAGGATCT	PCR, qRT-PCR(*108*)
pioB (Rpal_0816)	pioBqRTPCRfor	TCGCGCCAGGGTTCTATG	PCR, qRT-PCR(*108*)
pioB (Rpal_0816)	pioBqRTPCRrev	TTCCAGTAGGTGCCGTCCTT	PCR, qRT-PCR(*108*)
pioC (Rpal_0815)	pioCqRTPCRfor	ACGCCCAGGTCACCAAGA	PCR, qRT-PCR(*108*)
pioC (Rpal_0815)	pioCqRTPCRrev	GTTGGGCGACTCCTGATAGC	PCR, qRT-PCR(*108*)
pioC homolog (Rpal_4085)	Rpal_4085qPCRfor	CTATCAGGCACCCAACCAGT	qRT-PCR
pioC homolog (Rpal_4085)	Rpal_4085qPCRrev	CACAGATTGCACACCGAATC	qRT-PCR
ruBisCO form I (Rpal_1747)	Rpal_1747qPCRfor	GCAAGGAACGCTACAAGTCC	qRT-PCR
ruBisCO form I (Rpal_1747)	Rpal_1747qPCRrev	CCCAGTAGCCCATCTTCTTG	qRT-PCR
ruBisCO form II (Rpal_5122)	Rpal_5122qPCRfor	GGCTTCGGTAACTTCATCCA	qRT-PCR
ruBisCO form II (Rpal_5122)	Rpal_5122qPCRrev	GTGGAGACTTCGACGTTGGT	qRT-PCR
Exopolysaccharide synthesis gene I (Rpal_3203)	Rpal_3203qPCRfor	GCTACTACCTCGACGGCATC	qRT-PCR
Exopolysaccharide synthesis gene I (Rpal_3203)	Rpal_3203qPCRrev	GCGGCGTAGGAGAACATCT	qRT-PCR
Exopolysaccharide synthesis gene II (Rpal_3763)	Rpal_3763qPCRfor	GGCTTCGCTCTCATGATCTC	qRT-PCR
Exopolysaccharide synthesis gene II (Rpal_3763)	Rpal_3763qPCRrev	ACACCAGAACAGGGACCAAC	qRT-PCR
Exopolysaccharide synthesis gene IV (Rpal_3771)	Rpal_3771qPCRfor	GGTGTGGACCTGTTCTTCGT	qRT-PCR
Exopolysaccharide synthesis gene IV (Rpal_3771)	Rpal_3771qPCRrev	ATCGTTCCGATGCACATACA	qRT-PCR
Exopolysaccharide synthesis gene VI (Rpal_3777)	Rpal_3777qPCRfor	CTCGAGGGCTACTCGTATCG	qRT-PCR
Exopolysaccharide synthesis gene VI (Rpal_3777)	Rpal_3777qPCRrev	TTGGTCTGCTCATTCTCGTG	qRT-PCR
recA (Rpal_4376)	TIE-1recAqRT-PCRFor	ATCGGCCAGATCAAGGAAC	qRT-PCR(*108*)
recA (Rpal_4376)	TIE-1recAqRT-PCRRev	GAATTCGACCTGCTTGAACG	qRT-PCR(*108*)
clpX (Rpal_3308)	TIE-1clpXqRT-PCRFor	GGAGATCTGCAAGGTTCTCG	qRT-PCR(*108*)

3.2.2 Bioelectrochemical system and conditions

The bioelectrochemical systems (BESs) consisted of new, acid-washed (10% HCl), combusted 350 mL borosilicate glass H-cell reactors equipped with two butyl rubber sampling ports in the cathodic chamber (Adams and Chittenden Scientific Glass, Berkeley, CA, USA). A vacuum clamp held the anodic and cathodic chambers together, and electrolytes were separated using a cation-exchange membrane (Nafion® 117) with an active cross-section of 20 cm^2 (Fuel Cell Store, Boulder, CO, USA). The working electrodes consisted of spectroscopically pure 3/16" diameter graphite evaporation rods (SPI 01685-FA, Structure Probe Inc, West Chester, PA, USA) that were mechanically polished with 1200 grit sandpaper, soaked in 5% HCl for 12 hours and stored in ultrapure deionized water. The graphite rods were thoroughly dried prior to use by allowing the water to evaporate.

Each reactor was fitted with three graphite rods to provide a total immersed projected electrode surface area of 18 cm^2. The rods were sealed with fittings and ferrules on the reactor cap (Upchurch Scientific, Oak Harbor, WA, USA). Outside the reactor, rods were electrically connected to one potentiostat using alligator clips (described below). The counter electrode consisted of carbon cloth (Fuel Cell Store, Boulder, CO, USA), which was mechanically attached to a titanium wire pierced through a rubber stopper (VWR) and suspended in the

counter chamber. The distance between the working and counter electrodes was approximately 11 cm. Assembled BES reactors were sterilized by autoclaving in sterilization pouches and placed inside an anaerobic chamber (Coy, 2% hydrogen and palladium catalysts). Ag/AgCl reference electrodes were custom-made using glass tubing (4 mm KIMAX®), silver wire (0.5 mm diameter) and porous vycor tips (1/8" diameter, MF-2064, BASi). Reference electrodes were calibrated prior to each experiment, placed in the anaerobic chamber, sterilized with 70% ethanol, and placed in the counter chamber for the duration of the experiments. While inside the anaerobic chamber, media and counter buffer were added to the cathode and anode chambers, respectively. Inoculation of the BESs occurred inside the anaerobic chamber prior to transferring them outside the anaerobic chamber to establish electrical connections. The reactor system was purged continuously with a 1 cm^3 min^{-1} stream of 0.2 μm filter-sterilized, deoxygenated gas stream of 80%:20% N_2:CO_2 and 100% N_2 on the cathodic and anodic side, respectively, using a hypodermic needle immersed 1 cm below the media surface. The gases were deoxygenated using a high capacity oxygen trap lowering the oxygen levels to <0.01 ppm (Restek, Bellefonte, PA, USA). Each BES was individually housed with a fresh incandescent 60 W bulb providing a total irradiance of ~ 40 W m^{-2} total irradiance. Dark BESs lacked a bulb and were covered thoroughly with black paper to prevent light exposure. All working chambers were stirred gently with

a magnetic bar and incubated at 30◦C. All incubations, across all treatments, lasted 24 hours.

3.2.3 Electrical conditions and cyclic voltammograms

The reactors were poised using custom-built potentiostats engineered for microbial chronoamperometry (Karma Electronics Inc., Somerville, MA, USA). Data was collected through an Omega DAQ (OMB-DAQ-56) every 5 seconds using provided software (Omega Engineering, Inc.). Based on preliminary analyses of electroactivity in WT *R. palustris* TIE-1, the reactors were poised at +100 mV vs. Standard Hydrogen Electrode (SHE, -100 mV of the biological E_{pc} roughly at +200 mV vs. SHE) to assure cathodic conditions during the experiment. Cyclic voltammetry (CV) was conducted using a Gamry R600 potentiostat (Gamry, Warminster, PA, USA). Biofilm CVs were obtained with a scan range of -100 mV to +900 mV vs. SHE at a rate of 20 mV per second. Supernatant voltammograms were obtained using a 3 mm diameter glassy carbon electrode (Part no. A-002012, BioLogic, Claix, France), under a N_2 atmosphere, scanned between 0 to +500 mV vs. SHE at 20 mV per second. We were unable to detect any electro-active soluble species in the 0.2 mM filtered spent medium. To assess the active surface area variability between electrodes,

CVs were collected abiotically in fresh water medium. Potential is referenced to the SHE unless otherwise specified.

3.2.4 Experiment sampling

The reactors were inoculated with 10 mL of cells in the mid-exponential phase of photoautotrophic growth on 80% H_2: 20% CO_2. One mL of media was withdrawn from the reactors immediately following inoculation and used for optical density (OD_{660}) determination with a 4802 spectrophotometer (Cole Parmer, Vernon Hills, IL, USA), and for pH measurements (Inlab® Expert Pro pH meter and probe, Mettler Toledo, Schwerzback, Switzerland). Four mL of culture was also withdrawn from the reactors for cell counts. Cells were fixed in 4% paraformaldehyde for cell counting (Electron Microscopy Sciences, Hatfield, PA, USA). At the end of each experiment, one of the electrodes was immediately dipped into RNA*later*™ (Qiagen, Valencia, CA, USA) for RNA extraction. Also, 5 mL of planktonic cells were immediately preserved in RNA*later*™ and filtered on a polyethersulfone (PES) membrane for RNA extraction (Corning, Tewksbury, MA, USA). All RNA samples were stored at -80°C. A second electrode was cut into ~5 mm pieces and transferred into fixatives or staining solutions for microscopic analyses (described below). Post experimentation, 1 mL of planktonic cells were sampled for OD_{660}

determination, and 2 to 4 mL for pH measurements. The remaining culture volume was then filtered on a 0.2 μm cellulose acetate filter (Corning, Tewksbury, MA, USA). After resuspension in 8 mL of media, these planktonic cells were pelleted in two 2 mL microcentrifuge tubes (18000 g for 10 min) and kept at -80°C along with the filtered spent medium.

3.2.5 Fluorescence microscopy sample preparation and imaging

Sections of the electrode were placed into one of three solutions containing 1 μM 4',6-diamidino-2-phenylindole (DAPI, Life Technologies, Grand Island, NY, USA) as well as 1) LIVE/DEAD® stain (0.5 μM SYTO 9 and 3 μM propidium iodide, L7012, Life Technologies, Grand Island, NY, USA), 2) Exopolysaccharide (EPS) stain (200 mg L^{-1} Concanavalin A and Alexa 488, Life Technologies, Grand Island, NY, USA), and 3) Protein stain (undiluted FilmTracer SYPRO Ruby Biofilm Matrix Stain, Life Technologies, Grand Island, NY, USA). Tubes were wrapped in aluminum foil and kept at room temperature for at least 30 minutes. Samples were then placed in 1X phosphate-buffered saline (PBS) in a glass-bottom dish (MatTek Corporation), and imaged with a Zeiss 700 inverted confocal microscope with the following imaging lasers and Zeiss filters: 1) Live/Dead = 555 nm and 488 nm, SP490;

405 nm, SP555, 2) EPS = 488 nm and 405 nm, SP490 and LP490, 3) Protein = 555 nm, SP 490; 405 nm, SP555. This work was performed at the Harvard Center for Biological Imaging.

3.2.6 Scanning electron microscopy (SEM) sample preparation and imaging

Sections of the electrode were cut using sterile technique and immediately placed into a sterile microcentrifuge tube containing one of three solutions: 1) 5% glutaraldehyde (Electron Microscopy Sciences, Hatfield, PA, USA) in 1X PBS, 2) 2% paraformaldehyde (Electron Microscopy Sciences, Hatfield, PA, USA) in 1X PBS, and 3) 2% glutaraldehyde in in 1X PBS with 0.15% Safranin O (Sigma-Aldrich, St. Louis, MO, USA), which has previously been shown to aid in EPS preservation (*107*). Samples were held at 4°C for 24 hours before being subjected to ethanol dehydration by placing them in 35%, 50%, 70%, 95%, 100% ethanol (200 proof) in PBS or 0.1 M PBS solutions for ten minutes each. The 100% ethanol solution was changed five times, and the sample was left in ethanol for critical point drying (Autosamdri 815 A; Tousimis, Inc.) with a 15-minute purge time. The samples were adhered to SEM posts with carbon film tape and then imaged with a SEM at 5 kV (JEOL, Inc.). Cell counts for electrode samples were performed by analyzing microscopy fields taken at the

same working distance (4.5 mm) to image, counting at least 500 cells or examining 12 fields of view if cell density was low and normalized to total area. This work was performed at the Harvard Center for Nanoscale Systems (CNS).

3.2.7 RNA isolation and amplification

For planktonic assessments, preserved cells were dislodged from the PES membrane before RNA extraction by vortexing for three minutes in a TRIS-EDTA (TE) buffer. For biofilm assessment, the cells were dislodged from the graphite by scraping with a sterile razor, then vortexing vigorously in TE buffer. RNA was extracted as described previously (*108*). The RNA concentration was quantified using a NanoDrop ND1000 (Thermo Scientific, Wilmington, DE, USA).

The RNA obtained from the biofilm on the graphite was cleaned with the MEGAclear™ Kit (Life Technologies, Grand Island, NY, USA) as per the manufacturer's guidelines. The purified RNA was precipitated using ammonium acetate. The reconstituted RNA was used as template for the MessageAmp™ II-Bacteria Kit as per the manufacturer's guidelines (Life Technologies, Grand Island, NY, USA).

3.2.8 Quantitative reverse transcription PCR (qRT-PCR)

Gene expression analysis was performed using qRT-PCR. The comparative Ct method was used as described previously to assess expression of the *pioABC* operon and other relevant genes (*108*). Primer efficiencies were determined using the manufacturer's method (Applied Biosystems Inc. User Bulletin #2). *clpX* and *recA* were used as the two internal standards, which have been previously used and validated as internal standards (*101*). The primers used for the assays are indicated in Table 3.2. The iScript cDNA synthesis kit was used for reverse transcription (Biorad, Hercules, CA, USA). The iTaq FAST SYBR Green Supermix with ROX (Biorad, Hercules, CA, USA) and the Stratagene Mx3005P QPCR System (Agilent, Santa Clara, CA, USA) were used for all quantitative assays.

3.2.9 Cell counting

The paraformaldehyde fixed samples were transferred into Amicon centrifuge filters (Amicon Ultrael 100k, regenerated cellulose membrane, Millipore, Carrigtwohill, CO, Ireland) and centrifuged for 10 min at 1000 g. The pellet was resuspended in PBS and washed twice. The cells were recovered by

centrifugation of the Amicon in reverse position for 15 min at 3000 g. The resulting samples had less than 0.04% paraformaldehyde. Picogreen was added to the cells (Quant-iT PicoGreen® dsDNA, Life Technologies, Grand Island, NY, USA), and the cells were counted in 96 well plates along with 50 µL of Sphero™ AccuCount blank beads (Spheroteck, Lake Forest, IL, USA). Cell-density was estimated with a LSRII flow cytometer (BD, Sparks, MD, USA) using a 488 nm laser. A calibration curve relating the ratio of cell events to bead events with cell-density was constructed by analyzing a dilution series of a cell sample, the density of which has been determined by microscopy (with a Helber Bacteria Cell counting chamber with Thoma ruling, Hawksley, Lancing, Sussex, UK).

3.2.10 ICP-MS

To measure the concentration of iron present in FW medium ICP-MS was performed using an Agilent 7700x ICP-MS with an octopole MS (Agilent, Santa Clara, CA, USA). Internal standards used were Germanium and Manganese, which were within the detection limit of our system. The amount of iron in the basal medium was 4 µM and ranged from 2-4 µM in the spent medium obtained from filtering the media from the reactors after the duration of the experiment.

3.3 Results

Electron uptake by *Rhodopseudomonas palustris* TIE-1 was characterized by illuminated BESs that were configured with electrodes poised at +100 mV vs. Standard Hydrogen Electrode (SHE). This potential was selected because it falls within the range of Fe(II) (-0.3 V to +0.3 V) utilized by TIE-1 (Table 3.1) (*1*, *95*). TIE-1 was subjected to three treatments in bioelectrochemical reactors: 1) illuminated reactors with poised electrodes (illuminated treatment); 2) non-illuminated reactors with poised electrodes (dark treatment); and 3) illuminated reactors with open-circuit, non-poised electrodes (control treatment).

3.3.1 Electron uptake by TIE-1

The highest rates of electron uptake by TIE-1 wild-type (WT) were observed in illuminated treatments, up to ~1.5 $\mu A \cdot cm^{-2}$ (Fig. 3.2). In the dark treatment, the observed current density (~0.25 $\mu A \cdot cm^{-2}$) was ~70% lower than when illuminated (Fig. 3.2A). To test the role of PioABC in electron uptake, a ΔpioABC mutant was used in BES treatments. ΔpioABC illuminated biofilms accepted 30% less current than the WT (Fig. 3.2B). Cyclic voltammetry of intact illuminated biofilms (cells attached to the electrodes in the illuminated treatments) revealed two modest but discernible cathodic peaks at +0.27 V and

+0.4 V (vs. SHE) in the WT, which were absent in the abiotic control and ΔpioABC mutant (Fig. 3.3). These values are more positive than the forms of Fe(II) oxidized by microbes, which range from -0.3 V to +0.3 V (*95*), and the +0.1 V potential of the poised electrode.

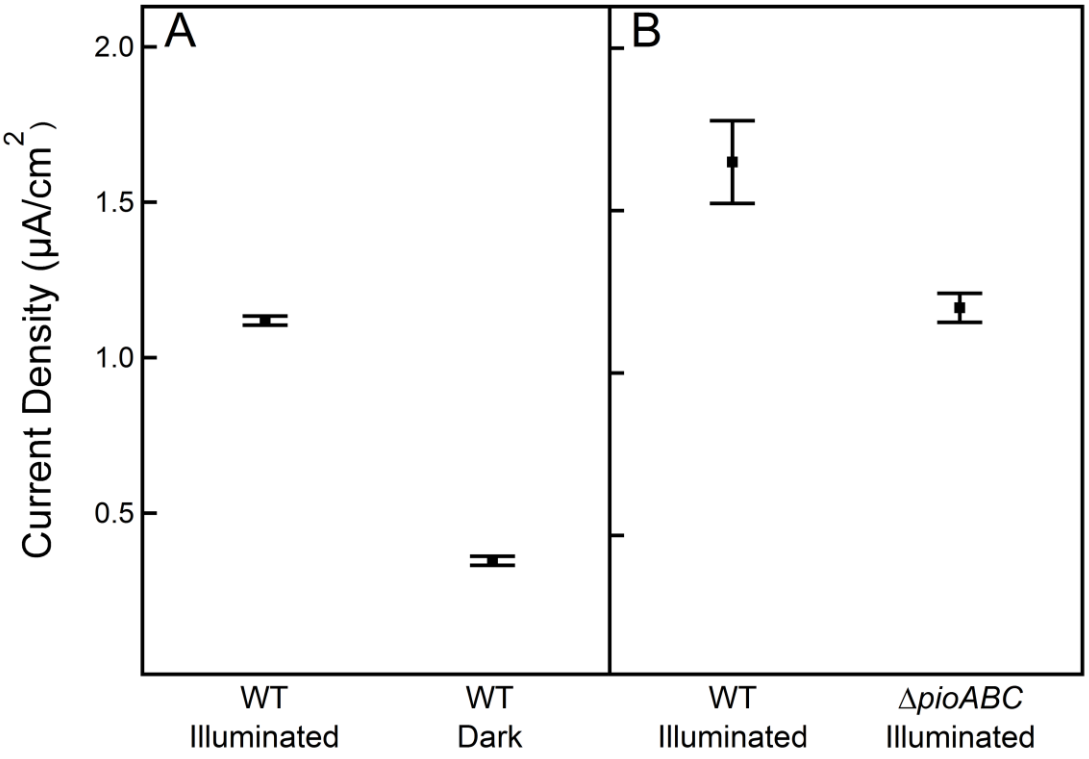

Figure. 3.2. A) Average current densities of wild-type Rhodopseudomonas palustris TIE-1 (WT) under illuminated and dark conditions. B) Average current densities of WT and ΔpioABC mutant under illuminated conditions with an incandescent 60 W bulb. These values were obtained by averaging regions of at least 8 hours of stable current for duplicate reactors. The same time points were used for the duplicates. Error bars indicate standard deviations of these averages. Data reported are for two separate experiments and are representative of >10 independent runs.

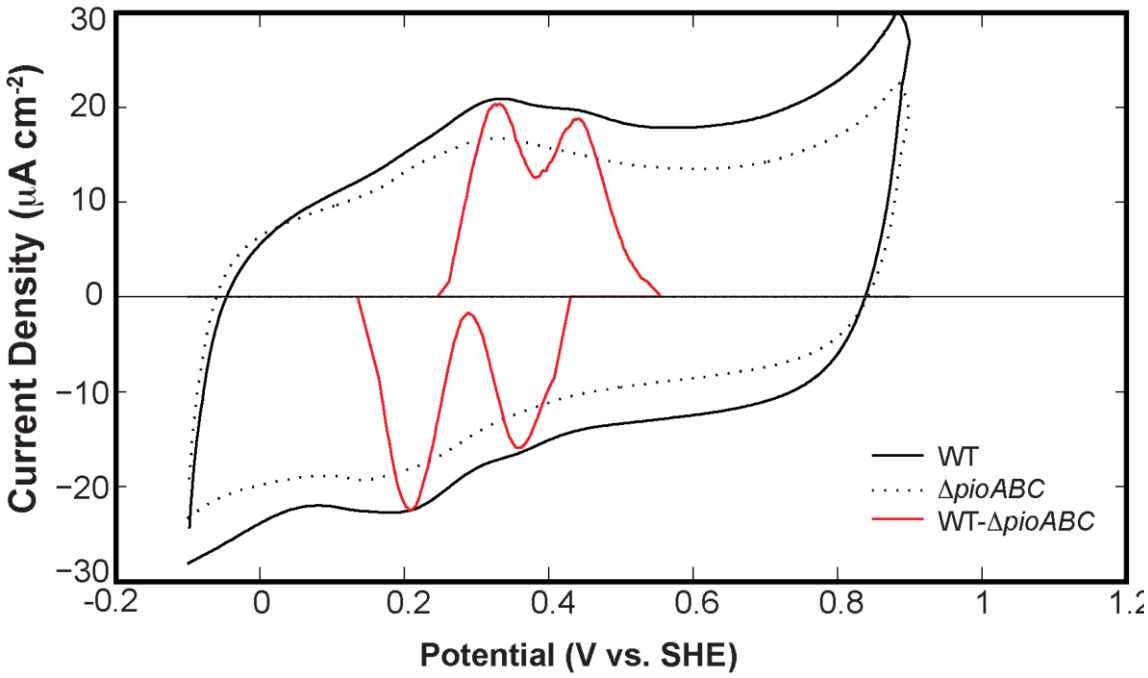

Figure 3.3. Cyclic voltammograms of WT and ΔpioABC mutant after 96 hours of treatment in bioelectrochemical reactors with electrodes poised at +100 mV vs. SHE. Two sets of anodic-cathodic peak pairs were identified at 0.27 and 0.40 V, respectively. The red trace depicts the difference in magnitude between the WT and the ΔpioABC mutant strain.

3.3.2 Changes in planktonic cell densities

Planktonic cell densities increased during the 24 hour incubation period in all treatments but were ~10-fold lower in the dark (Table 3.3). There was no significant difference in the planktonic cell increase between the WT and the ΔpioABC mutant (Table 3.3).

Table 3.3. Increase in planktonic cell densities of *Rhodopseudomonas palustris* TIE-1 in the experimental reactors.

The initial cell number was subtracted from the final cell number to report the change in cell density. Data reported are the average and range values for two replicate reactors per experimental set-up. Control = open circuit reactors exposed to light; Illuminated = closed circuit reactors exposed to light (incandescent 60 W bulb); Dark = closed circuit reactors without exposure to light.

A. Wild-type experiment

Strain, Condition	Cell Density (10^6 cells mL^{-1})
WT, control	111.4 ± 24.9
WT, dark	6.5 ± 4.8
WT, illuminated	84.9 ± 5.8

B. *ΔpioABC* experiment

Strain, Condition	Cell Density (10^6 cells mL^{-1})
ΔpioABC, control	98.4 ± 16.1
ΔpioABC, illuminated	68.4 ± 10.4
WT, illuminated	70.7 ± 6.2

3.3.3 Cell attachment to electrode

TIE-1 cells adhered to the electrode surface during illuminated conditions (Fig. 3.4). SEM imaging shows rosettes of TIE-1 cells (Fig. 3.4B) which are

indicative of growth patterns typically formed by *Rhodopseudomonas* species as it divides and multiplies (*109*). The dark biofilms were ~50 fold less dense than the WT (Table 3.4). The ΔpioABC mutant illuminated biofilms were ~8 to 10 fold less dense than the WT (Table 3.4).

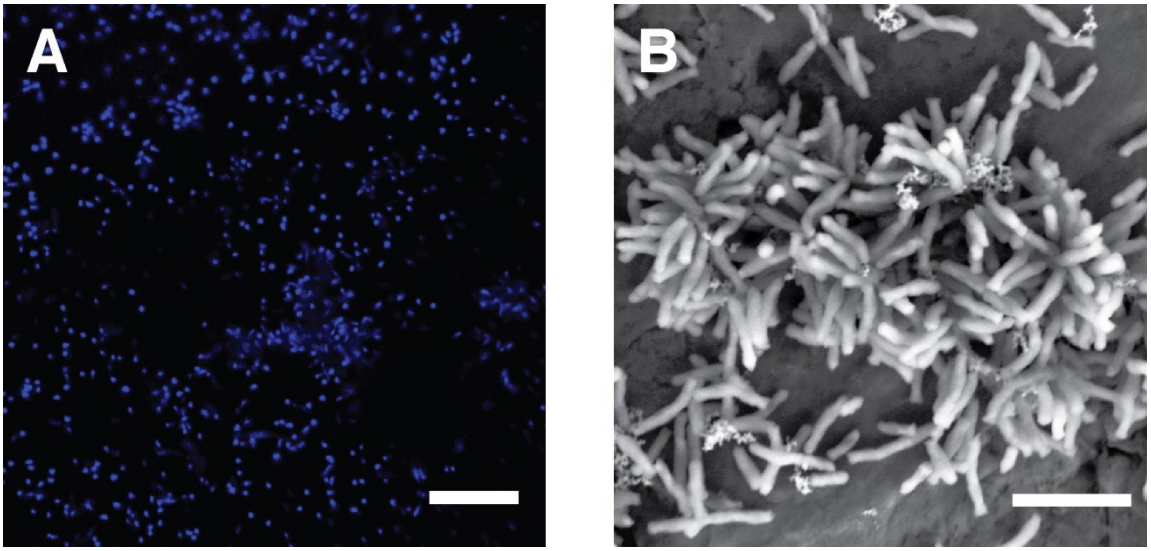

Figure 3.4. A) Fluorescence micrographs (FM) of a Rhodopseudomonas palustris TIE-1 wild-type (WT) illuminated biofilm (DAPI stain). The scale bar is 10 μm. B) Scanning electron micrograph (SEM) of a WT illuminated biofilm. The scale bar is 3 μm.

Although cells attached to electrodes during all biotic treatments, the absence of light results in lower viable cell colonization (Fig. 3.5). The viability of ΔpioABC cells was significantly decreased on the open circuit control (~13%) compared to normal illuminated conditions (~60%) Fig. 3.5). Extensive exopolysaccharide and protein deposits on the electrode was present under WT

illuminated closed circuit conditions, but was significantly reduced in the dark (Fig. 3.6).

Table 3.4. Biofilm cell densities of *Rhodopseudomonas palustris* TIE-1 growing on poised electrodes.

Using scanning electron microscopy, at least 12 fields were counted at the same working distance (covering at least >50 individual cells) and normalized to surface area. Data reported are the average and range values for two replicates per experimental set-up. Control = open circuit reactors exposed to light; Illuminated = closed circuit reactors exposed to light; Dark = closed circuit reactors without exposure to light.

A. Wild-type experiment

Strain, Condition	**Viable Cell Density (10^6 cells cm^{-2})**
WT, control	20 ± 10
WT, dark	0.19 ± 0.03
WT, illuminated	11± 1

B. *ΔpioABC* experiment

Strain, Condition	**Viable Cell Density (10^6 cells cm^{-2})**
ΔpioABC, control	0.4 ± 0.2
ΔpioABC, illuminated	0.28 ± 0.01
WT, illuminated	2.3 ± 0.5

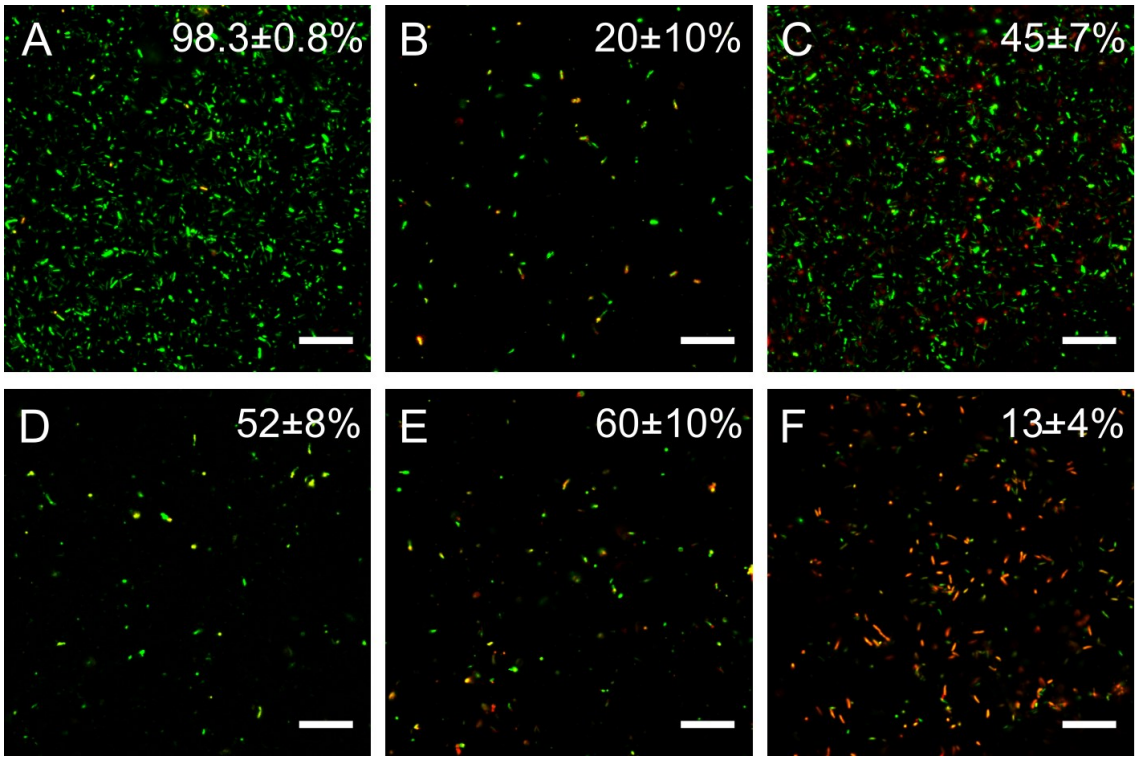

Figure 3.5. Fluorescent micrographs of Rhodopseudomonas palustris TIE-1 wild-type (WT) and ΔpioABC biofilms stained with LIVE/DEAD® dyes. A) WT illuminated treatment, B) WT dark treatment, and C) WT control treatment. D) WT illuminated treatment, E) ΔpioABC illuminated treatment, and F) ΔpioABC control treatment. The green stain is a DNA dye while the red stain shows metabolically inactive, dead cells. Percentage of viable cells on the electrode surface is reported on each image for duplicate reactor conditions. Total values were obtained by examining at least 5 fields of view. Error bars are the standard deviation between the two total numbers from the duplicate reactors. Scale bars are 15 μm. Illuminated = closed-circuit with illumination. Control = open-circuit with illumination. Dark = closed-circuit without illumination.

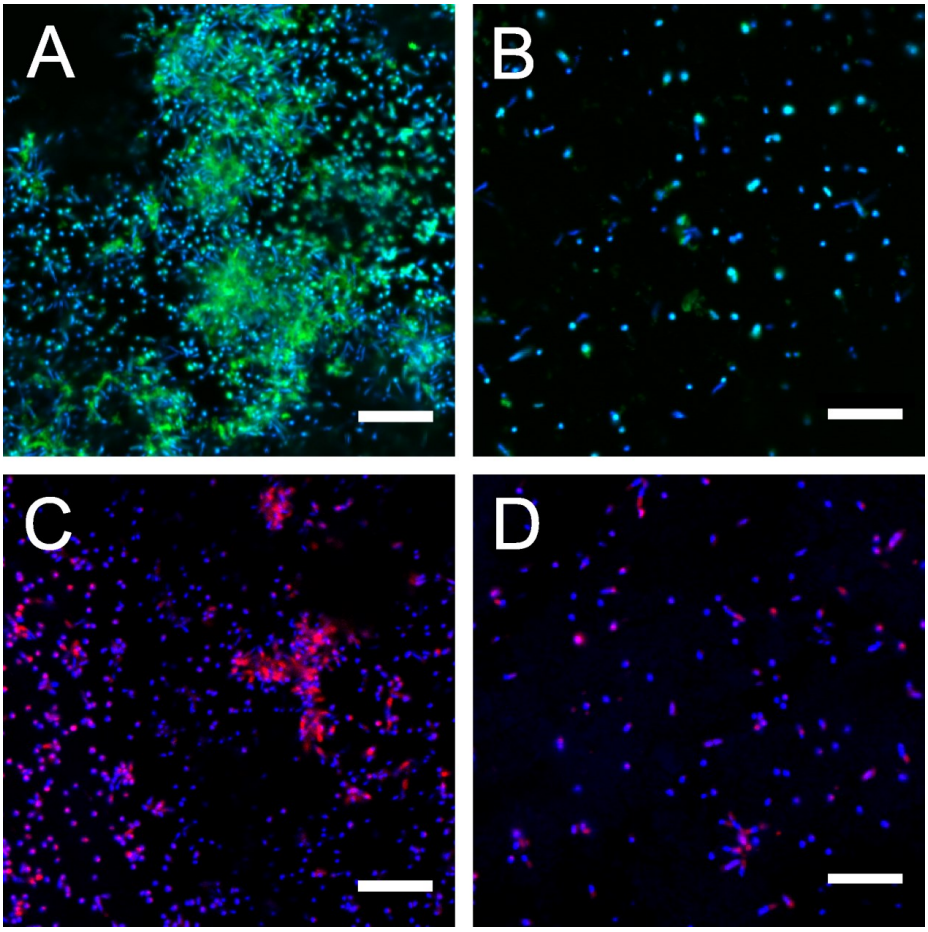

Figure 3.6. A, C) Fluorescence micrographs (FM) of a R. palustris TIE-1 wild-type (WT) illuminated biofilm dual-stained with DAPI (blue) for labeling DNA and either Concanavalin A (green) for labeling exopolysaccharide (A) or SYPRO (red) for labeling protein (C). B, D) Fluorescence micrographs (FM) of a R. palustris TIE-1 wild-type (WT) dark biofilm dual-stained with DAPI (blue) for labeling DNA and either Concanavalin A (green) for labeling exopolysaccharide (B) or SYPRO (red) for labeling protein (D). Scale bars are 10 μm.

3.3.4 Gene expression

The expression of the genes encoding the PioABC proteins was assessed across all WT treatments in the BES system. Expression of pioA in the WT

illuminated biofilms was ~48-fold upregulated while pioB and pioC showed more modest upregulation compared to the control treatment (11- and 3-fold respectively; Fig. 3.7A). The observed levels of pioA in the WT illuminated biofilm were comparable to that observed during photoferrotrophic growth on soluble Fe(II), and well above those of the inoculum (grown on H2:CO2; Fig. 3.7A). Additionally there is a ~5-fold higher pioABC expression in the dark vs. control treatment (Fig. 3.7A). Exopolysaccharide genes were highly upregulated in the WT and some of these genes were also upregulated in the ΔpioABC illuminated biofilms (Fig. 3.7C). Ribulose-1, 5-bisphosphate carboxylase/oxygenase (ruBisCo), a key enzyme in the Calvin cycle, directly reduces CO_2 using NAD(P)H to fix carbon (*110*, *111*). TIE-1 and related microbes have genes encoding two forms of ruBisCo, namely form I and II (*110*, *111*). Using mRNA abundance studies in TIE-1 ruBisCO form I, was observed to be most highly expressed in WT illuminated biofilms while ruBisCo form II expression decreased (Fig. 3.7B). Notably, ruBisCo form I expression was not induced in the dark treatment, suggesting that this enzyme functions most effectively in the presence of light under these conditions (Fig. 3.7B). The reduced expression of the electron sink, ruBisCo form I (23-fold lower than WT), in the ΔpioABC illuminated biofilms (Fig. 3.8A) further supported the role of PioABC in electron uptake.

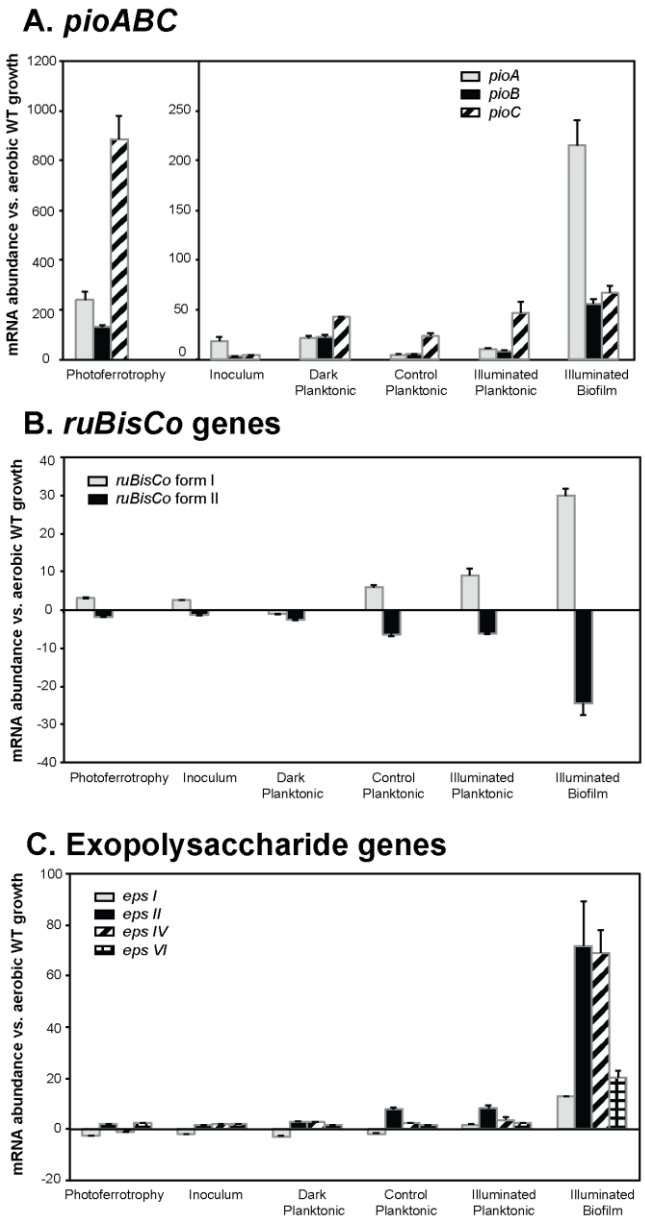

Figure 3.7. mRNA abundance determined in the wild-type (WT) using qRT-PCR for the A) *pioABC* genes B) the *ruBisCo* form I and II genes and C) exopolysaccharide (*eps*) genes. Cells were grown photoautotrophically with 5 mM $FeCl_2$ for photoferrotrophy. Photoautotrophic growth on hydrogen as an electron donor was the inoculum. qRT-PCR data are the averages ± standard error for two biological replicates assayed in triplicate. Illuminated = closed-circuit with illumination. Control = open-circuit with illumination. Dark = closed-circuit without illumination. *eps I* = Rpal_3203, *eps II* = Rpal_3763, *eps IV* = Rpal_3771, *eps VI* = Rpal_3777.

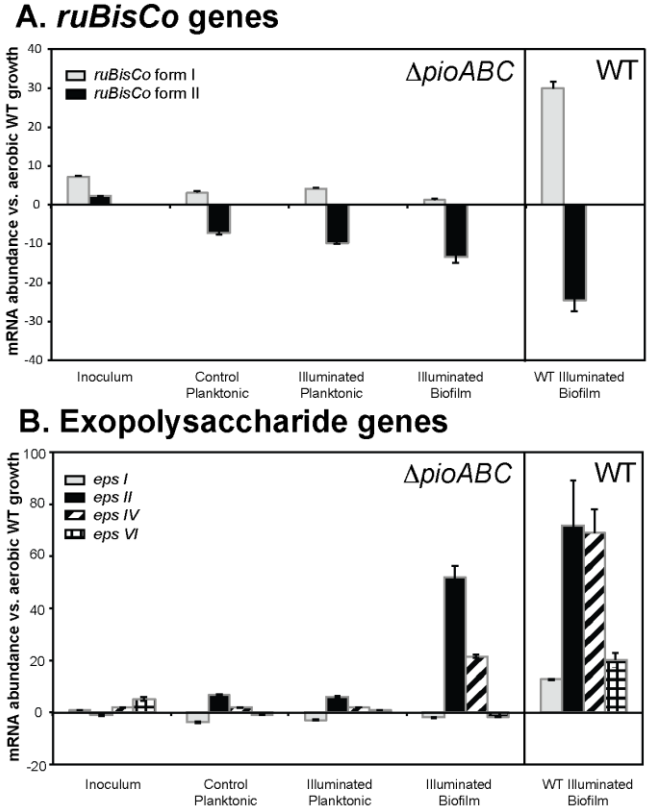

Figure 3.8. mRNA abundance determined in the Δ*pioABC* and wild-type (WT) using qRT-PCR for the A) the *ruBisCo* form I and II genes and B) exopolysaccharide (*eps*) genes. Photoautotrophic growth on hydrogen as an electron donor was the inoculum. qRT-PCR data are the averages ± standard error for two biological replicates assayed in triplicate. Illuminated = closed-circuit with illumination. Control = open-circuit with illumination. Dark = closed-circuit without illumination. *eps I* = Rpal_3203, *eps II* = Rpal_3763, *eps IV* = Rpal_3771, *eps VI* = Rpal_3777.

3.4 Discussion

The data shows that TIE-1 accepts electrons from a solid-phase conductor, with carbon dioxide as the sole carbon source/electron acceptor. Treatments with and without illumination revealed the important role of light for TIE-1 to

access electrons from the electrode. Additional studies using a TIE-1 pioABC mutant identify the Pio system to be important in electron uptake from the electrode. A previous study cultured *Mariprofundus ferroxydans* PV-1, a neutrophilic obligate Fe(II)-oxidizing autotroph, using a poised electrode as the sole electron donor (*98*). *M. ferroxydans* PV-1 were closely associated with the graphite electrode, typically attached as single cells and never as layered films or microcolonies (*98*), which is similar to the microscope observations of TIE-1(Fig. 3.4). These TIE-1 results broaden this phenomena by demonstrating a phototrophic Fe(II) oxidizer is capable of using a poised electrode as the electron donor.

The ability for TIE-1 to accept electrons from an electrode is stimulated by light. The significant more cathodic current under illuminated conditions indicates the degree to which light facilitated electron uptake by TIE-1. WT illuminated treatment increases cell attachment to the electrodes and planktonic cell number, indicating that light plays a key role in stimulating electron uptake. Cyclic voltammetry measurements suggest the presence of redox active components in the illuminated biofilms with potentials around +0.27 V and +0.4 V. These values are more positive than the forms of Fe(II) oxidized by microbes (-0.3 V to +0.3 V (*95*)) and the potential of the poised electrode (+0.1 V), allowing for these redox active compounds to mediate electron transfer from the mineral/electrode to the microbe. Many microbes

produce compounds that aid in extracellular electron transfer, including soluble mediators and insoluble membrane components (*2*). While the form of the redox active components produced by TIE-1 is unknown and warrants further investigation, such as examining the spent media soluble mediators, it is apparent that there are electroactive compounds made by TIE-1 that can shuttle electrons from a solid to the cell.

It has been unclear whether Fe(II) enters the cell for oxidation or if it is oxidized on the surface. It is thought that Fe(II) enters the cell through PioB and is then oxidized in the periplasm where the identified electron transfer proteins, PioA and PioC, reside (*95*). In these experiments, electrons are only accessible from outside the cell and these results demonstrate that TIE-1 is capable of oxidizing a solid electron donor without having a soluble component entering the cell. This coincides with environmental studies that demonstrate microorganisms capable of using iron containing minerals, phyllosilicate-Fe, for Fe(II) oxidation (*97*).

Under dark conditions, the lower cathodic current suggests TIE-1 is still able to maintain cellular metabolism, but at a lower level than under illuminated conditions. Phototrophic microbes related to TIE-1 use the energy of light to generate a proton motive force (PMF) for ATP synthesis through cyclic electron flow with no need for an electron donor (*112*). An electron donor is only required when the PMF is used to produce reducing equivalents for cellular

metabolism. In the dark, no PMF can be generated but cellular metabolism continues (*112*), requiring an electron donor, which is an electrode in this case. The PMF generated using the energy of light is dissipated by cellular metabolism necessitating a higher level of electron uptake. The data supports a model where electron uptake and photosynthesis are modular in TIE-1 with the two processes being linked via PMF.

Previous studies have shown that PioABC is essential for photoferrotrophy, and have speculated that the Pio proteins might be involved in electron transfer from Fe(II) to the electron transport chain (*100*, *113*). The decrease in cathodic current of ΔpioABC compared to WT suggests the role of pioABC in electron uptake. Additionally, the upregulation of the Pio genes in response to a poised electrode suggest it may be involved in electron uptake by TIE-1 under these conditions. Because the ΔpioABC mutant accepted current under illuminated conditions, additional mechanisms of electron uptake are likely to be employed by TIE-1. Using expression analysis, we observed that exopolysaccharide (EPS) genes were highly upregulated in both the WT and ΔpioABC biofilms, and microscopy revealed that EPS production was most evident in illuminated biofilms. Though the precise role of EPS, extracellular proteins, and other extracellular features in electron uptake remain to be determined, it is plausible that they might also play in electron transfer with a conductive material (*5*, *95*, *114*).

Electrons accepted by TIE-1 likely enter the cell and serve roles similar to those known for soluble electron donors. In organisms related to TIE-1, electron donors are required for generation of reducing equivalents namely NAD(P)H, which serves as a reductant for processes such as carbon fixation via the Calvin cycle (*110–112*). Protein abundance studies in a closely related strain CGA009 show that in addition to its role in carbon fixation, RuBisCo form I also aids in maintenance of redox regulation during photolithoautotrophy (*110*). In TIE-1, ruBisCO form I was most highly expressed in WT illuminated biofilms and not induced in the dark treatment (Fig. 3B). These data suggest that under illuminated conditions electrons accepted from the electrode are directed toward the Calvin cycle, via RuBisCo form I.

3.5 Environmental and biotechnological relevance

TIE-1's ability to access electrons from a solid outside the cell means that it has the protein machinery to transfer electrons from outside to inside the cell, and ultimately has the capacity to oxidize Fe(II) outside the cell. However, all the proteins involved in phototrophic Fe(II) oxidation described so far (PioA, PioC), are predicted to be periplasmic based on their sequence and some

biochemical evidence in the case of PioA (*100*). The redox proteins are predicted to be perplasmic for another phototrophic Fe(II)-oxidizing bacteria related to TIE-1, *Rhodobacter* sp. strain SW2A (*115*) where Fe precipitation has been observed to take place outside the cell (*96*). These combined results further the evidence for Fe(II) oxidation to occur extracellularly.

Additionally, Fe(III), a byproduct of Fe(II) oxidation, readily precipitates into insoluble Fe(III) oxides outside the cell (*1*, *95*). TIE-1 produces poorly crystalline Fe(III) hydroxides, which over time are abiotically transformed to the conductive minerals goethite and magnetite (*99*). Conduction of electrons through this matrix would allow TIE-1 access to electrons from remote electron donors, including Fe(II), via electron conduction or iron atom exchange (*102*, *103*, *116*). Recent studies have shown that conductive minerals can facilitate transfer to microbes from remote electron donors, including other microbes (*117–119*). These data extend microbial extracellular electron transfer processes to photoautotrophs, which being restricted by the maximum penetration of light to a depth of 200μm (*120*), have limited access to reductants in anaerobic zones deeper in the sediment column.

TIE-1 combines carbon dioxide fixation with forming complex carbon molecules in the form of biomass with the input of electricity via an electrode, offering interesting future biotechnology applications, particularly microbial electrosynthesis (*5*). Although a direct biofuel or readily used byproduct was

not produced by TIE-1, future genetic engineering of TIE-1 could lead to such a goal. TIE-1 offers the possiblity of combining the use of alternative energy sources as the electron source with carbon sequestration, and the possibility of producing organic compounds that do not degrade readily and/or have some commercial application (*22*). By learning more about the mechanisms of Fe(II) oxidizers to accept electrical current from an electrode and the various carbon byproducts they form, such technologies can be closer to becoming a reality.

Chapter 4

Poised Electrodes Increase Methanogenesis by *Methanosarcina barkeri*

4.1 Introduction

The majority of methane in nature is produced biologically (nearly 85%) by methane-producing archaea (*121*, *122*). These methanogens are a phylogenetically diverse group of strictly anaerobic Euryarchaeota with an energy metabolism that is restricted to the formation of methane from CO_2 and H_2, formate, methanol, methylamines and/or acetate (*121*, *123*). Methanogens are distinguished by their ability to obtain all or most of their energy for growth from the process of methane biosynthesis or methanogenesis. No

methanogens have been identified that can grow without producing methane. Methanogens are strict anaerobes, requiring them to generally be present in anoxic environments.

Some members of the Methanosarcinales order are predicted to electrically interact with electrodes because they contain metal containing protein subunits on membrane bound or associated hydrogenases that catalyze the oxidation of hydrogen (*124*), though to date this has not been adequately tested. Among the Methanosarcinales, species contain both hydrogenases and cytochromes or only cytochromes (*121*). *Methanosarcina barkeri* contains both cytochromes and hydrogenases, while the closely related *Methanosarcina acetivorans* have only cytochromes and cannot reduce carbon dioxide with hydrogen to form methane (*121*). These hydrogenases contain nickel and iron components that are involved in electron transfer and located in both the membrane and the cytoplasm. Some nickel-iron reaction centers are located inside (cytoplasmic side) the cell membrane, such as energy-converting [NiFe]-hydrogenases that catalyze the reversible reduction of ferredoxin (see 1.3.4), with hydrogen driven by a proton or sodium ion motive force (*124*). The energy-converting EchA-F [NiFe]-hydrogenase is found in *M. barkeri* but not in *M. acetivorans* (*124*). However, in order for a methanogen to electrically interact with a conductive solid, possible electron transfer sites should be located on the outside surface of the membrane. The active-site-harboring subunit is on the periplasmic side of

the membrane in the cytochrome b-containing [NiFe]-hydrogenase that catalyzes the reduction of methanophenazine with hydrogen and couples this reaction with the buildup of an electrochemical proton potential (*124*). Methanophenazine (E_0' = -170 mV) is a phenazine derivative and is a lipid-soluble electron and proton carrier in the cytoplasmic membrane like ubiquinone (E_0' = +110 mV) and menaquinone (E_0' = -80 mV), but with a lower redox potential (*124*). Methanophenazine has recently been shown to function as a key membrane bound electron shuttle during methanogenesis (*19*). An example is the methanophenazine-reducing hydrogenases Vht and Vht are found in *M. barkeri* (*125*, *126*). These redox active sites on these hydrogenases located outside the cell membrane on the periplasmic side that could potentially allow electron transfer between the methanogen and a conductive solid.

This study examines how methanogens metabolically interact with solid-phase materials. Several previous studies indicate evidence of methanogens capable of extracellular electron transfer (EET). In corrosion research, there is evidence that methanogens are responsible for iron-corrosion in anaerobic environments (*127*). Additionally, methanogenic archea (including *M. barkeri*) have been shown to use elemental iron as sole electron donor (*127*, *128*). In environmental bioelectrochemical systems, there are results that demonstrate conversion of biological current into methane by electromethanogenesis (*129*).

Previous studies demonstrate methanogens use Fe(III) oxide as an electron acceptor with hydrogen as electron donor; AQDS greatly accelerated Fe(III) reduction (*130*). Possible hydrogen production both in bioelectrochemical systems and elemental iron (and other metals) (*131*) complicate the ability to determine if methanogens are directly accepting electrons from these solid-phase materials or if they are using the hydrogen that is most likely produced. Most bioelectrochemical systems poise electrodes at negative potentials, in some cases negative enough that hydrogen is likely to be produced (*132*). This study examines a range of potentials well above the potential where hydrogen (-410 mV) can be produced at the electrode.

Only recently has the possibility of methane producing biocathodes been demonstrated (*129*), however here also the mechanisms remain unclear. Energetically, methanogens should be able to reduce carbon dioxide by an electrode because ATP synthesis can occur from both proton and sodium pumps (*133*). In this study, bioelectrochemical systems were developed to study isolated, cultured methanogens, *M. barkeri* and *M. acetivorans*, to determine their EET capabilities, specifically whether they are capable of using a solid-phase conductor for methangenesis and growth. The methanogens chosen for these experiments allow us to determine how the presence of these [NiFe]-hydrogenases dictate the EET abilities of methanogens (*134*). Additionally, methane has practical applications as a clean and renewable energy source.

The production and utilization of methane as an energy source can close an important loop in biogeochemical cycling of carbon, allowing for a recycling of energy that is initially trapped in organic compounds through the conversion of solar energy.

4.2 Materials and methods

4.2.1 Methanogen species, media, and growth conditions

Methanosarcina barkeri Fusaro and *Methanosarcina acetivorans* C2A were the methanogen species used in these experiments. *M. barkeri* Fusaro and *M. acetivorans* C2A were grown on the same media high-salt (HS) medium as described previously (*135*) dithiothreitol (0.4 mM) instead of Na2S·9H2O was used as the reductant for growth at 37°C. For experiments, *M. barkeri* Fusaro inoculum was grown on 80% hydrogen / 20% carbon dioxide (H2/CO2) at 20 kPa to OD_{420} of 0.2-0.4 and *M. acetivorans* C2A inoculum was grown on methanol (125 mM) to OD_{420} of 0.6-0.8. Optical density (OD_{420}) was determined with a 4802 spectrophotometer (Cole Parmer, Vernon Hills, IL, USA).

4.2.2 Bioelectrochemical system and conditions

The bioelectrochemical systems (BES) consisted of new, acid-washed 150 mL borosilicate glass H-cell reactors equipped with two butyl rubber sampling ports in the cathodic and anodic chambers (Adams and Chittenden Scientific Glass, Berkeley, CA, USA) (Fig. 4.1). A vacuum clamp held the anodic and cathodic chambers together, and electrolytes were separated using a cation-exchange membrane (Nafion® 117) with an active cross-section of 20 cm^2 (Fuel Cell Store, Boulder, CO, USA). The working electrodes consisted of spectroscopically pure 3/16" diameter graphite evaporation rods (SPI 01688-FA, Structure Probe Inc, West Chester, PA, USA) that were mechanically polished with 1200 grit sandpaper. Each reactor was fitted with three graphite rods to provide a total immersed projected electrode surface area of 20 cm^2. The rods were sealed into fitted rubber stoppers which were then secured with a modified cap to expose rod ends outside the reactor. Outside the reactor, rods were electrically connected to one potentiostat using alligator clips (described below). The counter electrode consisted of graphite cloth which was mechanically attached to a titanium wire and suspended in the counter chamber. The distance between working and counter electrode was approximately 10 cm. Assembled BES reactors were sterilized by autoclaving and placed inside an anaerobic chamber (Coy) by a combination of 2% hydrogen

and palladium catalysts. The temperature of the anaerobic chamber was maintained at 37°C. Ag/AgCl reference electrodes were custom-made using glass tubing (4 mm KIMAX®), silver wire (0.5 mm diameter) and porous Vycor tips (1/8" diameter, MF-2064, BASi). Reference electrodes were calibrated prior to each experiment before reaching anaerobic conditions, sterilized with ethanol, and placed in the counter chamber for the duration of the experiments. Each experiment consisted of at least one closed abiotic, two or three closed biotic reactors, and two or three open biotic reactors. All reactors were assembled the same way and only the biotic reactors were inoculated with cells.

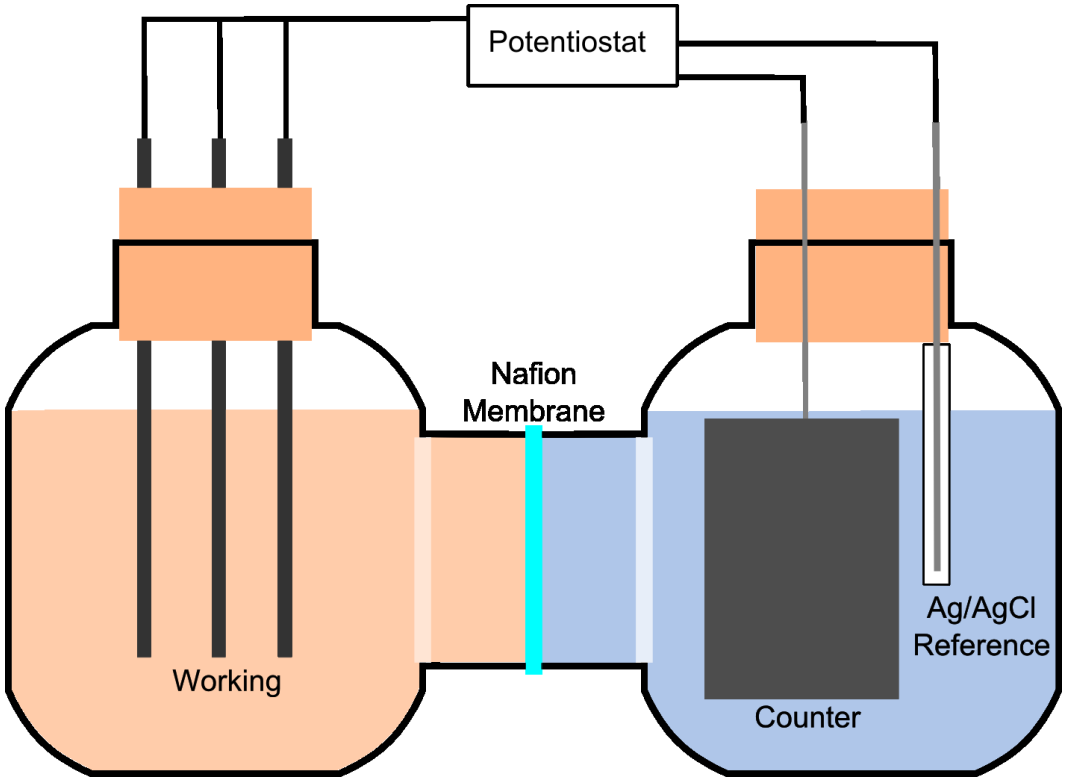

Figure 4.1. The bioelectrochemical system design (as described in section 4.2.2)

4.2.3 Electrical conditions

The closed or connected reactors were poised using custom-built potentiostats engineered for microbial chronoamperometry (Karma Electronics Inc., Somerville, MA, USA). Data was collected through an Omega DAQ (OMB-DAQ-56) every 5 seconds using provided software (Omega Engineering, Inc.) The reactors were poised at varying potentials of +400 mV and -300 mV vs. Standard Hydrogen Electrode (SHE). The open reactors had no electrical connections and were used as a biotic control. Closed reactors with the same growth media and not inoculated with methanogen cells were used as an abiotic control.

4.2.4 Experimental process and sampling

The reactors assembled with anerobic media (HS for *M. barkeri* Fusaro and *M. acetivorans* C2A) in the working side of the reactor and anaerobic PIPES (50 mM, pH 6.8) with added salts to be isosmotic with the media was in the counter side. The working sides of the reactors were inoculated with a volume of cells corresponding to an initial OD_{420} of 0.04-0.1 for *M. barkeri* or 0.4-0.5 for *M. acetivorans*. Prior to experimentation, a 1 to 2 mL sample of each culture was pelleted and stored at -80°C for total protein determination. Also, 1 mL of media was withdrawn from the reactors immediately following inoculation and

used for optical density (OD_{420}) determination with a 4802 spectrophotometer (Cole Parmer, Vernon Hills, IL, USA), and for pH measurements (Inlab® Expert Pro pH meter and probe, Mettler Toledo, Schwerzback, Switzerland). Due to the slow growth of methanogens, experiments lasted 3-4 days. At the end of each experiment, two of the electrodes were immediately dipped into RNA*later*™ for RNA extraction. Also, 50 mL of planktonic cells were immediately preserved in RNA*later*™ (Qiagen, Valencia, CA, USA) and filtered on a polyethersulfone (PES) membrane for RNA extraction (Corning, Tewksbury, MA, USA). All RNA samples were stored at -80°C. A second electrode was cut into ~5 mm pieces and transferred into fixatives or staining solutions for microscopic analyses (described below). Post experimentation, 1 mL of planktonic cells was sampled for OD_{420} determination and 2 to 4 mL for pH measurements. The remaining culture volume was then filtered on a 0.2 μm cellulose acetate filter (Corning, Tewksbury, MA, USA) and kept at -80°C until processed for total protein analysis.

4.2.5 Methane and hydrogen measurements

Initial and final methane headshot measurements (50ul) were taken from both sides of each reactor, since methane can cross Nafion membrane, and measured on a gas chromatograph (Hewlett Packard, 5890 Series II). To

determine the measured concentration, a five point calibration was conducted by taking different volumes from a 2% methane stock. Hydrogen headshot measurements from a *M. barkeri Fusaro* experiment at -300 mV vs. SHE were measured on a gas chromatograph mass spectrometer (Agilent Technologies, 5975C inert XC MSD) along with three calibration samples to determine concentration.

4.2.6 Scanning electron microscopy (SEM) sample preparation and imaging

Sections of the electrode were cut using sterile techniques and immediately placed into a sterile microcentrifuge tube containing 5% glutaraldehyde (Electron Microscopy Sciences, Hatfield, PA, USA) in 1X PBS. Samples were held at 4°C for 24 hours before being subjected to ethanol dehydration by placing them in 35%, 50%, 70%, 95%, 100% ethanol (200 proof) in PBS or 0.1 M PBS solutions for ten minutes each. The 100% ethanol solution was changed five times, and the sample was left in ethanol for critical point drying (Autosamdri 815 A; Tousimis, Inc.) with a 15-minute purge time. The samples were adhered to SEM posts with carbon film tape and then imaged with a SEM at 5 kV (JEOL, Inc.). This work was performed at the Harvard Center for Nanoscale Systems (CNS).

4.2.7 Total protein measurements

Protein estimations were performed by dissolving total protein in cell pellets or cells on membranes with 2 M Urea and using the BCA kit (Thermo Fisher Scientific, Rockford , IL) as previously described (*101*). Bovine serum albumin was used as the standard as previously described (*136*).

4.3 Results

4.3.1 Methane production dependence on potential

The primary motivation for these experiments was to ascertain if two methanogens, *M. acetivorans* and *M. barkeri*, were able to use current derived from a poised electrode for the production of methane. In all experiments, open circuit controls with no electrical connection were conducted to evaluate the effects of introducing a poised electrode to these methanogens. The methane produced under closed and open circuit conditions are reported for each experiment at a given potential (Figs. 4.2 and 4.3). Any deviation of the closed circuit value from open circuit is due to the effect of having a poised electrode present. From these results, *M. barkeri* produces more methane with an electrode with under any of the potentials tested (Fig. 4.2). While for *M. acetivorans*, there is no difference between open and closed circuit methane

(Fig. 4.3) production values indicating that *M. acetivorans* does not have an increase in methanogenesis under the presence of a poised electrode. The change in methane production due to having a poised electrode is calculated from the final minus initial amounts of methane measured. Variation in these values between experiments could be accounted for by differences in initial cell density.

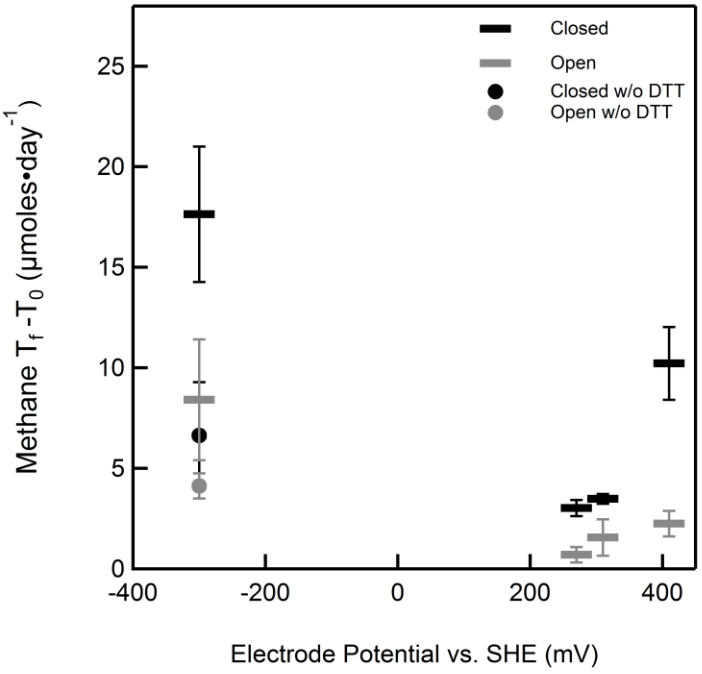

Figure 4.2. Methane production versus electrode potential for *M. barkeri.* The rate of change of methane production versus for electrically closed BES reactors at different working electrode potentials (-300, 270, 310, and 410 mV versus SHE) and for the corresponding open circuit reactor at that given potential. For each potential, the difference in methane production between closed and open circuits should be examined for the effect of the poised electrode on methanogenesis. Experiments with methanogen media containing 0.4 mM of dithiothreitol (DTT) and one with no DTT in the media are reported.

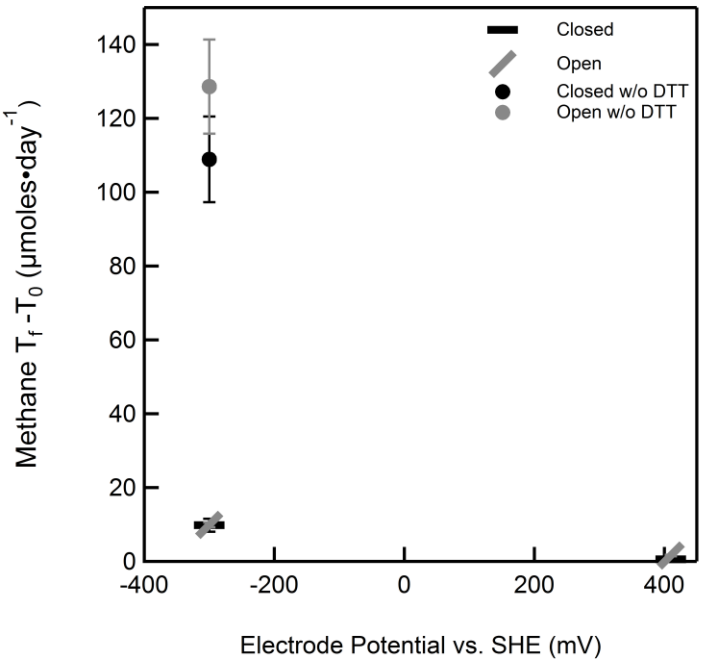

Figure 4.3. Methane production versus electrode potential for *M. acetivorans.*
The rate of change of methane production versus for electrically closed BES reactors at different working electrode potentials (-300 and 410 mV versus SHE) and for the corresponding open circuit reactor at that given potential. For each potential, the difference in methane production between closed and open circuits should be examined for the effect of the poised electrode on methanogenesis. Experiments with methanogen media containing 0.4 mM of dithiothreitol (DTT) and one with no DTT in the media are reported.

Normalizing to optical density of the initial cell density reconciles any contribution to varying cell density among different experiments (Table 4.2). The final optical density was recorded, but it was clear from this data that cell lysis and/or clumping occurred because of the reduced values measured at the final time point. However, any lysed cells did contribute to any methane production so normalizing by an initial measure of cell density is the most

comprehensive way to account for this variation among experiments. By assuming that the open circuit methane production values are a baseline for the amount of methane produced for a given experimental conditions, the difference between closed and open circuit values indicate the degree to which having a poised electrode enhances methane production by methanogenesis. By plotting this difference in methane production, a net positive value indicates that methane production increases under that experimental condition (Fig. 4.4). This is the case for *M. barkeri*, where the delta values are greater than zero for all potentials (~100 $\mu moles \cdot day^{-1}$). Additionally, removing DTT from the media increased the methane production in the closed circuit for *M. acetivorans*.

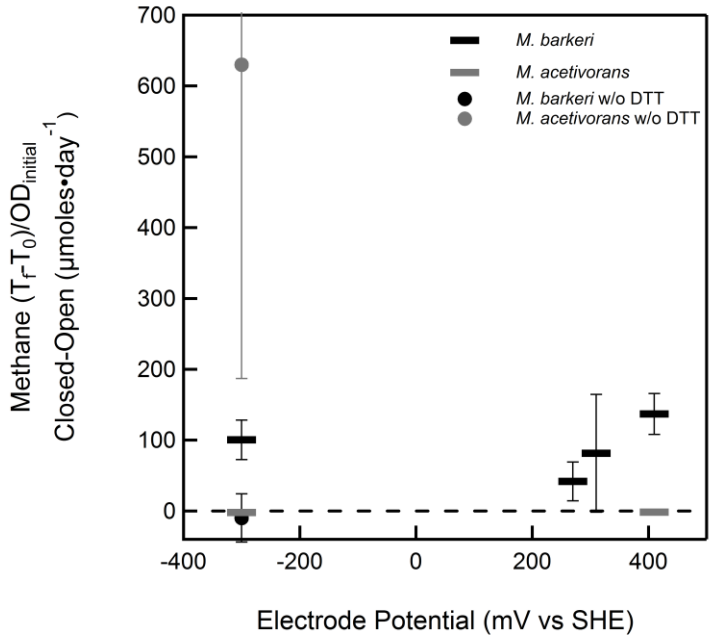

Figure 4.4. Difference between closed and open circuit methane production normalized to initial optical density versus electrode potential.
The rate of change of methane production between closed and open circuit BES reactors is normalized to initial optical density to normalize any differences due to cell density in the inoculum. This allows for comparison between the different potentials. A positive value indicates the poised electrode had a positive effect in increasing methane production. While values near zero indicate the treatment had a null effect.

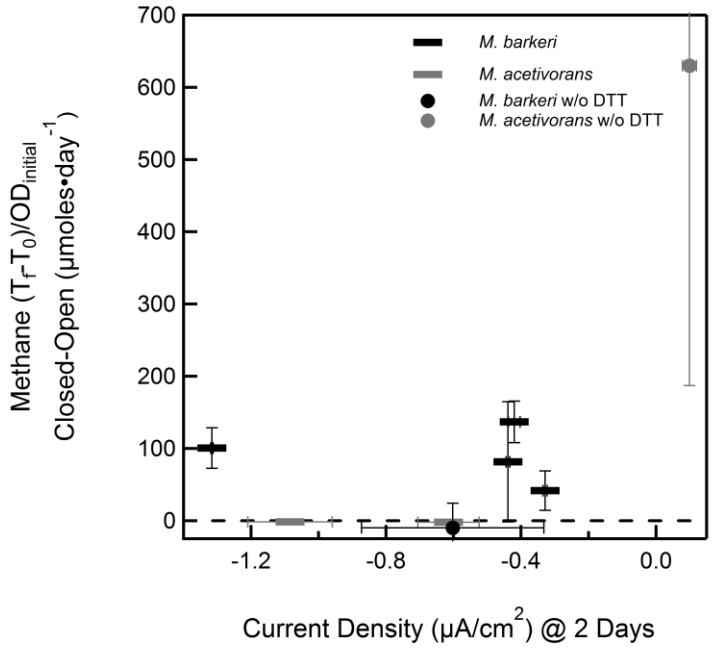

Figure 4.5. Difference between closed and open circuit methane production normalized to initial optical density versus current density.
The difference in methane production between closed and open circuit treatments is plotted against current density for the closed circuit BES reactors. The current density after two days was measured for each closed circuit experiment and plotted in the above graph on the x-axis. A negative current density corresponds to a net anodic current. The different media conditions with 0.4 mM DTT and without for both *M. barkeri* and *M. acetivorans* are shown. These different conditions appear to have more of an effect on methane production than the value of current density.

4.3.3 Total protein, OD, and imaging

The total protein was measured both in the initial and final time point samples for all experiments (Table 4.1). These values have comparable trends to the optical density (at a wavelength of 420nm) measurements for the initial and final samples (Table 4.2). Overall, the total protein values remain similar

or less than the starting values. This could occur due to cell lysis, which methanogens especially *M. barkeri* are known for. Another possibility is that not all of the cell material was removed from the filter prior to analysis. Imaging was conducted to determine if there were any trends on the population of methanogen cells on the surface of the electrode. In both open and closed circuit electrodes, there were patches of cells but no uniform cell coverage making it difficult to calculate a cell density on the electrode. In general, *M. acetivorans* had a higher coverage than *M. barkeri* most likely due to a higher cell density present in the BES reactor. These results indicate that the electrode, regardless if it was poised to a potential, was available as a surface for cell attachment.

Table 4.1. Total protein measurements
Total protein measurements reported in μg/mL for both initial and final time points in the experiments conducted for both methanogens.

M. barkeri				
Potential (mV vs. SHE)	**Closed**		**Open**	
	T_0	**T_f**	**T_0**	**T_f**
-300	510±80	600±400	550±90	1000±600
no DTT	640±40	100±20	500±90	100±10
+270	450±50	420±20	700±200	320±10
+310	600±300	350±20	600±200	430±30
+410	1600±100	300±100	3000±2000	340±3

M. acetivorans				
Potential (mV vs. SHE)	**Closed**		**Open**	
	T_0	**T_f**	**T_0**	**T_f**
-300	1300±200	2200±300	900±200	1500±600
no DTT	400±100	180±30	400±100	200±40
+410	2600±600	1300±800	1900±800	1100±200

Table 4.2. Optical density measurements
Optical density at a wavelength of 420 nm for both initial and final time points in the experiments conducted for both methanogens.

M. barkeri				
Potential (mV vs. SHE)	**Closed**		**Open**	
	T_0	**T_f**	**T_0**	**T_f**
-300	0.11±0.02	0.2±0.1	0.13±0.01	0.2±0.1
no DTT	0.054±0.008	0.007±0.009	0.032±0.005	0.005±0.004
+270	0.07±0.04	0.06±0.02	0.08±0.03	0.033±0.004
+310	0.04±0.04	0.07±0.04	0.06±0.05	0.06±0.05
+410	0.053±0.007	0.066±0.006	0.04±0.01	0.069±0.001

M. acetivorans				
Potential (mV vs. SHE)	**Closed**		**Open**	
	T_0	**T_f**	**T_0**	**T_f**
-300	0.48±0.05	0.8±0.3	0.44±0.02	0.9±3
no DTT	0.03±0.01	0.005±0.004	0.05±0.004	0.03±0.01
+410	0.60±0.08	0.9±0.2	0.6±0.1	0.8±0.4

4.3.4 Abiotic constituents contribute to overall current

The current direction for the majority of the biotic experiments (except for the *M. acetivorans* without DTT at -300 mV) was anodic which means that electrons are being donated to the electrode either by the microorganism or media constituent(s). To explore the effect of the potential, the abiotic current was evaluated as a function of potential (Fig. 4.6), because different media constituents might contribute to the current at different electrode potentials, including cysteine and DTT. In addition, media was prepared without DTT to

explore the effect of DTT in the media on abiotc current. Upon the removal of DTT, the abiotic current became positive, or a net cathodic current. Abiotic current densities with DTT are all within the same range (-0.2 to -0.4 $\mu A \cdot cm^{-2}$) while when DTT is removed the value increased (0.2 $\mu A \cdot cm^{-2}$).

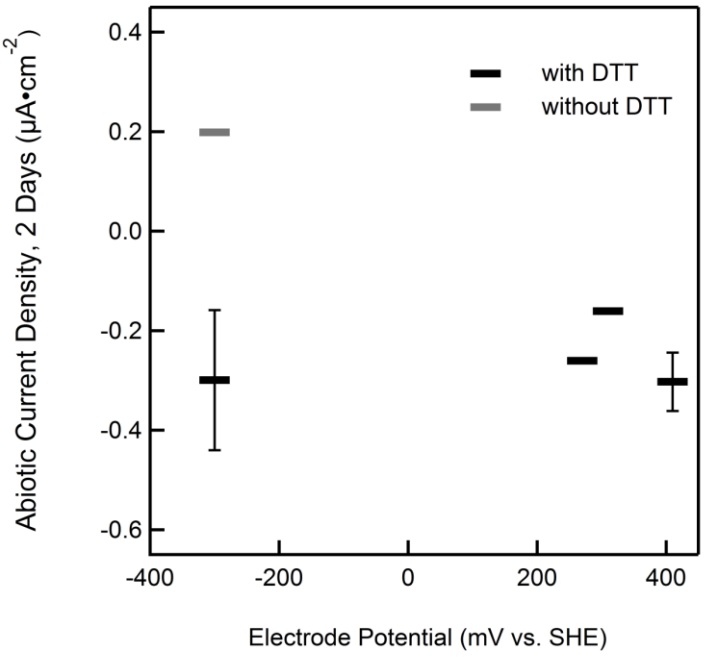

Figure 4.6 Abiotic current density versus electrode potential.
The abiotic current density at two days for the working electrode potentials used in these experiments is plotted above. Media containing the 0.4 mM DTT (in black) has a more negative current density value than media without the DTT (in grey).

4.4 Discussion

These experiments show that introducing a poised electrode stimulates methanogenesis for *M. barkeri* but not for *M. acetivorans*. A range of potentials (from -300 to +400 mV vs. SHE) show a range of similar response and are well above the potential where hydrogen (-410 mV vs. SHE) can be produced ruling out the possibility that *M. barkeri* is producing methane from hydrogen. Additionally, methanogenesis by *M. acetivorans* appears to be stimulated without the presence of DTT at -300 mV. These electrode potentials do fit within the range of iron minerals that could either be used as an electron donor or acceptor (-300 to +300 mV) (*95*).

Since there were few cells present on the electrodes, this suggests that indirect EET mechanisms were involved by *M. barkeri*. One possible electron shuttle is cysteine (E_0'= -204 mV), an essential amino acid commonly encountered in soils, and widely used reducing agent in growth media, including the media used in these experiments. Cysteine has been shown to mediate interspecies electron transfer in cocultures of *Geobacter sulfurreducens* and *Wolinella succinogenes* (*138*). Furthermore, addition of cysteine to a pure *G. sulfurreducens* culture increased 8 to 11 times the reduction rate of extracellular, poorly crystalline Fe(III) demonstrating its ability to act as an electron shuttle (*139*). Dithiothreitol (DTT) is also a redox

active molecule (E_0'= -330 mV). When DTT is removed from the media for a *M. barkeri* experiment, the increase in methane production due to an electrode is removed, suggesting that having a soluble redox active shuttle does play a role in the phenomena observed. Interestingly, when DTT is removed from *M. acetivorans* it is the only time when an increase in methane is observed by this methanogen throughout these experiments. These results suggest that the soluble cysteine and/or DTT in the media contribute to the ability for EET by these methanogens, but seem to have opposite effects.

The microbial mechanism for EET can be studied with this BES design. One major physiological difference between these two species is that *M. barkeri* contains both hydrogenases and cytochromes while *M. acetivorans* has only cytochromes. Since *M. barkeri* does show an increase in methane production in the presence of an electrode and *M. acetivorans* does not, these experiments suggest that membrane associated or bound [NiFe]-hydrogenases play an important role in electron transfer to an insoluble material. Many methanogen hydrogenases have metalloprotein components, such as the Vho and Vht hydrogenases which have a Ni-Fe subcomponents (*125*, *126*). The metalloprotein components of the hydrogenases are active sites that could transport electrons to the methanophenazine pool that has recently been shown to function as a key membrane bound electron shuttle during methanogenesis (*19*) and is most likely involved in electron transfer in this experiments.

While the methanogenesis by *M. barkeri* is stimulated by introducing a poised potential, developing a complete understanding of the direction of electron flow between methanogen and electrode is complex (Fig. 4.7). In methanogenesis where carbon dioxide or bicarbonate is the electron acceptor, the electrode would be the source of electrons. In all experiments, except for the experiment with *M. acetivorans* without DTT, the biotic current was more negative (anodic) than the abiotic current. This suggests that introducing methanogens to the BES reactors causes more electrons to be donated to the electrode.

If this is the case, how is methane being produced? One possible explanation is that *M. barkeri* is using energy stores, such as glycogen, as the electron donor and the electrode as the electron acceptor. It might be possible that as time progressed in these experiments, the direction of the current would slowly become more positive, indicating that a shift in the metabolism has occurred to where the electrode is the electron donor and carbon dioxide is the electron acceptor.

As part of conducting these experiments, understanding how the abiotic media components influence current density and direction was important. Abiotic experiments with and without DTT demonstrate that the presence of the reductant influences the overall net current direction. This stresses the importance of conducting abiotic controls for BES reactor experiments. There

are many factors (both abiotic and biotic) that can contribute to current flow in these systems (Fig. 4.7). Having an understanding of what the background current entails further informs the biological signal present.

These experiments demonstrate that for *M. barkeri*, and possibly other methanogens with [NiFe]-hydrogenases (*124*), having a poised electrode stimulates methane production. Here, an experimental design for studying isolated methanogens was developed and can be used for future investigations into this phenomenon. Such results have implications for understanding the ability of methanogens to use a solid-phase mineral in methanogenesis as well as biotechnological applications. Methane is a byproduct that can be readily used in our energy infrastructure (*5*). In future applications where methanogenesis already occurs, simply introducing an electrode can stimulate and increase overall methane production.

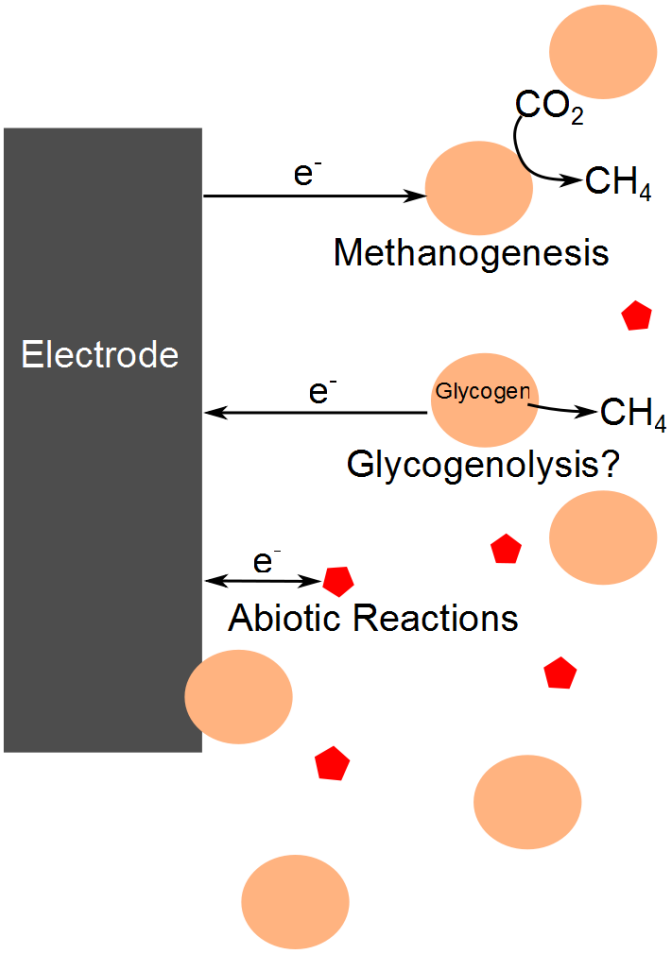

Figure 4.7. Possible biotic and abiotic reactions. This could include electron accepting reactions for methanogenesis from carbon dioxide, possible electron donating reactions by degrading glycogen stores in the methanogen, and electron transfer in either direction due to abiotic reactions from media components.

Bibliography

(1) Weber, K. A.; Achenbach, L. A.; Coates, J. D. Microorganisms pumping iron: anaerobic microbial iron oxidation and reduction. *Nat. Rev. Microbiol.* **2006**, *4*, 752–64.

(2) Hernandez, M. E.; Newman, D. K. Extracellular electron transfer. *Cell. Mol. Life Sci.* **2001**, *58*, 1562–1571.

(3) Logan, B. E. Exoelectrogenic bacteria that power microbial fuel cells. *Nat. Rev. Microbiol.* **2009**, *7*, 375–81.

(4) Du, Z.; Li, H.; Gu, T. A state of the art review on microbial fuel cells: a promising technology for wastewater treatment and bioenergy. *Biotechnol. Adv.* **2007**, *25*, 464–482.

(5) Rabaey, K.; Rozendal, R. A. Microbial electrosynthesis — revisiting the electrical route for microbial production. *Nat. Rev. Microbiol.* **2010**, *8*, 706–716.

(6) Rabaey, K.; Rodriguez, J.; Blackall, L. L.; Keller, J.; Gross, P.; Batstone, D.; Verstraete, W.; Nealson, K. H. Microbial ecology meets electrochemistry: electricity-driven and driving communities. *ISME J.* **2007**, *1*, 9–18.

(7) Madigan, M.; Martinko, J. *Brock Biology of Microorganisms*; 11th ed.; Pearson Prentice Hall: Upper Saddle River, NJ, 2006.

(8) Whitman, W. B.; Coleman, D. C.; Wiebe, W. J. Prokaryotes: the unseen majority. *PNAS* **1998**, *95*, 6578.

(9) White, D.; Drummond, J.; Fuqua, C. *The Physiology and Biochemsitry of Prokaryotes*; 4th ed.; Oxford University Press: New York, NY, 2012.

(10) Lovley, D. R. Extracellular electron transfer: wires, capacitors, iron lungs, and more. *Geobiology* **2008**, *6*, 225–31.

(11) Myers, C.; Nealson, K. H. Bacterial Manganese Reduction and Growth with Manganese Oxide as the Sole Electron Acceptor. *Science* **1988**, *240*, 1319–1321.

(12) Lovley, D. R.; Phillips, E. J. Novel mode of microbial energy metabolism: organic carbon oxidation coupled to dissimilatory reduction of iron or manganese. *Appl. Environ. Microbiol.* **1988**, *54*, 1472–80.

(13) Bond, D. R.; Lovley, D. R. Electricity Production by Geobacter sulfurreducens Attached to Electrodes. *Appl. Environ. Microbiol.* **2003**, *69*, 1548–1555.

(14) Hartshorne, R. S.; Reardon, C. L.; Ross, D.; Nuester, J.; Clarke, T. a; Gates, A. J.; Mills, P. C.; Fredrickson, J. K.; Zachara, J. M.; Shi, L.; Beliaev, A. S.; Marshall, M. J.; Tien, M.; Brantley, S.; Butt, J. N.; Richardson, D. J. Characterization of an electron conduit between bacteria and the extracellular environment. *PNAS* **2009**, *106*, 22169–74.

(15) Holmes, D. E.; Chaudhuri, S. K.; Nevin, K. P.; Mehta, T.; Methé, B. a; Liu, A.; Ward, J. E.; Woodard, T. L.; Webster, J.; Lovley, D. R. Microarray and genetic analysis of electron transfer to electrodes in Geobacter sulfurreducens. *Environ. Microbiol.* **2006**, *8*, 1805–15.

(16) Reguera, G.; McCarthy, K. D.; Mehta, T.; Nicoll, J. S.; Tuominen, M. T.; Lovley, D. R. Extracellular electron transfer via microbial nanowires. *Nature* **2005**, *435*, 1098–101.

(17) Reguera, G.; Nevin, K. P.; Nicoll, J. S.; Covalla, S. F.; Woodard, T. L.; Lovley, D. R. Biofilm and nanowire production leads to increased current in Geobacter sulfurreducens fuel cells. *Appl. Environ. Microbiol.* **2006**, *72*, 7345–7348.

(18) Marsili, E.; Baron, D. B.; Shikhare, I. D.; Coursolle, D.; Gralnick, J. A.; Bond, D. R. Shewanella secretes flavins that mediate extracellular electron transfer. *PNAS* **2008**, *105*, 3968 –3973.

(19) Abken, H.; Tietze, M.; Brodersen, J. Isolation and characterization of methanophenazine and function of phenazines in membrane-bound electron transport of Methanosarcina mazei Gö1. *J. Bacteri* **1998**, *180*, 2027–2032.

(20) Kim, T. S.; Kim, B. H. Electron flow shift in Clostridium Acetobutylicum fermentation by electrochemically introduced reducing equivalent. *Biotechnol. Lett* **1988**, *10*, 123–128.

(21) Potter, M. C. On the difference of potential due to the vital activity of microorganisms. *Proc. Durham Univ. Phil. Soc.* **1910**, *3*, 245–249.

(22) Lovley, D. R.; Nevin, K. P. A shift in the current: new applications and concepts for microbe-electrode electron exchange. *Curr. Opin. Biotechnol.* **2011**, *22*, 1–8.

(23) Logan, B. E.; Hamelers, B.; Rozendal, R.; Schroder, U.; Keller, J.; Freguia, S.; Aelterman, P.; Verstraete, W.; Rabaey, K. Microbial fuel cells: Methodology and technology. *Environ. Sci. Technol* **2006**, *40*, 5181–5192.

(24) Lovley, D. R. Bug juice: Harvesting electricity with microorganisms. *Nat. Rev. Microbiol.* **2006**, *4*, 497–508.

(25) Lies, D. P.; Hernandez, M. E.; Kappler, A.; Mielke, R. E.; Gralnick, J. A.; Newman, D. K. Shewanella oneidensis MR-1 uses overlapping pathways for iron reduction at a distance and by direct contact under conditions relevant for biofilms. *Appl. Environ. Microbiol.* **2005**, *71*, 4414–4426.

(26) Rabaey, K.; Boon, N.; Höfte, M.; Verstraete, W. Microbial phenazine production enhances electron transfer in biofuel cells. *Environ. Sci. Technol.* **2005**, *39*, 3401–3408.

(27) Watanabe, K.; Manefield, M.; Lee, M.; Kouzuma, A. Electron shuttles in biotechnology. *Curr. Opin. Biotechnol.* **2009**, *20*, 633–641.

(28) Gorby, Y. A.; Yanina, S.; McLean, J. S.; Rosso, K. M.; Moyles, D.; Dohnalkova, A.; Beveridge, T. J.; Chang, I. S.; Kim, B. H.; Kim, K. S.; Culley, D. E.; Reed, S. B.; Romine, M. F.; Saffarini, D. A.; Hill, E. A.; Shi, L.; Elias, D. A.; Kennedy, D. W.; Pinchuk, G.; Watanabe, K.; Ishii, S.; Logan, B.; Nealson, K. H.; Fredrickson, J. K. Electrically conductive bacterial nanowires produced by Shewanella oneidensis strain MR-1 and other microorganisms. *PNAS* **2006**, *103*, 11358–11363.

(29) Logan, B. E.; Regan, J. M. Electricity-producing bacterial communities in microbial fuel cells. *Trends Microbiol.* **2006**, *14*, 512–518.

(30) Girguis, P. R.; Nielsen, M. E.; Figueroa, I. Harnessing energy from marine productivity using bioelectrochemical systems. *Curr. Opin. Biotechnol.* **2010**, *21*, 252–258.

(31) Oh, S. T.; Kim, J. R.; Premier, G. C.; Lee, T. H.; Kim, C.; Sloan, W. T. Sustainable wastewater treatment: How might microbial fuel cells contribute. *Biotechnol. Adv.* **2010**, *28*, 871–881.

(32) Feng, Y.; Wang, X.; Logan, B. E.; Lee, H. Brewery wastewater treatment using air-cathode microbial fuel cells. *Appl. Microbiol. Biotechnol.* **2008**, *78*, 873–880.

(33) Rabaey, K.; Bützer, S.; Brown, S.; Keller, J.; Rozendal, R. A. High current generation coupled to caustic production using a lamellar bioelectrochemical system. *Environ. Sci. Technol.* **2010**, *44*, 4315–4321.

(34) Bullen, R. A.; Arnot, T. C.; Lakeman, J. B.; Walsh, F. C. Biofuel cells and their development. *Biosens. Bioelectron.* **2006**, *21*, 2015–2045.

(35) Logan, B. E. Simultaneous wastewater treatment and biological electricity generation. *Water Sci. Technol.* **2005**, *52*, 31–37.

(36) Shukla, A. K.; Suresh, P.; Berchmans, S.; Rajendran, A. Biological fuel cells and their applications. *Curr. Sci.* **2004**, *87*, 455–468.

(37) Tender, L. M.; Gray, S. A.; Groveman, E.; Lowy, D. A.; Kauffman, P.; Melhado, J.; Tyce, R. C.; Flynn, D.; Petrecca, R.; Dobarro, J. The first demonstration of a microbial fuel cell as a viable power supply: Powering a meteorological buoy. *J. Power Sources* **2008**, *179*, 571–575.

(38) Shantaram, A.; Beyenal, H.; Raajan, R.; Veluchamy, A.; Lewandowski, Z. Wireless sensors powered by microbial fuel cells. *Environ. Sci. Technol.* **2005**, *39*, 5037–5042.

(39) Nielsen, M. E.; Reimers, C. E.; Stecher, H. A. Enhanced power from chambered benthic microbial fuel cells. *Environ. Sci. Technol.* **2007**, *41*, 7895–7900.

(40) Rezaei, F.; Richard, T. L.; Brennan, R. A.; Logan, B. E. Substrate-enhanced microbial fuel cells for improved remote power generation from sediment-based systems. *Environ. Sci. Technol.* **2007**, *41*, 4053–4058.

(41) Tender, L. M.; Reimers, C. E.; Stecher, H. A.; Holmes, D. E.; Bond, D. R.; Lowy, D. A.; Pilobello, K.; Fertig, S. J.; Lovley, D. R. Harnessing microbially generated power on the seafloor. *Nat. Biotechnol.* **2002**, *20*, 821–825.

(42) Zuo, Y.; Maness, P.-C.; Logan, B. E. Electricity production from steam-exploded corn stover biomass. *Energy Fuels* **2006**, *20*, 1716–1721.

(43) Reimers, C. E.; Girguis, P.; Stecher, H. A.; Tender, L. M.; Ryckelynck, N.; Whaling, P. Microbial fuel cell energy from an ocean cold seep. *Geobiology* **2006**, *4*, 123–136.

(44) Fan, Y.; Hu, H.; Liu, H. Sustainable power generation in microbial fuel cells using bicarbonate buffer and proton transfer mechanisms. *Environ. Sci. Technol.* **2007**, *41*, 8154–8158.

(45) Liu, H.; Cheng, S.; Huang, L.; Logan, B. E. Scale-up of membrane-free single-chamber microbial fuel cells. *J. Power Sources* **2008**, *179*, 274–279.

(46) Rozendal, R. A.; Hamelers, H. V. M.; Rabaey, K.; Keller, J.; Buisman, C. J. N. Towards practical implementation of bioelectrochemical wastewater treatment. *Trends Biotechnol.* **2008**, *26*, 450–459.

(47) Dewan, A.; Beyenal, H.; Lewandowski, Z. Scaling up microbial fuel cells. *Environ. Sci. Technol.* **2008**, *42*, 7643–7648.

(48) Rabaey, K.; Clauwaert, P.; Aelterman, P.; Verstraete, W. Tubular microbial fuel cells for efficient electricity generation. *Environ. Sci. Technol.* **2005**, *39*, 8077–82.

(49) *Bioelectrochemical Systems*; Rabaey, K.; Angenent, L.; Schroder, U.; Keller, J., Eds.; IWA Publishing, 2010.

(50) Abrevaya, X. C.; Sacco, N.; Mauas, P. J. D.; Cortón, E. Archaea-based microbial fuel cell operating at high ionic strength conditions. *Extremophiles* **2011**, *15*, 633–642.

(51) Raghavulu, S. V.; Goud, R. K.; Sarma, P. N.; Mohan, S. V. Saccharomyces cerevisiae as anodic biocatalyst for power generation in biofuel cell: Influence of redox condition and substrate load. *Bioresour. Technol.* **2011**, *102*, 2751–2757.

(52) Yi, H.; Nevin, K. P.; Kim, B.-C.; Franks, A. E.; Klimes, A.; Tender, L. M.; Lovley, D. R. Selection of a variant of Geobacter sulfurreducens with enhanced capacity for current production in microbial fuel cells. *Biosens. Bioelectron.* **2009**, *24*, 3498–3503.

(53) Rabaey, K.; Boon, N.; Siciliano, S. D.; Verhaege, M.; Verstraete, W. Biofuel cells select for microbial consortia that self-mediate electron transfer. *Appl. Environ. Microbiol.* **2004**, *70*, 5373–5382.

(54) Pant, D.; Van Bogaert, G.; Diels, L.; Vanbroekhoven, K. A review of the substrates used in microbial fuel cells (MFCs) for sustainable energy production. *Bioresour. Technol.* **2010**, *101*, 1533–1543.

(55) Nielsen, M. E.; Wu, D. M.; Girguis, P. R.; Reimers, C. E. Influence of substrate on electron transfer mechanisms in chambered benthic microbial fuel cells. *Environ. Sci. Technol.* **2009**, *43*, 8671–8677.

(56) Catal, T.; Li, K.; Bermek, H.; Liu, H. Electricity production from twelve monosaccharides using microbial fuel cells. *J. Power Sources* **2008**, *175*, 196–200.

(57) Scott, K.; Cotlarciuc, I.; Hall, D.; Lakeman, J. B.; Browning, D. Power from marine sediment fuel cells: the influence of anode material. *J. Appl. Electrochem.* **2008**, *38*, 1313–1319.

(58) Lowy, D. A.; Tender, L. M.; Zeikus, J. G.; Park, D. H.; Lovley, D. R. Harvesting energy from the marine sediment-water interface II kinetic activity of anode materials. *Biosens. Bioelectron.* **2006**, *21*, 2058–2063.

(59) Liu, R.-H.; Sheng, G.-P.; Sun, M.; Zang, G.-L.; Li, W.-W.; Tong, Z.-H.; Dong, F.; Lam, M. H.-W.; Yu, H.-Q.; Hon-Wah Lam, M. Enhanced reductive degradation of methyl orange in a microbial fuel cell through cathode modification with redox mediators. *Appl. Microbiol. Biotechnol.* **2011**, *89*, 201–208.

(60) Milliken, C. E.; May, H. D. Sustained generation of electricity by the spore-forming, Gram-positive, Desulfitobacterium hafniense strain DCB2. *Appl. Microbiol. Biotechnol.* **2007**, *73*, 1180–1189.

(61) Torres, C. I.; Marcus, A. K.; Rittmann, B. E.; Legacy, N. Z. Proton transport inside the biofilm limits electrical current generation by anode-respiring bacteria. *Biotechnol. Bioeng.* **2008**, *100*, 872–881.

(62) Rozendal, R. A.; Hamelers, H. V. M.; Molenkamp, R. J.; Buisman, C. J. N. Performance of single chamber biocatalyzed electrolysis with different types of ion exchange membranes. *Water Res.* **2007**, *41*, 1984–1994.

(63) Grondin, F.; Perrier, M.; Tartakovsky, B. Microbial fuel cell operation with intermittent connection of the electrical load. *J. Power Sources* **2012**, *208*, 18–23.

(64) Dewan, A.; Beyenal, H.; Lewandowski, Z. Intermittent energy harvesting improves the performance of microbial fuel cells. *Environ. Sci. Technol.* **2009**, *43*, 4600–4605.

(65) Liang, P.; Wu, W.; Wei, J.; Yuan, L.; Xia, X.; Huang, X. Alternate charging and discharging of capacitor to enhance the electron production of bioelectrochemical systems. *Environ. Sci. Technol.* **2011**, *45*, 6647–6653.

(66) White, H. K.; Reimers, C. E.; Cordes, E. E.; Dilly, G. F.; Girguis, P. R. Quantitative population dynamics of microbial communities in plankton-fed microbial fuel cells. *ISME J.* **2009**, *3*, 635–646.

(67) Torres, C. I.; Krajmalnik-Brown, R.; Parameswaran, P.; Marcus, A. K.; Wanger, G.; Gorby, Y. A.; Rittmann, B. E. Selecting anode-respiring bacteria based on anode potential: phylogenetic, electrochemical, and microscopic characterization. *Environ. Sci. Technol.* **2009**, *43*, 9519–9524.

(68) Donovan, C.; Dewan, A.; Heo, D.; Beyenal, H. Batteryless, wireless sensor powered by a sediment microbial fuel cell. *Environ. Sci. Technol.* **2008**, *42*, 8591–8596.

(69) Lee, H.-S.; Torres, C. I.; Rittmann, B. E. Effects of substrate diffusion and anode potential on kinetic parameters for anode-respiring bacteria. *Environ. Sci. Technol.* **2009**, *43*, 7571–7577.

(70) Margulies, M.; Egholm, M.; Altman, W. E.; Attiya, S.; Bader, J. S.; Bemben, L. A.; Berka, J.; Braverman, M. S.; Chen, Y.-J.; Chen, Z.; Dewell, S. B.; Du, L.; Fierro, J. M.; Gomes, X. V.; Godwin, B. C.; He, W.; Helgesen, S.; Ho, C. H.; Irzyk, G. P.; Jando, S. C.; Alenquer, M. L. I.; Jarvie, T. P.; Jirage, K. B.; Kim, J.-B.; Knight, J. R.; Lanza, J. R.; Leamon, J. H.; Lefkowitz, S. M.; Lei, M.; Li, J.; Lohman, K. L.; Lu, H.; Makhijani, V. B.; McDade, K. E.; McKenna, M. P.; Myers, E. W.; Nickerson, E.; Nobile, J. R.; Plant, R.; Puc, B. P.; Ronan, M. T.; Roth, G.

T.; Sarkis, G. J.; Simons, J. F.; Simpson, J. W.; Srinivasan, M.; Tartaro, K. R.; Tomasz, A.; Vogt, K. A.; Volkmer, G. A.; Wang, S. H.; Wang, Y.; Weiner, M. P.; Yu, P.; Begley, R. F.; Rothberg, J. M. Genome sequencing in microfabricated high-density picolitre reactors. *Nature* **2005**, *437*, 376–380.

(71) Caporaso, J. G.; Kuczynski, J.; Stombaugh, J.; Bittinger, K.; Bushman, F. D.; Costello, E. K.; Fierer, N.; Peña, A. G.; Goodrich, J. K.; Gordon, J. I.; Huttley, G. A.; Kelley, S. T.; Knights, D.; Koenig, J. E.; Ley, R. E.; Lozupone, C. A.; Mcdonald, D.; Muegge, B. D.; Pirrung, M.; Reeder, J.; Sevinsky, J. R.; Turnbaugh, P. J.; Walters, W. A.; Widmann, J.; Yatsunenko, T.; Zaneveld, J.; Knight, R. QIIME allows analysis of high-throughput community sequencing data intensity normalization improves color calling in SOLiD sequencing. *Nat. Methods* **2010**, *7*, 335–336.

(72) Nielsen, M. E.; Reimers, C. E.; White, H. K.; Sharma, S.; Girguis, P. R. Sustainable energy from deep ocean cold seeps. *Energy Environ. Sci.* **2008**, *1*, 584–593.

(73) DeLong, E. F. Archaea in coastal marine environments. *PNAS* **1992**, *89*, 5685–9.

(74) Girguis, P. R.; Cozen, A. E.; Delong, E. F. Growth and population dynamics of anaerobic methane-oxidizing archaea and sulfate-reducing bacteria in a continuous-flow bioreactor. *Appl. Environ. Microbiol.* **2005**, *71*, 3725–3733.

(75) Girguis, P. R.; Orphan, V. J.; Hallam, S. J.; Delong, E. F. Growth and methane oxidation rates of anaerobic methanotrophic archaea in a continuous-flow bioreactor. *Appl. Environ. Microbiol.* **2003**, *69*, 5472–5482.

(76) Silva FISH Protocols. http://www.arb-silva.de/fish-probes/fish-protocols/.

(77) Bard, A. J.; Faulkner, L. R. *Electrochemical Methods: Fundamentals and Applications*; 2nd ed.; John Wiley & Sons, Inc.: New York, NY, USA, 2000; p. 35.

(78) Uría, N.; Berbel, X. M.; Sánchez, O.; Muñoz, F. X.; Mas, J. Transient storage of electrical charge in biofilms of Shewanella oneidensis MR-1 growing in a microbial fuel cell. *Environ. Sci. Technol.* **2011**, *45*, 10250–10256.

(79) Schrott, G. D.; Bonanni, P. S.; Robuschi, L.; Esteve-Nunez, Abraham Busalmen, J. P. Electrochemical insight into the mechanism of electron transport in biofilms of Geobacter sulfurreducens. *Electrochim. Acta* **2011**, *56*, 10791–10795.

(80) He, Z.; Wagner, N.; Minteer, S. D.; Angenent, L. T. An upflow microbial fuel cell with an interior cathode: assessment of the internal resistance by impedance spectroscopy. *Environ. Sci. Technol.* **2006**, *40*, 5212–5217.

(81) Ramasamy, R. P.; Ren, Z.; Mench, M. M.; Regan, J. M. Impact of initial biofilm growth on the anode impedance of microbial fuel cells. *Biotechnol. Bioeng.* **2008**, *101*, 101–108.

(82) Millero, F. J.; Lee, K.; Roche, M. Distribution of alkalinity in the surface waters of the major oceans. *Mar. Chem.* **1998**, *60*, 111–130.

(83) Franks, A. E.; Nevin, K. P.; Jia, H.; Izallalen, M.; Woodard, T. L.; Lovley, D. R. Novel strategy for three-dimensional real-time imaging of microbial fuel cell communities: monitoring the inhibitory effects of proton accumulation within the anode biofilm. *Energy Environ. Sci.* **2009**, *2*, 113–119.

(84) Millero, F. J. Thermodynamics of the carbon dioxide system in the oceans. *Science* **1995**, *59*, 661–677.

(85) Lovley, D. R.; Roden, E. E.; Phillips, E. J. Enzymatic iron and uranium reduction by sulfate-reducing bacteria. *Mar. Geol.* **1993**, *113*, 41–53.

(86) Holmes, D. E.; Bond, D. R.; Lovley, D. R. Electron transfer by Desulfobulbus propionicus to Fe(III) and graphite electrodes. *Appl. Environ. Microbiol.* **2004**, *70*, 1234–1237.

(87) Lovley, D. R.; Phillips, E. J. Novel processes for anaerobic sulfate production from elemental sulfur by sulfate-reducing bacteria. *Appl. Environ. Microbiol.* **1994**, *60*, 2394–2399.

(88) Holmes, D. E.; Bond, D. R.; O'Neil, R. A.; Reimers, C. E.; Tender, L. R.; Lovley, D. R. Microbial communities associated with electrodes harvesting electricity from a variety of aquatic sediments. *Microb. Ecol.* **2004**, *48*, 178–190.

(89) Finster, K.; Liesack, W.; Thamdrup, B. Elemental sulfur and thiosulfate disproportionation by Desulfocapsa sulfoexigens sp. nov., a new anaerobic bacterium isolated from marine surface sediment. *Appl. Environ. Microbiol.* **1998**, *64*, 119–125.

(90) Knittel, K.; Boetius, A. Anaerobic oxidation of methane: progress with an unknown process. *Annu. Rev. Microbiol.* **2009**, *63*, 311–334.

(91) Boetius, A.; Ravenschlag, K.; Schubert, C. J.; Rickert, D.; Widdel, F.; Gieseke, A.; Amann, R.; Jørgensen, B. B.; Witte, U.; Pfannkuche, O. A marine microbial consortium apparently mediating anaerobic oxidation of methane. *Nature* **2000**, *407*, 623–626.

(92) Lovley, D. R. Dissimilatory Fe(III) and Mn(IV) reduction. *Microbiol. Rev.* **1991**, *55*, 259–287.

(93) Baker, B. J.; Banfield, J. F. Microbial communities in acid mine drainage. *FEMS Microbiol. Ecol.* **2003**, *44*, 139–152.

(94) Edwards, K. J.; Bach, W.; Rogers, D. R. Geomicrobiology of the ocean crust: a role for chemoautotrophic Fe-bacteria. *Biol. Bull.* **2003**, *204*, 180–185.

(95) Bird, L. J.; Bonnefoy, V.; Newman, D. K. Bioenergetic challenges of microbial iron metabolisms. *Trends Microbiol.* **2011**, *19*, 330–340.

(96) Miot, J.; Benzerara, K.; Obst, M.; Kappler, A.; Hegler, F.; Schädler, S.; Bouchez, C.; Guyot, F.; Morin, G. Extracellular iron biomineralization by photoautotrophic iron-oxidizing bacteria. *Appl. Environ. Microbiol.* **2009**, *75*, 5586–5591.

(97) Shelobolina, E.; Konishi, H.; Xu, H.; Benzine, J.; Xiong, M. Y.; Wu, T.; Blöthe, M.; Roden, E. Isolation of phyllosilicate-iron redox cycling microorganisms from an illite-smectite rich hydromorphic soil. *Fronti. Microbiol.* **2012**, *3*, 1–10.

(98) Summers, Z. M.; Gralnick, J. A.; Bond, D. R. Cultivation of an obligate Fe(II)-oxidizing lithoautotrophic bacterium using electrodes. *mBio* **2013**, *4*, 1–4.

(99) Jiao, Y.; Kappler, A.; Croal, L. R.; Newman, D. K. Isolation and characterization of a genetically tractable photoautotrophic Fe (II) -

oxidizing bacterium , Rhodopseudomonas palustris strain TIE-1. *Appl. Environ. Microbiol.* **2005**, *71*, 4487–4496.

(100) Jiao, Y.; Newman, D. K. The pio operon is essential for phototrophic Fe(II) oxidation in Rhodopseudomonas palustris TIE-1. *J. Bacteriol.* **2007**, *189*, 1765–1773.

(101) Bose, A.; Newman, D. K. Regulation of the phototrophic iron oxidation (pio) genes in Rhodopseudomonas palustris TIE-1 is mediated by the global regulator, FixK. *Mol. Microbiol.* **2011**, *79*, 63–75.

(102) Gorski, C. a; Handler, R. M.; Beard, B. L.; Pasakarnis, T.; Johnson, C. M.; Scherer, M. M. Fe atom exchange between aqueous Fe2+ and magnetite. *Environ. Sci. Technol.* **2012**, *46*, 12399–12407.

(103) Handler, R. M.; Beard, B. L.; Johnson, C. M.; Scherer, M. M. Atom exchange between aqueous Fe(II) and goethite: an Fe isotope tracer study. *Environ. Sci. Technol.* **2009**, *43*, 1102–1107.

(104) Rosenbaum, M.; Aulenta, F.; Villano, M.; Angenent, L. T. Cathodes as electron donors for microbial metabolism: Which extracellular electron transfer mechanisms are involved? *Bioresour. Technol.* **2011**, *102*, 324–333.

(105) Nevin, K. P.; Woodard, T. L.; Franks, A. E.; Summers, Z. M.; Lovley, D. R. Microbial electrosynthesis: Feeding microbes electricity to convert carbon dioxide and water to multicarbon extracellular organic compounds. *mBio* **2010**, *1*, 1–4.

(106) Ross, D. E.; Flynn, J. M.; Baron, D. B.; Gralnick, J. a; Bond, D. R. Towards electrosynthesis in Shewanella: Energetics of reversing the mtr pathway for reductive metabolism. *PlLoS One* **2011**, *6*, e16649.

(107) Erlandsen, S. L.; Kristich, C. J.; Dunny, G. M.; Wells, C. L. High-resolution visualization of the microbial glycocalyx with low-voltage scanning electron microscopy: Dependence on cationic dyes. *J. Histochem. Cytochem.* **2004**, *52*, 1427–1435.

(108) Markowitz, V. M.; Chen, I.-M. a; Palaniappan, K.; Chu, K.; Szeto, E.; Grechkin, Y.; Ratner, A.; Jacob, B.; Huang, J.; Williams, P.; Huntemann, M.; Anderson, I.; Mavromatis, K.; Ivanova, N. N.; Kyrpides, N. C. IMG:

the integrated microbial genomes database and comparative analysis system. *Nucleic Acid Res.* **2012**, *40*, D115–D122.

(109) Whittenbury, R.; McLee, a G. Rhodopseudomonas palustris and Rh. viridis--photosynthetic budding bacteria. *Archiv für Mikrobiologie* **1967**, *59*, 324–334.

(110) Romagnoli, S.; Tabita, F. R. A novel three-protein two-component system provides a regulatory twist on an established circuit to modulate expression of the cbbI region of Rhodopseudomonas palustris CGA010. *J. Bacteriol.* **2006**, *188*, 2780–2791.

(111) Wang, X.; Falcone, D. L.; Tabita, F. R. Reductive pentose phosphate-independent CO2 fixation in Rhodobacter sphaeroides and evidence that ribulose bisphosphate carboxylase/oxygenase activity serves to maintain the redox balance of the cell. *J. Bacteriol.* **1993**, *175*, 3372–3379.

(112) Overmann, J.; Garcia-Pichel, F. The Phototrophic Way of Life. In *The Prokaryotes*; Dworkin, M., Ed.; Springer, 2006; pp. 32–85.

(113) Xing, D.; Zuo, Y.; Cheng, S.; Regan, J. M.; Logan, B. E. Electricity generation by Rhodopseudomonas palustris DX-1. *Environ. Sci. Technol.* **2008**, *42*, 4146–4151.

(114) Cao, B.; Shi, L.; Brown, R. N.; Xiong, Y.; Fredrickson, J. K.; Romine, M. F.; Marshall, M. J.; Lipton, M. S.; Beyenal, H. Extracellular polymeric substances from Shewanella sp. HRCR-1 biofilms: Characterization by infrared spectroscopy and proteomics. *Environ. Microbiol.* **2011**, *13*, 1018–1031.

(115) Croal, L. R.; Jiao, Y.; Newman, D. K. The fox operon from Rhodobacter strain SW2 promotes phototrophic Fe(II) oxidation in Rhodobacter capsulatus SB1003. *J. Bacteriol.* **2007**, *189*, 1774–1782.

(116) Felmy, A. R.; Ilton, E. S.; Rosso, K. M.; Zachara, J. M. Interfacial reactivity of radionuclides: emerging paradigms from molecular-level observations. *Mineral. Mag.* **2011**, *75*, 2379–2391.

(117) Lu, A.; Li, Y.; Jin, S.; Wang, X.; Wu, X.-L.; Zeng, C.; Ding, H.; Hao, R.; Lv, M.; Wang, C.; Tang, Y.; Dong, H. Growth of non-phototrophic microorganisms using solar energy through mineral photocatalysis. *Nat. Commun.* **2012**, *3*, 768.

(118) Kato, S.; Hashimoto, K.; Watanabe, K. Microbial interspecies electron transfer via electric currents through conductive minerals. *PNAS* **2012**, *109*, 10042–10046.

(119) Nielsen, L. P.; Risgaard-Petersen, N.; Fossing, H.; Christensen, P. B.; Sayama, M. Electric currents couple spatially separated biogeochemical processes in marine sediment. *Nature* **2010**, *463*, 1071–1074.

(120) Ciani, A.; Goss, K.-U.; Schwarzenbach, R. P. Light penetration in soil and particulate minerals. *Eur. J. Soil Sci.* **2005**, *56*, 561–574.

(121) Thauer, R. K.; Kaster, A.-K.; Seedorf, H.; Buckel, W.; Hedderich, R. Methanogenic archaea: Ecologically relevant differences in energy conservation. *Nat. Rev. Microbiol.* **2008**, *6*, 579–591.

(122) Schoell, M. Multiple origins of methane in the earth. *Chem. Geol.* **1988**, *71*, 1–10.

(123) Hedderich, R.; Whitman, W. B. Physiology and Biochemistry of the Methane-Producing Archea. In *The Prokaryotes*; Dworkin, M.; Falkow, S.; Rosenberg, E.; Schleifer, K.-H.; Stackebrandt, E., Eds.; Springer New York: New York, NY, 2006; pp. 1050–1079.

(124) Thauer, R. K.; Kaster, A.-K.; Goenrich, M.; Schick, M.; Hiromoto, T.; Shima, S. Hydrogenases from methanogenic archaea, nickel, a novel cofactor, and H2 storage. *Annu. Rev. Biochem.* **2010**, *79*, 507–536.

(125) Deppenmeier, U. Purification and properties of a F420-nonreactive, membrane-bound hydrogenase from Methanosarcina strain Go1. *Arch. Microbiol.* **1992**, *157*, 505–511.

(126) Deppenmeier, U.; Göttingen, U.; Germany, G. Redox-driven proton translocation in methanogenic Archaea. *Cell. Mol. Life Sci.* **2002**, *59*, 1513–1533.

(127) Dinh, H. T.; Kuever, J.; Mußmann, M.; Hassel, A. W. Iron corrosion by novel anaerobic microorganisms. *Nature* **2004**, *427*, 829–832.

(128) Daniels, L.; Belay, N.; Rajagopal, B. S.; Weimer, P. J. Bacterial methanogenesis and growth from CO2 with elemental iron as the sole source of electrons. *Science (New York, N.Y.)* **1987**, *237*, 509–511.

(129) Cheng, S.; Xing, D.; Call, D. F.; Logan, B. E. Direct biological conversion of electrical current into methane by electromethanogenesis. *Environ. Sci. Technol.* **2009**, *43*, 3953–3958.

(130) Bond, D. R.; Lovley, D. R. Reduction of Fe(III) oxide by methanogens in the presence and absence of extracellular quinones. *Environ. Microbiol.* **2002**, *4*, 115–124.

(131) Lorowitz, W. H.; Nagle Jr., D. P.; Tanner, R. S. Anaerobic oxidation of elemental metals coupled to methanogenesis by Methanobacterium thermoautotrophicum. *Environ. Sci. Technol* **1992**, *26*, 1606–1610.

(132) Villano, M.; Aulenta, F.; Ciucci, C.; Ferri, T.; Giuliano, A.; Majone, M. Bioelectrochemical reduction of CO2 to CH4 via direct and indirect extracellular electron transfer by a hydrogenophilic methanogenic culture. *Bioresour. Technol.* **2010**, *101*, 3085–3090.

(133) Deppenmeier, U.; Müller, V.; Gottschalk, G. Pathways of energy conservation in methanogenic archaea. *Arch. Microbiol.* **1996**, *165*, 149–163.

(134) Maeder, D. L.; Anderson, I.; Brettin, T. S.; Bruce, D. C.; Gilna, P.; Han, C. S.; Lapidus, A.; Metcalf, W. W.; Saunders, E.; Tapia, R.; Sowers, K. R. The Methanosarcina barkeri genome: comparative analysis with Methanosarcina acetivorans and Methanosarcina mazei reveals extensive rearrangement within methanosarcinal genomes. *J. Bacteriol.* **2006**, *188*, 7922–7931.

(135) Sowers, K. R.; Boone, J. E.; Gunsalus, R. P. Disaggregation of Methanosarcina spp . and growth as single cells at elevated osmolarity. *Appl. Environ. Microbiol.* **1993**, *59*, 3832–3839.

(136) Bose, A.; Kulkarni, G.; Metcalf, W. W. Regulation of putative methyl-sulphide methyltransferases in Methanosarcina acetivorans C2A. *Mol. Microbiol.* **2009**, *74*, 227–238.

(137) Tietze, M.; Beuchle, A.; Lamla, I.; Orth, N.; Dehler, M.; Greiner, G.; Beifuss, U. Redox potentials of methanophenazine and CoB-S-S-CoM, factors involved in electron transport in Methanogenic archaea. *ChemBioChem* **2003**, *4*, 333–335.

(138) Kaden, J.; S Galushko, A.; Schink, B. Cysteine-mediated electron transfer in syntrophic acetate oxidation by cocultures of Geobacter sulfurreducens and Wolinella succinogenes. *Arch. Microbiol.* **2002**, *178*, 53–58.

(139) Doong, R.-A.; Schink, B. Cysteine-mediated reductive dissolution of poorly crystalline iron(III) oxides by Geobacter sulfurreducens. *Environ. Sci. Technol.* **2002**, *36*, 2939–2945.

(140) Harold, F. *The Vital Force: A study of Bioenergetics*; W. H. Freeman and Company, 1986.

Appendix

Fluorescence in situ hybridization (FISH) methods

I. Detailed FISH sample preparation protocol

1. Heat two ovens: one to 46°C and another to 48°C. If you don't have two ovens, a 48°C water bath can be used.
2. Use PCR water to make a probe working solution (usually 50 ng DNA/ul).
3. Prepare both the hybridization and washing buffers (Table 1 and 2).
4. Prepare hybridization mixtures by adding 1 volume of probe working solution to 9 volumes of hybridization buffer. Keep probe solutions dark and on ice.
5. Prepare hybridization vessels.
   a. For slides, prepare hybridization vessels from 50 ml polyethylene tubes: insert a folded Kimwipe into a tube and soak it with about 1 ml of the correct formamide percentage in water or left over hybridization buffer. Use separate tubes for each correct formamide concentration.
   b. Or you might not need vessels because of small sample sizes and you could hybridize in a small volume of hybridization mixture.
6. Incubate at 46°C for at least 90 minutes, maximum of 3 hours.
7. Prepare washing buffer to an appropriate volume for each sample (maybe 50 mL). Preheat to 48°C.
8. After the incubation time, take sample and immerse it in washing buffer and incubate for 25 min. at 48°C.
9. Rinse in distilled H2O by dipping the sample into a container with H2O, let air-dry.
10. Counter stain with DAPI for 3-5 minutes, rinse with distilled H2O and let air dry.
11. Mount samples with some antibleaching reagent and prepare for imaging.
12. Dried samples can be frozen overnight at -20°C. Some say it even improves fluorescence.
13. When imaging, it is safer to image the probe and then DAPI to reduce the amount spent in UV excitation. Probe fluorescence fades more rapidly than DAPI fluorescence while imaging.

Table A.1. Hybridization Buffer

Stock Reagent	Volume	Final Concentration
5 M NaCl	360 µl	900 mM
1 M Tris/HCl	40 µl	20 mM
Formamide	% depending on probe (see Table 3)	
Distilled H_2O	Add to 2 mL	
10% SDS (add SDS last to avoid precipitation)	2 µl	0.01%

Table A.2. Washing Buffer

Stock Reagent	Volume	Final Concentration
5 M NaCl	Depends on % Formamide Concentration (see Table 3)	
1 M Tris/HCl	1 mL	20 mM
0.5 M EDTA	500 µl	5 mM
Distilled H_2O	Add to 50 mL	
10% SDS (add SDS last to avoid precipitation)	50 µl	0.01%

Table A.3. Volume Calculations for Different Formamide %

	Hybridization Buffer (46°C)	Washing Buffer (48°C)	
% Formamide in Hybridization Buffer	µl Formamide Volume in 2 mL	NaCl Concentration (M)	µl 5M NaCl for 50 ml of buffer
0	0	0.900	9000
5	100	0.636	6300
10	200	0.450	4500
15	300	0.318	3180
20	400	0.225	2150
25	500	0.159	1490
30	600	0.112	1020
35	700	0.080	700
40	800	0.056	460
45	900	0.040	300
50	1000	0.028	180

II. Preparation of planktonic samples for FISH – useful for preparing control samples to test FISH probes

1. Starting with planktonic cultures, mix one volume of the sample with three volumes of 4% paraformaldehyde in phosphate buffer saline (PBS) solution. Incubate for 3-12 hours at 4°C (do not freeze).
2. Pellet cells (15,000 g for 5 minutes).
3. Resuspend pellet in PBS. Repeat 2 times.
4. Resuspend pellet in PBS and add equal volume of 96% ethanol.
5. Apply 20 µl drop of fixed sample onto a glass microscope slide.
6. Dry slide until all the liquid has been evaporated.
7. Continue to dry drops of sample onto the same area until a visible residue of the cells forms.
8. Dip the slide horizontally in molten agarose (~1%) for 5 seconds.
9. Allow the agarose to solidify. Wipe off the excess agarose from the bottom of the slide.
10. Dehydrate the samples by incubating the slides through a graded series of ethanol concentrations (50%, 80%, 96%) for 3 minutes each.
11. Dry slides and use for FISH protocols.